Analyzing feedbacks in a forest soil-vegetation-atmosphere system

vorgelegt von

Inken Rabbel

aus

Eckernförde, Deutschland

Bonn, Dezember 2018

Angefertigt mit Genehmigung der Mathematisch-Naturwissenschaftlichen Fakultät
der Rheinischen Friedrich-Wilhelms-Universität Bonn

Acknowledgements

Zusammenfassung

In dieser Arbeit wurden verschiedene Rückkopplungen im Boden-Pflanze-Atmosphärensystem eines 38 ha großen bewaldeten Einzugsgebietes in der Eifel (Westdeutschland) analysiert. Ziel war, das Verständnis der Auswirkungen von Klimavariablen und Bodenwasserverfügbarkeit auf Wasserverbrauch und Wachstum von Bäumen bzw. Wäldern zu verbessern. Im Fokus der Studie stand die Gemeine Fichte (*Picea abies* [L.] H. Karst.). Diese Art reagiert besonders empfindlich auf Trockenheit und Hitze.

Der Wasserverbrauch der Bäume wurde anhand von Saftflussmessungen untersucht. Zur Verarbeitung von Saftflussdaten stehen verschiedene Methoden zur Verfügung. Je nach Methode fallen die Berechnungen des Wasserverbrauches allerdings sehr unterschiedlich aus. Daher wurde in einem ersten Schritt eine vergleichende Analyse verschiedener Datenbearbeitungsverfahren durchgeführt. Ziel war dabei, die Unsicherheit von Saftflussmessungen in Bezug auf die gewählte Datenverarbeitungsmethode zu quantifizieren.

Anschließend wurden die Saftflussdaten verwendet, um einen alternativen Wasserstressfaktor zu entwickeln. Dieser wurde genutzt, um das Wasserstressmodell nach Feddes für die Gemeine Fichte zu parameterisieren. Die Analysen ergaben, dass Trockenstress bei Fichten ab einer mittleren Saugspannung von -4100 cm Wassersäule (-402 kPa) einsetzt. Damit ist die Baumart resistenter gegen Trockenheit als bislang angenommen. Der permanente Welkepunkt liegt bei einer mittleren Saugspannung von 15,000 cm Wassersäule (-1471 kPa). Belüftungsstress durch Staunässe konnte für Fichten im Rahmen dieser Studie nicht nachgewiesen werden.

Die neu parameterisierte Wasserstressfunktion wurde in das bodenhydrologische Modell HYDRUS-1D implementiert um zu testen, ob die artspezifische Parametrisierung standortbasierte Wasserhaushaltsmodellierungen verbessern kann. Tatsächlich konnten für einen Standort mit zeitweise limitierter Bodenwasserverfügbarkeit realistischere Modellergebnisse erzielt werden. Die Berücksichtigung von Bodenfeuchtevariabilitäten und artspezifischen Grenzwerten für Bodenwasserstress kann somit auch zur Verbesserung der Simulation von Transpirationsflüssen auf Einzugsgebietsebene beitragen.

In einem weiteren Schritt wurden Langzeitsimulationen der Bodenwasserverfügbarkeit an 48 Standorten innerhalb des Untersuchungsgebietes durchgeführt. Die Ergebnisse und weitere kleinräumige Standortvariabilitäten wurden anhand von Jahrringdaten mit Jahr-zu-Jahr Variabilitäten im Baumwachstum in Bezug gesetzt. Es konnte nachgewiesen werden, dass die Bodenwasserverfügbarkeit skalenübergreifende Auswirkungen auf das Klima-Wachstumssignal von Fichten hat. So korreliert das regionale Klima-Wachstumssignal auf Einzugsgebietsebene besser mit der simulierten Bodenwasserverfügbarkeit also mit monatlichen Niederschlägen. Auch die Bildung von Wachstumsclustern innerhalb des Untersuchungsgebietes orientiert sich vorwiegend an räumlichen Bodenfeuchtemustern. Dabei zeigte das Wachstumscluster mit den trockensten Bedingungen die stärkste Klima-Wachstumsbeziehung, während das Cluster mit den feuchtesten

Bedingungen mit einer Ausnahme keine signifikante Klima-Wachstumsbeziehungen aufwies. Die Analyse der Klima-Wachstumssignale aller 48 Einzelstandorte ergab, dass diese in ihrer Ausprägung sowohl direkt über die simulierte Bodenwasserverfügbarkeit, als auch indirekt über die Pflanzdichte an den Bodenwasserhaushalt gekoppelt sind.

Daraus lässt sich schlussfolgern, dass kleinräumig aufgelöste Daten über die Bodenwasserverfügbarkeit am Untersuchungsstandort die Interpretierbarkeit von Jahrringdaten verbessern und dazu beitragen können, artenspezifische Wachstumsgrenzen zu identifizieren.

Summary

In this study, the soil-vegetation-atmosphere system of a 38 ha forested headwater catchment in the Eifel region (western Germany) was analyzed with the aim to improve the understanding of the impacts of climate forcings and soil water supply on tree/forest water use and growth. The focus species was Norway spruce (*Picea abies* [L.] H. Karst.), a species, which is known to be particularly vulnerable to heat and drought.

Tree water use was assessed on the basis of sap flow measurements. The choice of the data processing approach for sap flow measurements has considerable impacts on the resulting estimates of absolute tree water use. Therefore, a comparative study of different data processing approaches was conducted to quantify the uncertainty in sap flow estimates, which is related to the data processing procedure.

In a second step, the sap flow series of two plots with contrasting soil moisture regimes were used to derive a new water stress factor and to parameterize the Feddes water stress model for Norway spruce. The onset of drought stress was observed at a root-zone pressure head of -4100 cm water column (-402 kPa). With that, the trees showed a higher drought resistance than previously assumed. Maximum drought stress was determined for a root zone pressure head of -15,000 cm water column (-1471 kPa), while aeration stress was not observed.

The newly parameterized water stress function was implemented in the soil hydrological model HYDRUS-1D with the aim to improve site specific water balance simulations. This aim was achieved for a plot with temporarily limited soil water supply. Considering soil moisture patterns and species specific critical limits of soil water supply in the model setup can thus improve the simulation of transpiration fluxes on the catchment scale.

Based on this finding, long-term water balance simulations were carried out for 48 plots within the catchment. These and other microsite conditions were set into context with inter-annual growth variations in terms of tree ring data. The data showed that soil water supply strongly affects the climate-growth responsiveness of Norway spruce across different levels of data aggregation. On the regional scale, inter-annual growth variations were better explained by soil water supply than by monthly precipitation sums. Also the formation of growth clusters within the catchment mainly followed spatial patterns of soil water supply. While the driest cluster showed the strongest climate-growth reaction, the climate-growth response of the wettest cluster was almost completely insignificant. Across all investigated microsites within the test-site, the climate-growth response of Norway spruce was directly (simulated soil suction of the root-zone) and indirectly (planting density) related to local soil water supply.

Small-scale information on soil water supply can thus help to improve the interpretability of tree ring data and to investigate species-specific growth limitations.

Contents

List of Figures

List of Tables

List of Abbreviations

α	empirical parameter of the Mualem-van Genuchten model related to the air-entry pressure value
A_{qh}	empirical parameter needed for the deep drainage option in HYDRUS-1D
B_{qh}	empirical parameter needed for the deep drainage option in HYDRUS-1D
CA	projected crown area
CAL	current calendar year
CAL_p	previous calendar year
Cfb climate	temperate oceanic climate according to the Köppen-Geiger classification
CL chronology	cluster chronology
DOY	day of year
D	ΔT_{max} determination approach: daily ΔT_{max} determination
DBH	diameter at breast height
DFG	Deutsche Forschungsgesellschaft (German Research Foundation)
DHC-station	dendro-hydro-climate station
DR	ΔT_{max} determination approach: double regression based on linear regression (LR)
DR_{sub}	ΔT_{max} determination approach: double regression approach applied to a sub-period of the vegetation period
ΔT_{max}	maximum temperature gradient between Granier-type sap flow probes in a given time period
$\Delta T_{ref\_1/2}$	additional reference probes in improved sap flow systems
DWD	Deutscher Wetterdienst (German Meteorological Service)
E	east
E_0	reference evaporation
EC system	eddy-covariance system
ESE	east-south-east
ET_0	grass reference evapotranspiration
ET_{act}	actual evapotranspiration
ET_{pot}	potential evapotranspiration
ETp*	transformed potential evapotranspiration
FC	field capacity
F_d	sap flow density
$F_{d,n}$	normalized sap flow density
GWL_{ref}	reference groundwater level
h	pressure head
$h_{1/2/3/4}$	Feddes parameters

JJA	June, July, and August of the current year
JJA_p	June, July, and August of the previous year
K_s	saturated hydraulic conductivity
K_c	crop coefficient
LAI	leaf area index
LR	ΔT_{max} determination approach: linear regression based on local maxima of 9 day period
LR_{sub}	ΔT_{max} determination approach: linear regression approach (LR) applied to a sub-period of the vegetation period
m	retention curve shape parameter of the Mualem-van Genuchten model
MAM	March, April, and May of the current year
MAM_p	March, April, and May of the previous year
MW	moving window
MW3-MW14	ΔT_{max} determination approach: ΔT_{max} determination based on dynamic time windows of 3 (MW3) to 14 days (MW14)
N	nitrogen
n	empirical parameter of the Mualem-van Genuchten model related to the pore size distribution
OB	ΔT_{max} determination approach: Oishi baseliner
P	phosphate
Φ	objective function
P-signal	precipitation signal of a tree ring chronology
q	discharge rate
R	solar radiation
R^2	coefficient of determination
REW	relative extractable soil water
RMSE	root mean square error
RR	ΔT_{max} determination approach: daily simulation of ΔT_{max} based on the relationship between potential evapotranspiration and sap flow readings
RWI	ring width index
S_e	relative soil saturation
SM	soil moisture
SN	TERENO SoilNet
SON	September, October, and November of the current year
SON_p	September, October, and November of the previous year
SWC	soil water content
SWD	sapwood depth
T_0	reference transpiration
T_{act}	actual transpiration
TERENO	TERrestrial ENviromental Observatoria
θ_r	residual water content
θ_s	saturated water content

TMC	tree mean curve
TR32	Transregional collaborative research center 32
T-signal	temperature signal of a tree ring chronology
VEG	vegetation period (April to October) of the current year
VEG_p	vegetation period (April to October) of the previous year
VPD	vapour pressure deficit of the air
VPD_{air}	vapour pressure deficit of the air above the forest canopy
VPD_{stand}	vapour pressure deficit of the air below the forest canopy
WP	permanent wilting point
WÜ chronology	regional chronology of the Wüstebach test-site

1 Introduction

1.1 Research framework

This doctorate thesis has been developed in the framework of the Transregional Collaborative Research Center 32 (TR32) funded by the German Research Foundation and in close collaboration with the TERENO-Rur Hydrological Observatory funded by the Helmholtz Association.

The key goals of these research programs are to study and monitor ecosystem controls on terrestrial system patterns and fluxes and to investigate the impact of global change on these across scales (Zacharias et al., 2011; Simmer et al., 2015; Bogena et al., 2018).

1.2 Problem statement

Forests cover 30% of the earth's land surface. Storing 45% of the terrestrial carbon and contributing 50% of the terrestrial net primary production, forest ecosystems provide significant climate services worldwide. However, the future development of the world's forest systems and the magnitude of change in species composition and energy and matter fluxes under climate change is highly uncertain (Bonan, 2008). For temperate forests, climate scenarios predict an increase of severe and recurrent droughts (Bréda et al., 2006). This also applies for the Rur catchment in western Germany, for which a strong increase in temperatures and a precipitation shift from summer to winter are currently expected (Zacharias et al., 2011).

Since water availability is one of the most important growth factors in temperate forest systems, such changes in the seasonal course of climate variables are likely to evoke a long-term shift in species composition (Bréda et al., 2006; Thompson et al., 2009; Hanewinkel et al., 2013). On the short to medium term, however, present species will be driven towards their physiological limits with unknown consequences for ecosystem processes and fluxes (Bréda et al., 2006; Thompson et al., 2009). To reduce the high uncertainty in the prediction of future forest traits, more research is needed on the assessment of energy and matter fluxes in the forest soil-vegetation-atmosphere system (Ammer et al., 2018; Thompson et al., 2009) and on the understanding and quantification of species specific growth and transpiration limitations (Keenan, 2015; Bréda et al., 2006). In this context, the recognition of belowground processes and soil conditions and the implementation of respective thresholds and feedbacks in mechanistic models are of particular importance (Keenan, 2015; Thompson et al., 2009; Bréda et al., 2006).

The aims of this study are to improve the uncertainty assessment for tree based transpiration estimates (chapter 2) and to investigate the species specific stress response of Norway spruce (*Picea abies* [L.] H. Karst.), which is a wide-spread and economically important species in Europe. Special emphasis is put on the response of transpiration (chapter 3) and growth (chapter 4) to climate forcings and soil water supply.

1.3 State of the art

1.3.1 Basic principles of water flow in trees

The water flowing through the xylem conduits of woody plants is generally called sap (Perämäki, 2005). While xylem anatomy and structure vary e.g. with the tree species (Cruiziat et al., 2002), the general organizational structure of the stem is always similar (Figure 1.1). The central spongy tissue of the trunk (pith) is surrounded by a wooden body, from which the inner, non-active part (heartwood) basically stabilizes the tree (Johnson and Schweingruber, 2012), while the outer part (xylem; sapwood) contains living ray cells and serves as a pathway for water flow from the roots to the branches and leaves (Cruiziat et al., 2002; Perämäki, 2005).
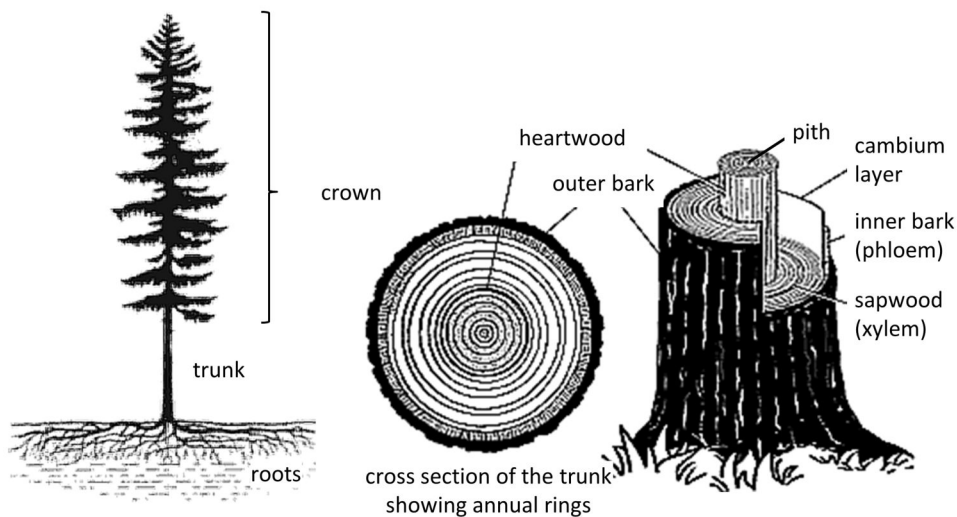
Figure 1.1: Organizational structure of a tree trunk. Modified after Johnson and Schweingruber (2012) and The Botanist (2012)[1].

The xylem structure of Norway spruce (*Picea abies*), which is the focus species of this dissertation, is characterized by so-called tracheids (Figure 1.2). This elongated cell type is typical for conifers and serves at the same time as both supporting and conductive tissue (Hacke and Sperry, 2015). The xylem body is surrounded by a thin tissue layer (cambium), which is responsible for cell division and thus for secondary growth and tree ring formation. This cell-dividing tissue layer is directly connected to the phloem, which forms the inner bark and consists of conducting cells that translocate photosynthetic products (mainly sugars) within the tree (Johnson and Schweingruber, 2012; De Schepper and Steppe, 2010). The outer bark prevents evaporation from the phloem and protects the tree from damage, e.g. by fungal or insect infestation (Perämäki, 2005).

---

[1]botanistbackyard.blogspot.com; last accessed in November 2018
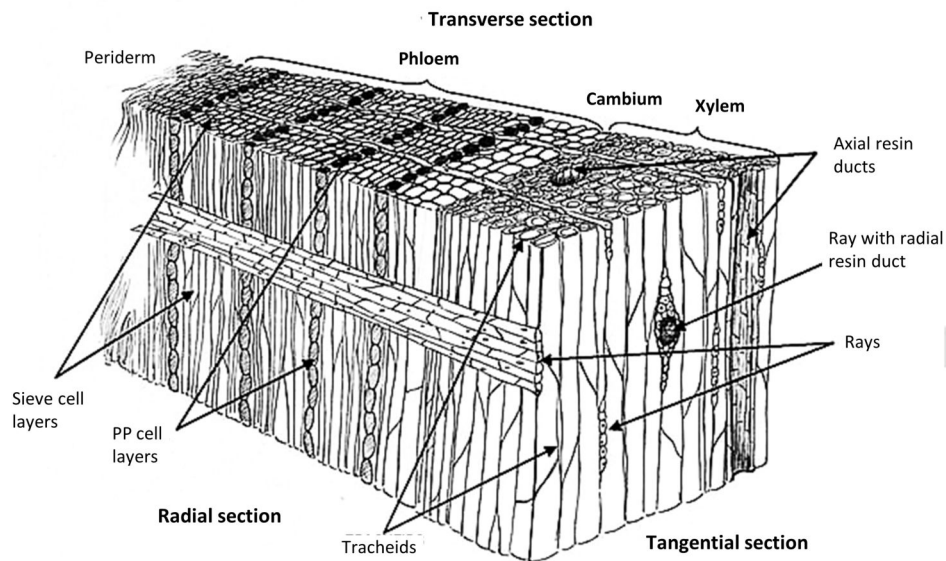
Figure 1.2: Scheme of the basic bark and sapwood anatomy of Norway spruce. Source: Krokene et al. (2008).

Far more than 90% of the water flow in trees ends up in transpiration, which pulls the water from the soil to the leaves (Hacke and Sperry, 2015; Perämäki, 2005; Cruiziat et al., 2002). On its way through the xylem conduits, the water (sap) follows dynamic gradients of water potential. With that, trees can be considered as "kind of hydraulic system[s]" (Cruiziat et al., 2002). These systems are basically governed by solar radiation, because solar radiation is the main driver of stomatal activity (Figure 1.3). When stomata open for photosysthesis, water molecules follow the atmospheric vapour pressure deficit and escape from the leaves. The induced negative pressure at the evaporating surface of the leaves then pulls the continuous water column upwards and the water ascents the trunk (Cruiziat et al., 2002; Hacke and Sperry, 2015; Tyree, 1997).

In general, this principle works fairly well, however, it is not immune against failure. Under certain pressure-temperature conditions, the water in the xylem conduits abruptly changes its phase from liquid to gas (water vapour) (Cruiziat et al., 2002; Hacke and Sperry, 2015; Perämäki, 2005). This process is called cavitation and directly leads to a reduction of hydraulic conductivity, which decouples the upper transpiration limit from atmospheric demand and sets it a function of soil water supply instead (Hacke and Sperry, 2015). Cavitation often occurs as a consequence of freezing-thawing cycles of xylem sap, but also as a consequence of drought (Cruiziat et al., 2002; Hacke and Sperry, 2015; Perämäki, 2005).

Following the dynamics of radiation and atmospheric demand, transpiration and thus sap flow typically show diurnal patterns going hand in hand with diurnal fluctuations of the water tension in the xylem (Perämäki, 2005; Steppe et al., 2005). The resulting changes in stem water storage (cf. Figure 1.3) lead to reversable stem diameter fluctuations, which can be monitored by dendrometers and are inverse to the diurnal sap flow pattern (Figure 1.4).
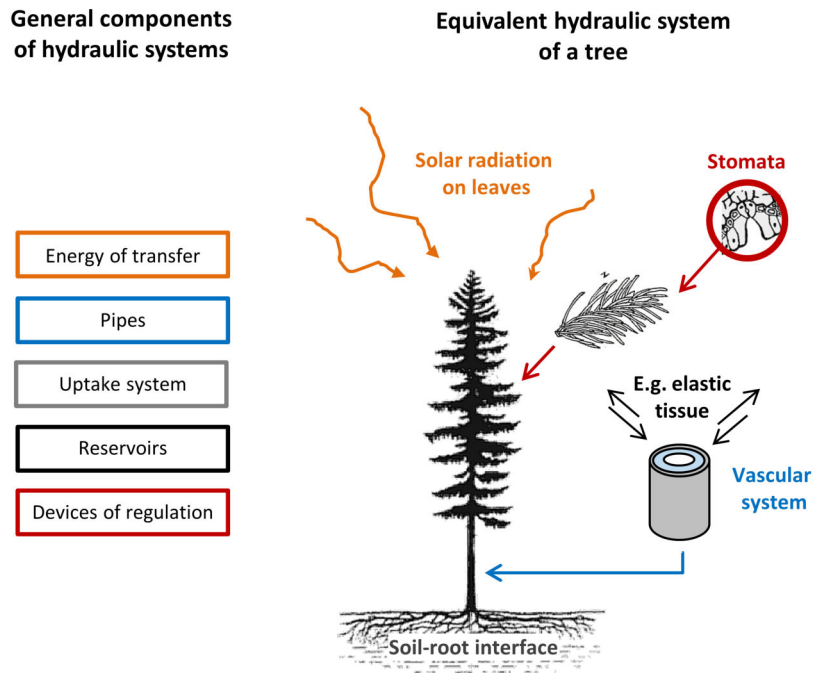
Figure 1.3: Hydraulic system of a tree. Modified and extended after Cruiziat et al. (2002) and Johnson and Schweingruber (2012).
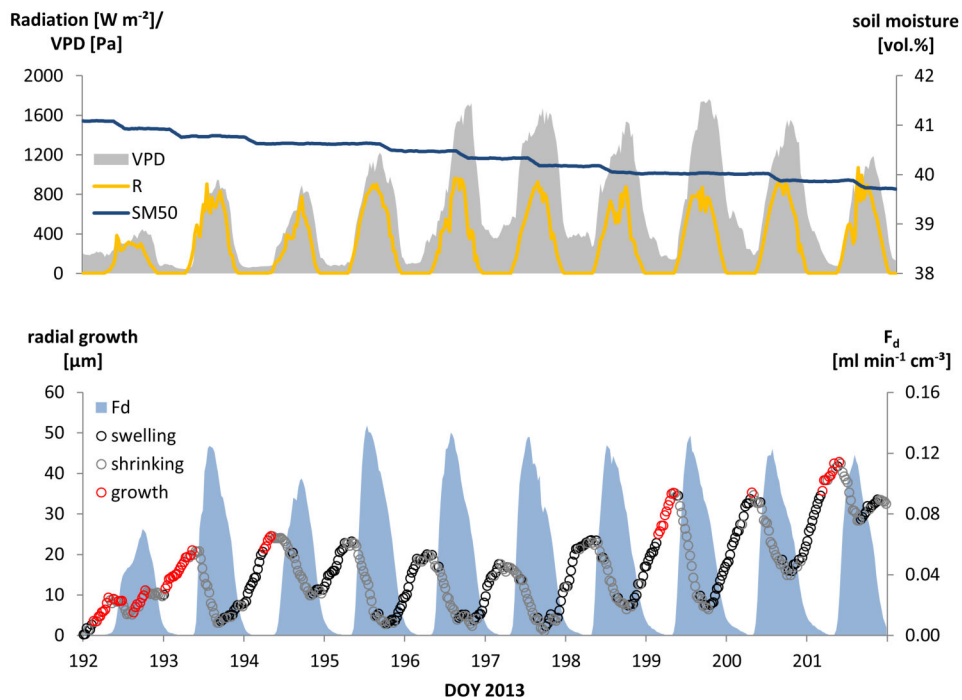
Figure 1.4: Example data from the Wüstebach of the year 2013 showing inverse patterns of sap flow dynamic and diurnal stem expansion (bottom illustration) and how these follow the patterns of incoming global radiation and atmospheric vapour pressure deficit (upper illustration). VPD: vapour pressure deficit; R: global radiation; SM50: volumetric soil moisture in 50 cm depth; F_d: sap flow density; DOY: day of year.

Additional to these swelling-shrinking cycles, dendrometers are able to detect phases of absolute stem increment (red dots in Figure 1.4). These can be attributed to either irreversable cell expansion or new cell formation (Deslauriers et al., 2007).

With that, dendrometers can not only be used to estimate tree water status, but also to monitor intra-annual growing patterns. However, one current challenge in dendroecology is to put these short-term observations into context with long-term intra-annual growth variations as obtained from tree ring data (cf. chapter 1.3.2).

1.3.2 Tree ring formation and growth assessment

Tree rings evolve as a results of the cambial activity of trees during the growing season. In temperate ecosystems with recurring interplay of growing periods and dormant seasons, trees generally form one distinct ring per year. The formation of a tree ring is "a complex process of cell division, growth and maturation" (Deslauriers et al., 2017). New cells are built in tangential orientation, whereas cells directed outwards become part of the phloem, while cells directed inwards become part of the xylem body (Cocozza et al., 2016; Deslauriers et al., 2017).

Normally, the cambial cell division starts simultaneously on the phloem and the xylem sides. However, since the first one or two layers of phloem cells generally differentiate without previous cell division, phloem formation actually starts earlier in the growing season than xylem formation. For Norway spruce, the shift between the onset of phloem and xylem formation amounts to 3-5 weeks (Deslauriers et al., 2017).

The rate and duration of cell division and enlargement are mainly determined by genetics and environmental conditions (Schweingruber, 1996; Cocozza et al., 2016). In temperate forests, the onset of stem growth is generally related to species-specific temperature thresholds or critical heat sums (Cocozza et al., 2016). During spring growth, the trees draw on internal nutrient reserves that they have stored during the previous year. Wide-lumened and thin-walled earlywood cells with a high hydraulic conductivity are built to cover the demand for water and nutrients at this stage. Therefore, the current year tree ring width of some species is more sensitively correlated to previous year climate conditions than to the climate in the year of ring formation (Schweingruber, 2007; Neuwirth, 2010).

Over the growing season, a transition of the huge earlywood cells to flatter latewood cells with narrow lumen and thicker walls can be observed (Figure 1.5). This earlywood to latewood transition is triggered by hormones and goes hand in hand with a shift in cell functionality. In the later growing season, matters like lignin, resin, dye and ferment are stored along the cell walls. This reduces the cell volume, but stabilizes the wood. The decreasing temperatures towards the end of the growing season go hand in hand with the cessation of cell division and thus growth. With that, the tree ring is completed (Schweingruber, 1996, 2007).

Timing and appearance of the earlywood to latewood transition are basically driven by genetics and climate. Norway spruce typically shows a continuous transition from earlywood to latewood (cf. Figure 1.5b). However, seasonal short-term climate oscillations or variations of the soil water supply may sometimes yield sharp earlywood to latewood transitions as well.
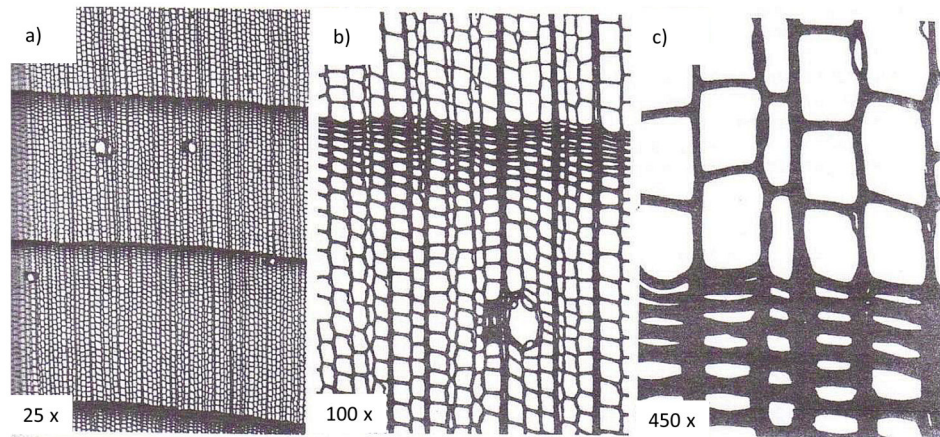
Figure 1.5: Tree ring structure of Norway spruce in 25x (a), 100x (b), and 450x magnification (c). The differing cell structure of earlywood and latewood is clearly visible in Figure (c), where the latewood earlywood border marks the beginning of a new tree ring. Source: Schweingruber (1990).

Consequently, intra-annual variations of cell size and structure hold important information of the intra-seasonal variability of environmental conditions in the year of ring formation (Schweingruber, 2007; Deslauriers et al., 2017).

One opportunity to close the gap between high resolution dendrometer data (cf. Figure 1.4) and annually-resolved tree ring data is therewith the analysis of cell growth and wood anatomy in intermediate time steps. To this end, small samples of wood (so-called microcores) are taken from the developing current year tree ring in bi-weekly or shorter time steps. On the basis of the resulting intra-seasonal microcore chronology, tree rings can be resolved intra-annually and actual cell growth can be related to the shape of the dendrometer curve (Cocozza et al., 2016; Michelot et al., 2012; Drew and Downes, 2009).

Nevertheless, the traditional way to analyse the climate-growth response of trees still includes the correlation of monthly mean climate data with annually-resolved time series of tree ring widths (Cocozza et al., 2016). Respective basic principles of site selection and data processing are described in chapter 1.3.4.

1.3.3 Measuring and scaling sap flow

Since more than 90% of the water flow in trees ends up in transpiration and all of that water passes the trunk (cf. chapter 1.3.1), sap flow measurements can serve as a proxy for tree and forest transpiration (Perämäki, 2005). With that, sap flow techniques are valuable tools in studies of forest water and energy budgets (Figure 1.6).

In contrast to classic water balancing approaches and micrometeorological techniques, sap flow measurements allow for the partitioning of species specific transpiration components from overall forest evapotranspiration and for the assessment of spatio-temporal transpiration patterns (Smith and Allen, 1996; Kool et al., 2014; Williams et al., 2004; Ringgaard et al., 2012, 2014; Oishi et al., 2008).
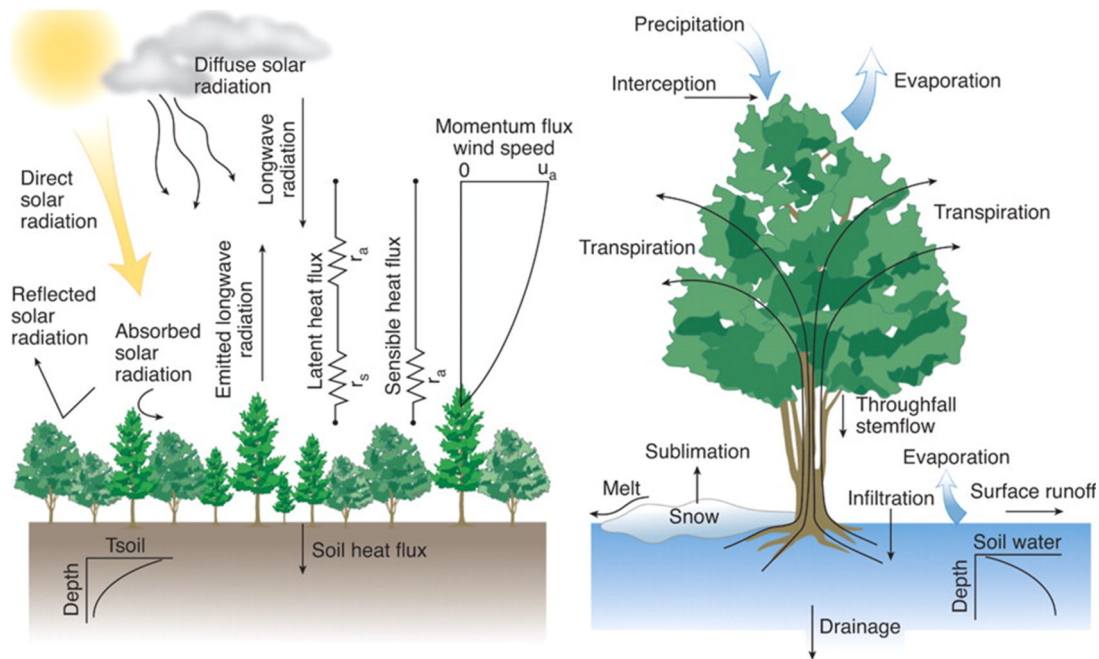
Figure 1.6: Overview of energy (left-hand illustration) and water fluxes (right-hand illustration) in forest soil-vegetation-atmosphere systems. Source: Bonan (2008).

In combination with measurements of other environmental variables, they provide important information on plant-physiological responses to varying hydro-climatic conditions (Bräuning and Steppe, 2016; Leo et al., 2014; Clausnitzer et al., 2011; Lundblad and Lindroth, 2002) and help to identify species- and site-specific limits of plant hydraulic functioning (Steppe et al., 2015).

Different sap flow systems are commonly in use and commercially available. However, all of them rely on the principle of heat being used as a tracer for sap movement in the tree (Smith and Allen, 1996). In heat balance methods, the trunk (Sakuratani, 1981) or a section of the trunk (Cermák et al., 1973) is "heated electrically and the heat balance is solved for the amount of heat taken up by the moving sap stream, which is then used to calculate the mass flow of sap in the stem" (Smith and Allen, 1996). With the heat pulse technique, "sap flux density is determined from the velocity of a short pulse of heat moving along xylem tissue through conduction and convection" (Steppe et al., 2010). One empirical approach to determine sap flow rates is the thermal dissipation technique (Granier, 1985, 1987), where sap flow densities are derived "from the temperature of sapwood near a continuously-powered heater implanted in the stem" (Smith and Allen, 1996).

All of these measuring systems have their advantages and disadvantages. In the TR32 project, we used the Granier system (Granier, 1985, 1987), because it is easily applicable to trees of larger size. A detailed description of our sensors and the principle of Granier-based sap flow measurements is given in chapter 2.

As with all sap flow systems, one key issue of the Granier technique is measuring accuracy (Steppe et al., 2010, 2015). In comparison to gravimetric measurements, Granier-based sap flow sensors tend to underestimate actual sap flow densities (Steppe et al., 2010). This is partly

related to the method applied for the conversion of the raw temperature signal into actual sap flow density (Peters et al., 2018). Different data processing approaches are in use, however, little attention has been paid to the uncertainty, which is related to the signal transformation. The research presented in chapter 2 addresses this issue by comparing existing data processing approaches and quantifying variations in the resulting sap flow densities on different time scales. The results show that absolute sap flow densities strongly vary with the underlying data processing procedure. Therefore, attention should be paid to the selection of the data processing approach.

Another critical point of Granier type sap flow systems is related to the assessment of natural radial and circumferential variations of sap velocities within the trunk (Figure 1.7). Granier-based measurements are point measurements. Since trunk internal velocity profiles may vary with tree species, tree size, tree age, social position of the tree, and also with ambient conditions, radial and circumferencial sap flow profiles need to be determined for a proper scaling to whole-tree water use. This requires sap flow measurements in different sapwood depths and from different sides of the tree. To further reduce the uncertainty of tree-scale sap flow estimates, a species- and site-specific calibration of the sensors is generally recommended (Peters et al., 2018; Steppe et al., 2015; Ford et al., 2004; Gebauer et al., 2008; Phillips et al., 1996; Fiora and Cescatti, 2006; Čermák et al., 2007).
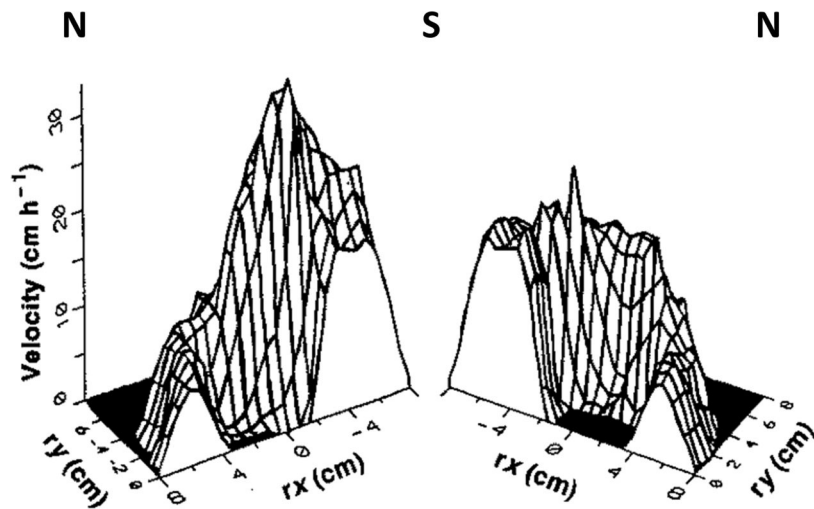
Figure 1.7: Example of a crossectional velocity profile of a Norway spruce stem. N: northern side of the stem; S: southern side of the stem; rx/ry: radius in x and y direction; Source: Čermák et al. (2004).

For the scaling of sap flow data from the tree to the forest stand, and therewith to a ground-area basis, scalars like leaf area, projected crown area or basal area can be used. Age and diameter distributions, crown-classes, and potential edge-effects should be considered in the sampling design (Asbjornsen et al., 2011; Köstner et al., 1998; Čermák et al., 2004; Ringgaard et al., 2012).

Respectively, extensive measurement campaigns are needed to obtain proper estimates of forest transpiration from sap flow measurements alone. Therefore, many researchers alternatively apply water balance models to estimate forest transpiration. These models calculate tran-

spiration as a function of atmospheric boundary conditions, soil water supply and vegetation characteristics (Asbjornsen et al., 2011; Arora, 2002). To account for the effects of limited soil water supply on stand transpiration, they commonly refer to plant water stress functions. These describe the species-specific water stress response of plants, but have rarely been parameterized for forest trees, because no common method is available. This issue is adressed in chapter 3, which shows how to make use of sap flow data to quantify the water stress response of trees and improve forest water balance simulations.

1.3.4 Analyzing climate-growth relations

Investigating the climate-growth response of specific sites and species is one of the main research subjects in classic tree ring studies. To maximise the climate signal in the tree ring data, a proper site selection is of critical importance. Typically, homogeneity in site conditions and social position of the sample trees are considered necessary prerequisites for building strong chronologies. These requirements can only be meet by selective sampling. To obtain a solid mean chronology of a geobotanically and climatically homogeneous site, 20-30 dominant trees are usually sampled from two opposite sides (Schweingruber et al., 2013). After preparing the cores for ring width measurements (for detailed information on sample preparation and measurement techniques cf. Pilcher (2013) and Stokes and Smiley (1968)), the samples typically undergo the following procedure:

1. Determination of the tree ring widths

Measurements of tree ring widths can either be done visually using microscopes and moveable object tables or with the help of measuring software that is based on scanned images of the cores (Pilcher, 2013).

2. Calculation of tree mean curves

A tree mean curve (TMC) is the tree ring chronology resulting from the average of all growth curves taken from one tree (Kaennel and Schweingruber, 1995). Therewith, TMCs represent the mean growth behaviour of a tree.

3. Cross-dating

Cross-dating describes the "procedure of matching variations in ring width or other ring characteristics among several tree ring series allowing the identification of the exact year in which each tree ring was formed" (Kaennel and Schweingruber, 1995). A proper cross-dating is essential in any tree ring study, because it is the only possibility to identify missing rings or false rings that may result from environmental anomalies during the growing season.

4. Standardization and indexing

Standardization, commonly termed indexation in the dendro community, describes the process of removing climatic or bio-ecological trends from tree ring series by substracting or dividing the measured tree ring widths by smoothed values obtained from a filter or a selected smoothing function (Figure 1.8a). The choice of the filter or smoothing function depends on the aims of the study. With low-pass filters (e.g. 31-year weighted running

means of the measured values), long-term environmental fluctuations can be emphasized, while high-pass-filters (e.g. weighted or unweigthed 5-year running means) are used to bring short-term fluctuations to the fore (Schweingruber, 1988). One trend that needs to be removed wherever tree ring series from individual trees of different cambial age are set into context, is the so-called age trend. This term describes the phenomenon that the absolute tree ring width typically decreases from the pith to the outermost ring because of the "geometric constraint of adding an annual volume of biomass to the stem of a tree that has an increasing radius [over time]" (Helama, 2015). The effect of the selected filter function on the resulting indexed tree ring series is illustrated in Figure 1.8b.
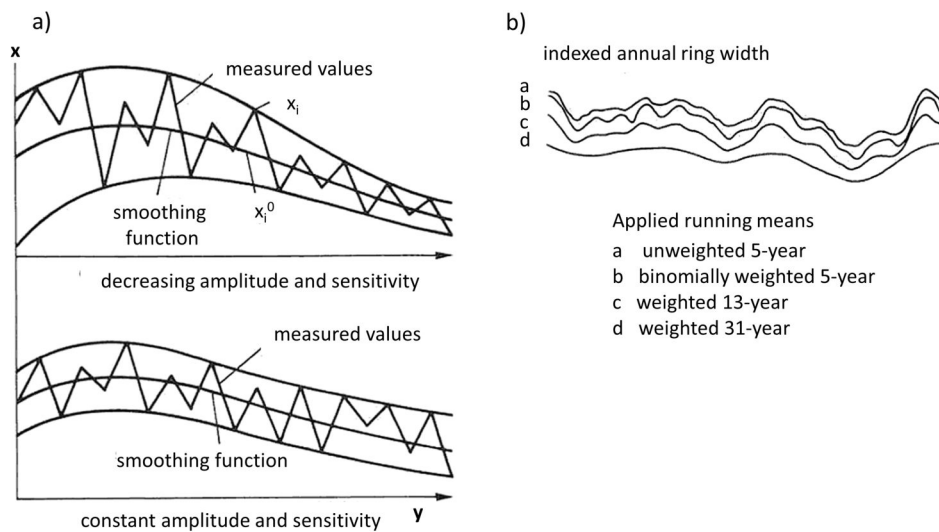
Figure 1.8: (a) Examples of smoothing functions. (b) Effect of the selected filter function on the resulting indexed tree ring series. 5-year filters are typically used to emphasize short-term environmental fluctuations, the 13-year filter can be used to investigate medium term fluctuations, while the 31-year filter puts long-term fluctuations to the fore; Modified after Schweingruber (1988).

5. Chronology building

After cross-dating and indexation, the tree ring series of individual trees are aggregated to mean chronologies (Kaennel and Schweingruber, 1995). The level of data aggregation depends on the study purpose and may range from individualistic approaches on the tree or microsite level (Carrer, 2011) over site chronologies regional chronologies (Kaennel and Schweingruber, 1995).

To investigate the climate-growth responsiveness of specific sites or species, the annual records of respective growth chronologies are typically correlated with monthly and seasonal mean temperatures or precipitation sums. The strength of the resulting climate-growth relations provides information on species- and site-specific growth limitations and may decide wether a chronology is suitable for climate reconstructions or not (Schweingruber, 1996).

One critical issue related to this standard procedure in analyzing the climate-growth response

of trees is the question of representativeness of the averaged growth chronology for entire populations and the actual conditions on site. Even though selective sampling is still acknowledged as appropriate approach for climate growth analysis and climate reconstructions, there is increasing evidence that also geobotanically and climatically homogeneous sites comprise small-scale heterogeneities in site conditions which may significantly alter the climate-growth responsiveness of individual trees (Carrer, 2011; Nehrbass-Ahles et al., 2014; Sullivan and Csank, 2016). Such small-scale heterogeneities are for example caused by management practice (Pretzsch and Dieler, 2011; Primicia et al., 2015), physical and chemical soil properties (Braun et al., 2010; Pretzsch and Dieler, 2011; Tromp-van Meerveld and McDonnell, 2006; Ibáñez et al., 2018), soil water state (Ashiq and Anand, 2016; Helama et al., 2016; Jiang et al., 2016; Lévesque et al., 2014; Linares et al., 2010; Primicia et al., 2015; Zhang et al., 2018), canopy structure (Adams and Kolb, 2004; Linares et al., 2010; Martín-Benito et al., 2008; Primicia et al., 2015), tree-to-tree competition (Linares et al., 2010; Primicia et al., 2015; Gleason et al., 2017; Piutti and Cescatti, 1997), and tree size (Carrer and Urbinati, 2004; Linares et al., 2010). The interplay of these parameters determines the range of climate signals detected among individual trees (Carrer, 2011).

One understudied question in this context is related to level of data aggregation at which such small-scale effects become significant for average site or stand chronologies. The research presented in chapter 4 adresses this issue by analyzing tree ring chronologies of 144 even-aged Norway spruce trees on different levels of data aggregation with the aim to identify the relevance of small-scale heterogeneities in site conditions for the detected climate-growth signal.

1.4 Study area

The major goal of the TR32 is to study and monitor ecosystem controls on terrestrial system patterns and fluxes and to investigate the impact of global change on these across scales (Zacharias et al., 2011; Simmer et al., 2015; Bogena et al., 2018). Covering a broad range of environmental gradients, e.g. in altitudes, temperatures, precipitation amounts, and land-use types, the Rur catchment in western Germany was selected as the central study area and has turned into a highly instrumented observation site since the beginning of the research activities in 2007 (Simmer et al., 2015; Bogena et al., 2018).

The total catchment area of the Rur covers about 2354 km². With 34%, a considerable proportion of the landcover consists of forests, mainly located in the southern upland part of the catchment (Simmer et al., 2015). Hence, forests play a significant role for the regional water, energy and matter cycles. To improve the understanding of respective processes and fluxes in the forest soil-vegetation-atmosphere system, the 27 ha Wüstebach test-site was implemented as one of three heavily instrumented research sites in the Rur catchment (Zacharias et al., 2011; Bogena et al., 2018). All studies of this dissertation were conducted in the setting of this site, which is not only one of the focus areas of the TR32 project, but was also set up as part of the TERENO Eifel/Lower Rhine Valley Observatory in 2007 (Bogena et al., 2018).

The Wüstebach test site is located in the catchment of the Wüstebach stream (50°30'N, 6°19'E), which covers an area of 38.5 ha and is situated in the German low mountain ranges close to the German-Belgian border (Figure 1.9a) (Bogena et al., 2010, 2014, 2018; Zacharias

et al., 2011).

Altitudes range from 595 m a.s.l. in the north to 628 m a.s.l. in the south. The main valley of the Wüstebach stream shows an asymmetric V-shape with steeper slopes (11-15°) on the eastern side than on the western side (7-11°) (Lehmkuhl et al., 2010). Situated in the northern part of the Eifel mountains, the area is part of the Rhenish Massif, which belongs to the Variscan orogenic belt. Respectively, the bedrock is characterized by Devonian shales with occasional sandstone inclusions covered by a periglacial solifluction layer of 1 to 3 m depth (Bogena et al., 2018; Lehmkuhl et al., 2010).

The present geomorphology of the Wüstebach site is strongly marked by anthropogenic interventions. During medieval and early modern times, the region was characterized by poor socioeconomic conditions. The population density was low and small and scattered field structures prevailed. Until the mid of the 19th century, however, the area developed to an important center for iron melting and other heavy industries. In this period, huge parts of the natural beech forests were deforested for charcoal production. Under Prussian governance, the first pine and spruce plantations were established to meet the continuing need for wood for mining and construction. During the Second World War, forests fell again victim to the high demand for firewood. In the final stage of the war, the region was the scene of heavy fighting in the Battle of Bulge. Dugouts, impact craters, and gun emplacements still dominate the small-scale geomorphology of the Wüstebach site (Lehmkuhl et al., 2010).

After the war the few remaining wood resources were soon exhausted. However, in the late 1940ies, spruce plantations were again established to produce timber and prevent erosion (Bogena et al., 2018; Lehmkuhl et al., 2010). The Wüstebach test-site is situated in one of these plantations. Meanwhile, the trees (*Picea abies* [L.] H. Karst.) are ∼70 years old and have reached a canopy height of ∼30 m (observations from 2016). Due to the high degree of shading, only sparse shrub, herb, and moss layers have developed below the forest canopy. The species composition within these layers is typical for acidic and nutrient-poor soils in montane and sub-Atlantic regions and comprises e.g. black elderberry (*Sambucus nigra*), common broom (*Cytisus scoparius*), white woodrush (*Luzula luzloides*), blueberry *(Vaccinium mytrillus)*, and red foxglove (*Digitalis purpurea*)(Deckers, 2010).

In 2004, the Eifel National Park was established and the Wüstebach catchment became part of it. Until 2034, about 75% of the conservation area is supposed to be transformed to an undisturbed landscape with near-natural vegetation. One goal of the National Park Forestry Service is therefore to convert former spruce plantations into European beech forests (*Fagus sylvatica*), which is the potential natural vegetation in the region (Wald und Holz NRW, 2017). To accelerate the conversion process, forest managers decided to remove a significant proportion of the spruce forest providing space for natural succession. In this context, a clear-cut experiment was conducted in the area of the Wüstebach test-site (Bogena et al., 2014, 2018).

To investigate the effects of deforestation on hydrological and biogeochemical cycling, the site was instrumented with a soil moisture measurement network (TERENO SoilNet; Bogena et al. (2010)) and observation platforms monitoring the main water and matter fluxes in the catchment (Bogena et al., 2018).
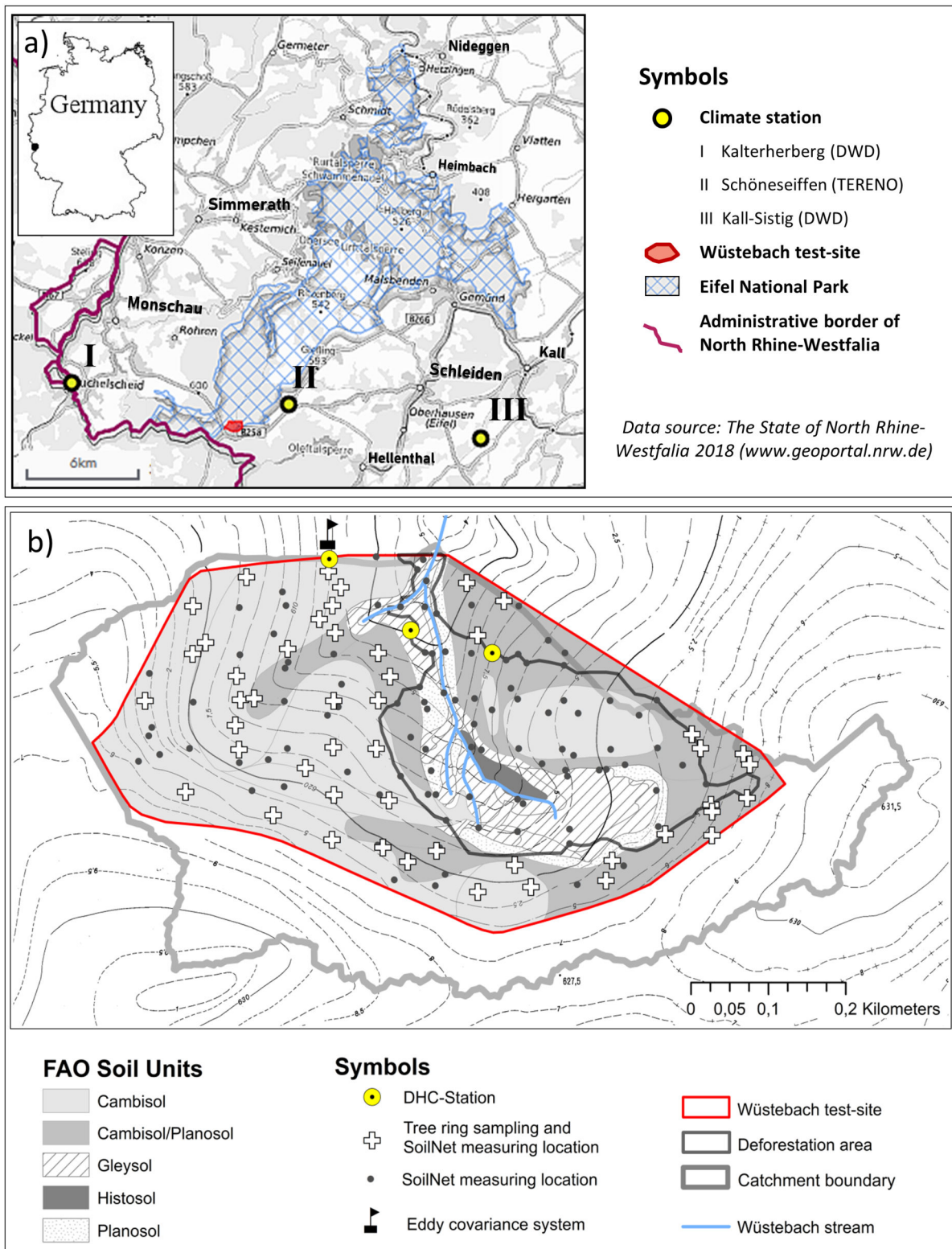
Figure 1.9: (a) Location of the Wüstebach test-site within the Eifel National Park and Germany and overview of nearby climate stations. (b) Overview of the Wüstebach test-site including relevant instrumentation and sampling sites. The installed dendro-hydro-climate stations (DHC-stations) include sap flow sensors and dendrometers on 3-4 trees and temperature and relative humidity sensors to monitor the micro-climate on site. The difference between the displayed contour lines is 2.5 m.

SoilNet operates wireless and monitors volumetric soil moisture in 5, 20, and 50 cm depth at 150 measuring locations across the test-site. An overview of the measuring locations is given in Figure 1.9b. Recording the data in 15 min time steps (Bogena et al., 2010), SoilNet provides high-resolution information on the spatio-temporal soil moisture variability since 2009.

Another centrepeace of the Wüstebach test-site is the micrometeorological tower, which was installed in 2010. The tower is about 38 m high and measures actual evapotranspiration fluxes above the forest canopy. The measurements are based on the eddy-covariance (EC) technique and yield mean estimates of fluxes from a dynamic footprint area (Graf et al., 2014). Shape and size of this footprint area depend on the wind direction and other micrometeorological conditions. The radius of the main EC tower footprint in the Wüstebach catchment reaches approximately 500 m downwind (Graf 2018, personal communication).

Other permanently installed measuring devices in the Wüstebach catchment include three runoff gauging stations, eight groundwater piezometers, two cosmic-ray neutron probes, a lysimeter station, and sampling stations for weekly determination and isotopic analysis of different components of the hydrological water cycle. For a detailed description of the measuring devices and additional sampling campaigns in the framework of TERENO, refer to Bogena et al. (2018) and to the TERENO data discovery portal TEODOOR[2].

The instrumentation of the Wüstebach test-site was completed between 2007 and 2010 and thus well before the deforestation in 2013. About 9 ha of spruce forest were then removed from the plantation (Figure 1.10) (Bogena et al., 2014, 2018).
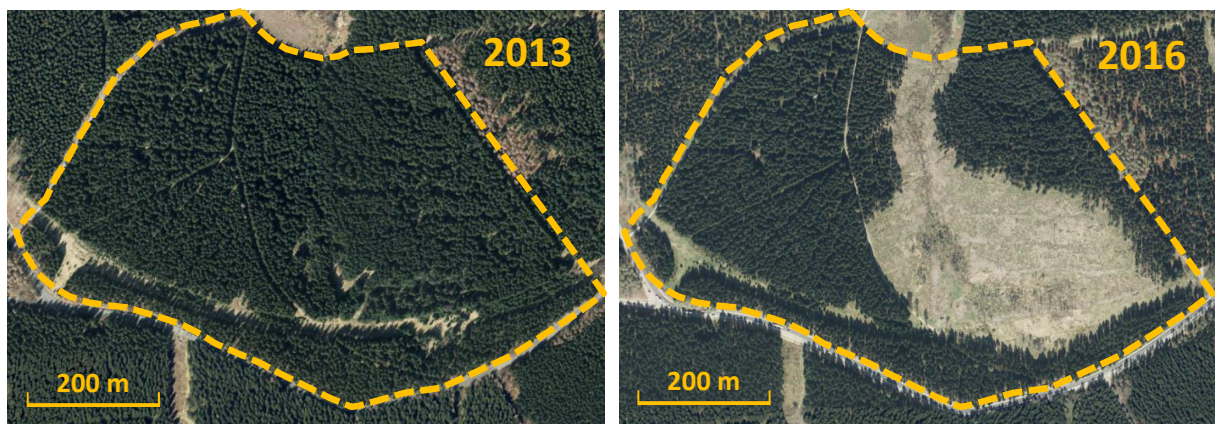
Figure 1.10: Aereal images of the Wüstebach test-site before (2013) and after the deforestation measure (2016). The dashed yellow lines indicate the border of the test-site. *Data source: The State of North Rhine-Westfalia* (`www.geoportal.nrw`; last accessed in October 2018)

During the clearcut, most trees were felled in the wettest part of the test-site, where Gleysols, and Histosols (half-bogs) have developed under the influence of groundwater in the riparian zone of the Wüstebach stream. On the drier hillslopes shallow Cambisols and Planosols prevail (Figure 1.9b) (Bogena et al., 2018). The soil texture on site is mainly clay loam with a medium to high coarse material fraction (Gottselig et al., 2017). Bulk densities are slightly higher, while skeleton contents and (macro-) porosities are lower in the valley bottom than on the slopes (Gottselig et al., 2017; Rosenbaum et al., 2012; Wiekenkamp et al., 2016).

---

[2]`teodoor.icg.kfa-juelich.de`; last accessed in October 2018

The weather in the Eifel region is influenced by relatively moist and temperate air originating from the North Atlantic (Simmer et al., 2015). The climate can thus be classified as a temperate oceanic (*Cfb* climate according to the Köppen-Geiger classification (Kottek et al., 2006)). Over the last decades, mean annual precipitation in the Wüstebach area slightly increased from 1234 mm in the period 1955-1985 to 1287 mm in the period 1985-2015 (DWD weather station Kalterherberg, cf. Figure 1.9a), while annually mean temperatures increased from 7.4 °C to 8.4 °C (DWD weather station Kall-Sistig, cf. Figure 1.9a). The shift in mean annual precipitation is mainly due to increasing monthly precipitation sums in spring (March) and fall (September and October), whereas the shift in the mean annual temperature is caused by increasing mean monthly temperatures in all months except from September (Figure 1.11).
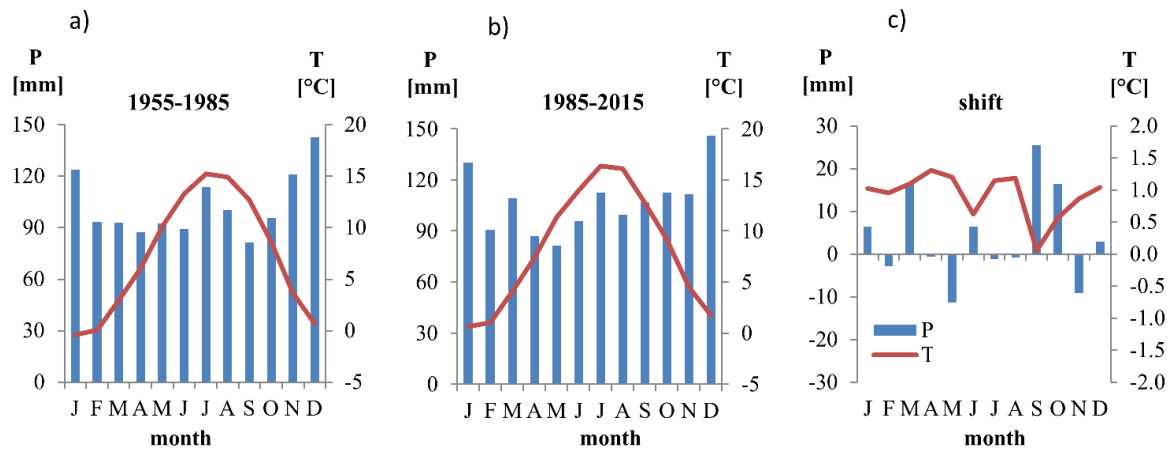
Figure 1.11: Mean monthly temperatures (T) and precipitation sums (P) for the periods 1955-1985 (a) and 1985-2015 (b), and shift in mean monthly values between these periods (c) according to the data recorded by the DWD weather stations Kall-Sistig (temperature) and Kalterherberg (precipitation).

Hence, the region is highly susceptible to climate change (Simmer et al., 2015), which makes it an ideal setting to investigate forest development under climate change and to study the limits of tree eco-hydrological functioning and growth.

To investigate short-term eco-hydrological processes on the tree level, three so-called dendro-hydro-climate stations (DHC-stations) were installed in the Wüstebach catchment. Two of them operated between 2009 and 2011 and were located on sites of contrasting soil moisture regimes ("wet" in the riparian zone and "dry" on the eastern slope of the Wüstebach stream), while the third DHC-station next to the eddy covariance tower (cf. Figure 1.9b) was installed in 2012 and is still operating. At each DHC-station 3 to 4 trees were equipped with dendrometers and sap flow sensors. Furthermore, temperature and relative humidity were monitored in 2 m above soil surface and thus below the forest canopy (Figure 1.12).

To investigate the long-term climate-growth relationships across the Wüstebach test-site, a tree ring sampling campaign was conducted in 2016. An overview of the test-site and instrumentation and sampling locations referred to in this dissertation is given in Figure 1.9b.

Figure 1.12: Experimental design of a DHC-station: (1) Granier-type sap flow sensors and point dendrometers; (2) Measurements of temperature and relative humidity; (3) Eddy-covariance system belonging to the TERENO project.

1.5 Research questions and overview of manuscripts

The aims of this study are to improve the uncertainty assessment for sap flow measurements in trees and to investigate the species specific stress response of Norway spruce to climate forcings and soil water supply. In this context, three individual manuscripts have been prepared and published in international peer-reviewed journals, namely *Sensors*, *Water*, and *Dendrochronologia*.

The **first manuscript** (chapter 2; Rabbel et al. (2016)) adresses the need for a reliable quantification of tree water use. As described in chapter 1.3.3, the estimation of absolute tree water use from Granier-based sap flow measurements comprises many uncertainties. While uncertainties related to the scaling of the point measurement to the tree have been adressed in many studies and are usually assessed by considering radial and circumferencial sap flow density profiles (e.g., Fiora and Cescatti (2006); Nadezhdina et al. (2002); Čermák et al. (2004)), little attention has been paid to the uncertainty in sap flow estimates, which is related to the parametrization of the empirical equation (Granier formula) that transfers the raw temperature signal to sap flow density. In chapter 2, different parameterization approaches are compared to quantify the effects of the data processing procedure on the resulting sap flow densities. The main research questions are: ***How does the parameterization of the Granier formula affect absolute sap flow density estimates on sub-daily, daily and (intra-) seasonal scales and which parameterization approach yields the most reliable results?***

The **second manuscript** (chapter 3; Rabbel et al. (2018a)) adresses the need for a better understanding and quantification of species specific transpiration limitations under considera-

tion of the soil conditions. An alternative water stress factor is derived from the sap flow density series of two DHC-stations with contrasting soil moisture regimes and used to parameterize the Feddes water stress model (Feddes et al., 1978) for Norway spruce. The newly parameterized Feddes function is implemented in site specific water balance simulations raising the question: ***Does the implementation of sap flow data help to improve forest water balance simulations?***

The ***third manuscript*** (chapter 4; Rabbel et al. (2018b)) adresses the need for a better understanding of the role of soil conditions for the climate growth response of trees. The Feddes parameters developed in manuscript 2 are implemented in long-term water balance simulations throughout the Wüstebach test-site. The resulting information on long-term spatiotemporal variations of soil water supply are set into context with tree ring data from 48 microsites (cf. Figure 1.9b). The underlying research question is: ***How important are small-scale heterogeneities in soil water supply for the growth responsiveness of trees?***

An overview of all manuscripts, research questions, and key findings is given in Table 1.1.

Table 1.1: Overview of manuscripts and related research questions.

Chapter	Publication	Research focus	Research questions	Key findings
2	Rabbel, I., Diekkrüger, B., Voigt, H., and Neuwirth, B. (2016): Comparing ΔT_{max} determination approaches for Granier-based sap flow estimations. *Sensors* 16(1): 2042. doi:10.3390/s16122042.	Sap flow data processing	How does the parameterization of the Granier formula effect absolute sap flow density estimates and which approach yields the most reliable results?	• absolute sap flow density estimates strongly vary with the underlying data processing approach • physically-based parameterizations of the Granier formula yields more reliable sap flow density estimates than empirical parameterization approaches
3	Rabbel, I., Bogena, H., Neuwirth, B., and B. Diekkrüger (2018): Using sap flow data to parameterize the Feddes water stress model for Norway spruce. *Water* 10(3): 279. doi:10.3390/w10030279	Water balance simulations	Does the implementation of sap flow data help to improve forest water balance simulations?	• sap flow data can be used to quantify the water stress response of trees and to determine critical limits of soil water supply • implementing respective information into models can help to improve forest water balance simulations
4	Rabbel, I., Neuwirth, B., Bogena, H., and Diekkrüger, B. (2018). Exploring the growth response of Norway spruce (Picea abies) along a small-scale gradient of soil water supply. *Dendrochronologia* 52: 123-130. doi:10.1016/j.dendro.2018.10.007	Climate-growth response	How important are small-scale heterogeneities in soil water supply for the growth responsiveness of trees?	• soil water supply and site characteristics, which modify the water availability for trees, dominate the growth responsiveness of forest microsites • small-scale information on soil water supply and site characteristics improve the interpretability of tree ring data and help to improve our understanding of species-specific growth limitations

2 Comparing $\triangle$T$_{\mathbf{max}}$ determination approaches for Granier-based sap flow estimations

Abbreviations of the original article have been adapted according to the standardized format of this dissertation.

Abstract: Granier-type thermal dissipation probes are common instruments for quantifying tree water use in forest hydrological studies. Estimating sap flow using Granier-type sap flow sensors requires determining the maximum temperature gradient (ΔT$_{\max}$) between the heated probe and the reference probe below. ΔT$_{\max}$ represents a state of zero sap flux, which was originally assumed to occur each night leading to a ΔT$_{\max}$ determination on a daily basis. However, researchers have proven that, under certain conditions, sap flow may continue throughout the night. Therefore alternative approaches to determining ΔT$_{\max}$ have been developed. Multiple ΔT$_{\max}$ approaches are now in use; however, sap flow estimates remain imprecise because the empirical equation that transfers the raw temperature signal (ΔT) to sap flux density (F$_{d}$) is strongly sensitive to ΔT$_{\max}$. In this study, we analyze the effects of different ΔT$_{\max}$ determination approaches on sub-daily, daily and (intra-)seasonal F$_{d}$ estimations. On this basis, we quantify the uncertainty of sap flow calculations, which is related to the raw signal processing. We show that the ΔT$_{\max}$ determination procedure has a major influence on absolute ΔT$_{\max}$ values and the respective sap flux density computations. Consequently, the choice of the ΔT$_{\max}$ determination approach may be a significant source of uncertainty in sap flow estimations.

Keywords: heat dissipation; thermal dissipation; maximum temperature gradient; data processing; transpiration; Norway spruce; *Picea abies*

2.1 Introduction

Granier-type thermal dissipation probes are common instruments for quantifying tree water use in forest hydrological studies (Verstraeten et al., 2008; Davis et al., 2012; Lu et al., 2004; Wullschleger et al., 1998; Köstner et al., 1996). Upscaled to a ground area basis, tree water use is particularly valuable in accounting for actual tree transpiration when partitioning forest evapotranspiration (Kool et al., 2014; Ringgaard et al., 2012; Wilson et al., 2001). The Granier

system consists of two sensor probes inserted radially into the sapwood, one above the other. The upper probe is equipped with a heating element and a thermocouple, thus recording the heat dissipation due to sap flow. The lower probe measures the ambient reference temperature of the wood (Granier et al., 1996). Sap flux density derived from the temperature gradient between the two probes using the empirical equation (Granier, 1985, 1987):

$$F_{\mathrm{d}} = 119 * \left(\frac{\Delta T_{\max} - \Delta T}{\Delta T} \right)^{1.231} \tag{2.1}$$

where F_{d} is the sap flux density ($\mathrm{g \cdot m^{-2} \cdot s^{-1}}$), ΔT is the actual temperature gradient between the two probes and $\Delta T_{\max}$ the maximum temperature gradient measured between the probes in a given time period.

Granier's formula is strongly sensitive to the parameter $\Delta T_{\max}$, which represents a state of zero sap flow ($F_{\mathrm{d}} = 0$). Such zero flow conditions were originally assumed to occur every night (Granier, 1985, 1987). This assumption led to a $\Delta T_{\max}$ determination on a daily basis (D). However, there is increased evidence that, under certain conditions, sap flow continues throughout the night (Zeppel et al., 2013; Phillips et al., 2010; Daley and Phillips, 2006). To improve nocturnal sap flow detection, researchers pay much attention to determining the zero flow conditions and respective $\Delta T_{\max}$ values. Consequently, alternative approaches to determining $\Delta T_{\max}$ have been developed, all based on the assumption that zero flow is related to erratically occurring ambient conditions.

There are two main approaches to including this assumption into sap flow calculations: (1) presuming the recurrence of zero flow within a given time period, during which $\Delta T_{\max}$ is determined (empirical approaches) or (2) defining $\Delta T_{\max}$ when accompanying environmental measures suggest that presumed zero flow conditions have been met (physically based approaches). Most commonly used are the empirical moving window approaches (MW), where $\Delta T_{\max}$ is determined within dynamic time windows of different widths. Within these time windows, zero flux is assumed to occur only once. While Lu et al. (2004) proposed estimating $\Delta T_{\max}$ over periods of 7–10 days, in practice researchers applied moving windows of 3 days (Ringgaard et al., 2012), 4- to 5-days (Reyes-García et al., 2012), 7 days (Moore et al., 2008; Moore and Owens, 2011), 10 days (Köstner and Clausnitzer, 2011; Schwärzel et al., 2009; Oliveras and Llorens, 2001) or even 14-day MWs (Ford et al., 2007) for $\Delta T_{\max}$ determination. The subjectivity of selecting the MW width has already been identified as a drawback of this approach (Regalado and Ritter, 2007). The advantage of MW approaches is that they are easy to implement and, due to their dynamic character, capable of compensating drifts in the data.

Another empirical procedure to overcome both the drift phenomena and the problem of nocturnal flow detection is performing a linear regression (LR) of $\Delta T_{\max}$ values that have first been determined by a 10-day moving window (Lu et al., 2004; Granier, 1987). This approach has been refined by (1) eliminating the data points that were below the values estimated by the linear regression and (2) performing a second linear regression through the remaining data points. This modified regression procedure is known as double regression (DR) (Lu et al., 2004).

However, DR has found limited use because its accuracy has not yet been validated (Regalado and Ritter, 2007).

By considering actual environmental conditions as zero flow criteria, Oishi et al. (2008, 2016) defined a baseline upon ΔT_{max} values that were observed on days with particularly low vapor pressure deficit (VPD). Phillips et al. (2010) also set their baseline on nights when VPD fell to zero for several hours. Regalado and Ritter (2007) dynamically computed ΔT_{max} depending mainly on potential evapotranspiration, while Ward et al. (2008) calculated their baseline from the relation between nocturnal sap flow estimates derived from the daily ΔT_{max} approach and nocturnal stomatal conductance that was simulated from data of whole-tree chamber experiments.

However, although various determination procedures are in use, little attention has been paid to assessing uncertainties related to the application of such alternative ΔT_{max} approaches. This study therefore aims to compare existing ΔT_{max} approaches and quantify their effects on sap flux density $(g \cdot m^{-2} \cdot s^{-1})$ estimations for mature Norway spruce trees in the Eifel National Park (Schleiden, Germany). Besides the described empirical ΔT_{max} approaches, we test the method of Oishi et al. (2008, 2016) as a representative for VPD-based ΔT_{max} approaches and the ΔT_{max} simulation method of Regalado and Ritter (2007). For lack of whole tree chambers, the approach of Ward et al. (2008) is not considered in this study. The outcome is analyzed on the sub-daily, daily and (intra-)seasonal scales.

Considering that the analyzed ΔT_{max} approaches have been designed to capture nocturnal sap flow where existing and that we only analyze days with unlikely nocturnal flow, the hypothesis is that all ΔT_{max} approaches yield the same sap flux density estimations as D. Deviations from D thus represent the uncertainty of sap flow computations, which is related to the ΔT_{max} determination approach.

2.2 Materials and methods

2.2.1 Study site

The study site (50°30' N, 06°19' E) is located in the 38 ha Wüstebach catchment (western Germany) where altitudes range from 595 m a.s.l. to 628 m a.s.l. (Bogena et al., 2014). Hillslopes are dominated by shallow Cambisols and Planosols while Gleysols and Histosols have developed in the groundwater-influenced riparian zone along the Wüstebach stream. The soils mainly show a silty clay loam texture with a medium to high coarse material fraction.

The climate is characterized by an annually mean temperature of 7 °C, a mean annual precipitation of 1100 to 1200 mm (Sciuto and Diekkrüger, 2010) and an average potential evapotranspiration of 630 mm (Graf et al., 2014). The precipitation is more or less evenly distributed over the seasons with a slight peak in fall (∼500 mm in contrast to ∼300 mm during the other seasons). Thus, even in summer, periods of high transpirative power alternate with rainy days and respective low transpiration and sap flow activity. With 320 trees ha^{-1}, the Wüstebach catchment is densely forested by Norway spruce (*Picea abies*). The trees were planted in 1949 (Etmann, 2009) and have now reached a canopy height of ∼25 m (Graf et al., 2014).

2.2.2 Sample trees

The three sample trees are located at 50°30'18" N/6°19'52" E, 620 m a.s.l. at an ESE facing slope with a gradient of 8°. Mean diameter at breast height (DBH) is 54.8 cm, mean projected crown area (CA) amounts to 54.8 m2 and mean sapwood depth (SWD) is 5.7 cm, which was determined by drillhole analyses (Table 2.1). To ensure that our investigations are not overlaid by effects related to the individual phenological development of the trees, we used the overlap of the trees' main growing periods as study period. The main growing period is defined as the time interval during which 5%–90% of the seasonal growth is reached (Jackson, 1952) and could thus be determined on the basis of dendrometer data (cf. 2.2.4). The study period started on 25 May and ended on 14 August 2012.

Table 2.1: Attributes of sample trees (DBH: diameter at breast height, SWD: sapwood depth, CA: projected crown area).

Tree	DBH (cm)	SWD (cm)	CA (cm^2)	Main growing period	
				Start	**End**
1	58.4	6.1	52.3	6 May	25 August
2	54.3	5.7	50.1	24 May	25 August
3	51.7	5.4	61.9	15 May	14 August
Means	54.8	5.7	54.8	25 May	14 August

2.2.3 Sap flow measurements and calculation

The improved Granier-type sap flow sensors that we used in our study (type SF-L 20/33, Ecomatik, Dachau, Germany) include an extra pair of thermocouples that are placed horizontally to the upper heated probe to account for natural innerwood temperature variations. For installation scheme and technical details of the sensors, see Figure 2.1. The mean of the inner-wood temperature variations recorded by the additional SF-L reference probes are subtracted from the values recorded by the classic Granier system before applying the Granier formula. This pre-processing of the Granier sensor signal slightly affects absolute sap flow estimates. In this study, accounting for inner-wood temperature variations reduced mean seasonal sap flow by 3.1%. The sap flow sensors were installed in the outermost 3.3 cm of the sapwood on the north side of the sample trees at ∼1.5 m above ground. We insulated our probes with reflective polystyrene and plastic boxes. Measured temperature gradients were recorded at a datalogger (type CR1000, Campbell Scientific Ltd., Logan, UT, USA) in 30-min intervals. Sap flux density (F_d) was estimated in line with Granier (1985; 1987).

Besides the classic Granier approach (Granier, 1985, 1987), we applied moving window approaches of different width (3, 5, 7 and 9 days), and the linear and double regression approaches (Lu et al., 2004). Furthermore, we tested the application of one single ΔT_{max} (absolute maximum) and the physically-based methods of Oishi et al. (2008, 2016) and Regalado and Ritter (2007).
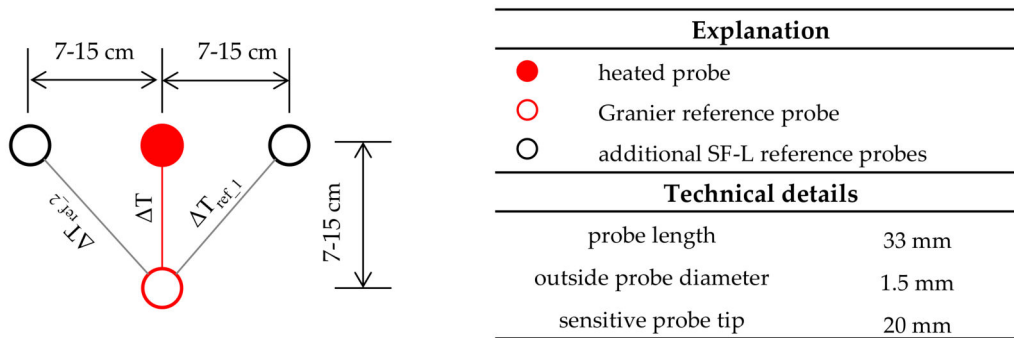
Figure 2.1: Installation scheme and technical details of the used Ecomatik sap flow sensors, type SF-L 20/33, according to (Ecomatik, 2000). The original ΔT between the heated probe and the Granier reference probe is corrected by substraction of the inner-wood temperature variations (ΔT_{ref_1}, ΔT_{ref_2}) recorded by the additional SF-L reference probes.

For the Oishi method, we applied the software baseliner 4.beta (Oishi et al., 2016) which identifies ΔT_{max} when the following conditions are met: (1) nighttime; (2) stable ΔT; and (3) low VPD. We determined nighttime based on global radiation and set the radiation threshold for nighttime definition $5.0 \text{ W} \cdot \text{m}^{-2}$. This value corresponds to the nighttime definition of Daley and Phillips (2006) that we also used for data selection (see below). Stable ΔT was identified when the coefficient of variation for a two-hour period was <0.01. Low VPD conditions were identified when mean VPD was less than 0.05 kPa for a two-hour period.

For the Regalado and Ritter approach, we applied the software FITDTMAX (available online: `https://aritter.webs.ull.es/software_FITDTMAX.html`) using the default transformed potential evapotranspiration (ETp*) limit of 0.1. Since our data had a temporal resolution of 30 min instead of the 15 min resolution used by Regalado and Ritter (2007), we raised the proportionality tolerance from the default value of 0.05 to 0.1. To ensure the reliability of the modelled ΔT_{max} values and respective sap flux density estimates, we excluded days from our investigations where the coefficients of determination between the selected transformed potential evapotranspiration and ΔT were below 0.75 (for more details on the modeling procedure, see Regalado and Ritter (2007)).

To assess the impacts of the study period length and the position of the study period within the main growing period on ΔT_{max}, we divided our study period into the following sub-periods: (1) 25 May to 22 June; (2) 23 June to 19 July; and (3) 19 July to 14 August. All ΔT_{max} approaches were applied to both the entire growing period and the sub-periods. Resulting sap flow densities were analyzed on the sub-daily (30 min resolution), daily and (intra-)seasonal scales. Although alternative ΔT_{max} approaches have been designed to capture nocturnal sap flux where existing and not to modify day-time sap flux densities, it is obvious that changes in ΔT_{max} affect both nocturnal and day-time F_d estimates (Oishi et al., 2008). To assess the magnitude of this effect, we separately investigated the effects of alternative ΔT_{max} approaches on nocturnal and day-time F_d estimates, respectively.

An overview of the applied ΔT_{max} approaches and their implementation and abbreviation are given in Table 2.2. All sap flux density estimations were evaluated with regard to (1) the results

Table 2.2: Theory and implementation of the applied ΔT_{max} approaches.

ΔT_{max} approach	ID	ΔT_{max} determination	References	Implementation in this study
Empirical approaches				
Daily maximum	D	Daily maximum	Granier (1985)	Daily ΔT_{max} determination
Moving window	MW	Dynamic determination based on dynamic time windows of 3 (MW3) to 14 days (MW14)	Lu et al. (2004), Ringgaard et al. (2012), Reyes-García et al. (2012), Ford et al. (2007)	Dynamic time windows of 3, 5, 7, 9 days, always starting 1, 2, 3, 4 days before the actual date of study
Linear regression	LR	First calculate local maxima of moving 10 day periods, then calculate new ΔT_{max} by LR of the local maxima and DOY	Lu et al. (2004), Granier (1987)	LR based on local maxima of 9 day period
Double regression	DR	Elimination of local ΔT_{max} below the LR line and new LR based on remaining data points	Lu et al. (2004)	Regression and data point selection based on local maxima of 9 day period
Absolute maximum	AM	Absolute maximum within selected study period		Absolute maximum within selected study period
Physically-based approaches				
Oishi baseliner	OB	Identification of points in time where flow is likely zero, based on ΔT stability and biophysical conditions; baseline is set by interpolation between selected points; measured ΔT values that exceed the interpolation line are integrated into the baseline	Oishi et al. (2008), Oishi et al. (2016)	Model setup for point selection: vapour pressure deficit threshold = 0.05 kPa; global radiation threshold for nighttime definition = 5.0 W $\cdot$ m^{-2}
Simulated ΔT_{max}	RR	Daily simulation of ΔT_{max} based on the relationship between potential evapotranspiration and sap flow readings	Regalado and Ritter (2007)	Model setup: transformed potential evapotranspiration limit (ETp*) for nighttime definition = 0.1; proportionality tolerance = 0.1; exclusion of days with coefficients of determination between selected ETp* and sap flow readings < 0.75

obtained by the original daily ΔT_{max} approach (D); (2) their applicability to data series of different length and (3) data plausibility in terms of climate feedback. Test statistics (one-sided Mann-Whitney U-tests) were applied to each data series.

To allow for taking D as the reference approach, days of potentially ongoing nocturnal sap flow were excluded from our investigations. We assumed nocturnal sap flow to potentially occur as a consequence of (1) nocturnal transpiration; (2) nocturnal tree growth or (3) nocturnal restoration of the tree's internal water storage during periods of droughts (Daley and Phillips, 2006; Zeppel et al., 2013).

Periods of ongoing nocturnal transpiration and tree growth were excluded by only using sap flow data from days on which nocturnal potential evapotranspiration fell to zero while at the same time relative stem extension (cf. 2.2.4) was zero or negative. Water limitations did not occur in our study period and could therefore be neglected as a driving factor for nocturnal water movements in the trees. Applying these criteria, from the original study period of 80 days, 76 days (Tree 1), 77 days (Tree 2) and 72 days (Tree 3) of unlikely nocturnal sap flow remained for investigation.

2.2.4 Environmental measurements and classification

Tree growth and diurnal stem extension were observed by point dendrometers (type DR, Ecomatik, Dachau, Germany). The relative stem extension was determined by taking the difference between two consecutive dendrometer measures. To monitor soil water content, we installed two SPADE sensor probes (SPADE, sceme.de GmbH, Horn-Bad Meinberg, Germany) in 5, 20 and 50 cm depths. Soil matric potential was recorded by an equitensiometer (EQ15, Ecomatik, Dachau, Germany) in 20 cm depth. To observe micro-climate on site, we measured air temperature and relative humidity at 2 m above soil surface (HygroClip2, Rotronic, Ettlingen, Germany). All data was recorded in a 30 min resolution (datalogger CR1000, Campbell Scientific).

For above-canopy meteorological investigations, we had access to half-hourly climate data (temperature, global radiation, relative humidity, potential evapotranspiration ET_{pot}) of the TERENO Observation Network (weather station Schöneseiffen, 3.4 km east of the Wüstebach). Daily precipitation data was provided by the German Meteorological Service (DWD), weather station Kalterherberg (9.6 km west of the Wüstebach).

Actual evapotranspiration (ET_{act}) was determined by an on-site eddy-covariance (EC) system installed at a height of about 38 m (Drüe et al., 2012). The tower is located in direct proximity to our sample trees within the Wüstebach catchment. Processed data was available in half-hourly resolution (Graf et al., 2014).

Based on the results of a pilot study in the same catchment, we divided the study period into days of distinct environmental conditions that were found to impact F_d. These were (1) days of low/high global radiation, on which the daily global radiation was 0.5 of the standard deviations below/above the mean daily global radiation between May and September 2012 and (2) wet days, on which daily precipitation was above 5 mm and dry days, which were defined as the second day without precipitation. Days that met these conditions were analyzed separately. Nighttime was defined as the period during which radiation was less than 5.0 W $\cdot$ m^{-2} (Daley and Phillips, 2006).

2.3 Results

2.3.1 Sub-daily scale

Maximum temperature gradients (ΔT_{max}) strongly vary depending on the ΔT_{max} approach (Figure 2.2). For the linear and double regressions, the reference period has a major impact on the resulting ΔT_{max} trend (Figure 2.2b, c). While the Oishi "baseliner" shows similar patterns as D, RR yields ΔT_{max} values that strongly vary about D (Figure 2.2d). All empirical ΔT_{max} approaches yielded higher mean sap flow densities (F_d) than D ($p < 0.01$). F_d generally increased with increasing MW width; based on the test statistics (cf. 2.2.3), MW9 and LR were evaluated as equal ($p > 0.1$). The largest difference in sap flow density was computed between approaches RR $<$ D $<$ MW3 $<$ MW7 $<$ DR $<$ AM (Figure 2.3).

Although the means of the sub-period LR distributions (hereinafter referred to as LR_{sub}) still equaled the respective means of the MW9 distributions, the minority of LR_{sub} distributions were found to equal the respective parts of the LR distributions obtained from the complete study period ΔT_{max} regression. Some LR_{sub} distributions were significantly smaller and some significantly larger than the respective parts of LR. Likewise, we could not identify a distinct relation between DR_{sub} (sub-period DR) and other ΔT_{max} approaches.

Since ΔT and ΔT_{max} were found to develop dynamically over the growing season (Figure 2.4), the static AM approach led to significantly biased sap flow density distributions and was therefore not considered for further analysis.

From the physically-based approaches, both OB and RR yielded lower mean F_d than D ($p < 0.01$) when applied to the complete study period; applied to the sub-periods, the majority of the means of the OB distributions equaled those of the D distributions, while RR still yielded lower sap flow densities than D ($p < 0.05$, two exceptions). Comparing RR with OB, RR yielded either equal or lower mean F_d than OB. All tested ΔT_{max} approaches yielded higher nocturnal sap flow densities after radiation intensive days than after days of below-average radiation ($p < 0.01$).

A comparison of empirical ΔT_{max} approaches and D showed that the averaged absolute daytime sap flux density increase was always higher than the mean F_d increase at nights ($p < 0.01$). For the physically-based approaches, in contrast, the difference to D during days and nights was either equal or higher during the nights than in the daytime (Figure 2.4).

Correlating F_d and climate variables (above-canopy vapor pressure deficit VPD_{air}, below-canopy vapor pressure deficit VPD_{stand}, radiation R; actual evapotranspiration ET_{act}) all ΔT_{max} approaches yielded satisfactory coefficients of determination (R^2 of 0.62 to 0.75).
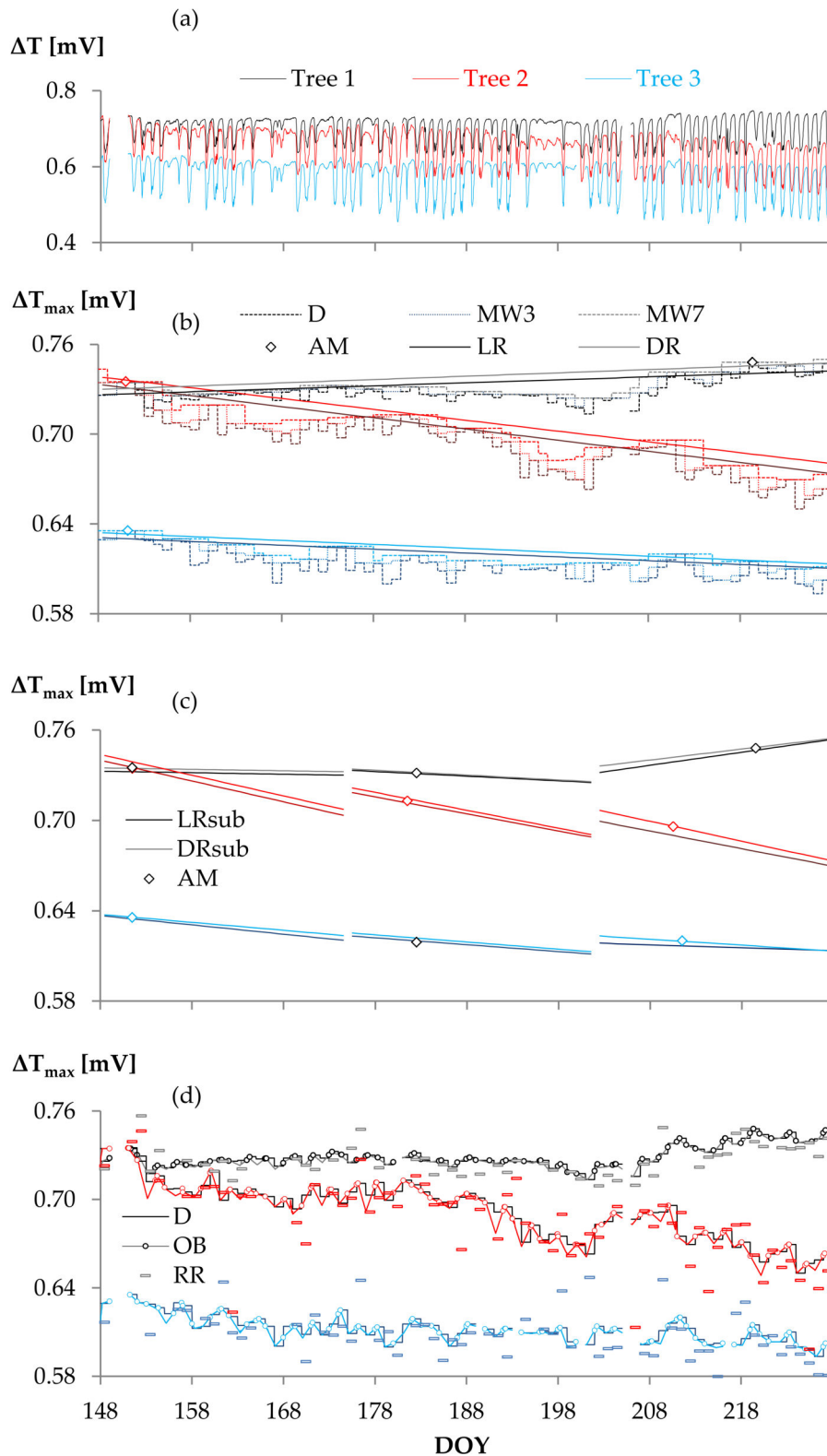
Figure 2.2: ΔT and ΔT_{max} by determination approach and tree: (a) ΔT over growing season; (b) ΔT_{max} by moving window (MW3, MW7) and regression approaches applied to complete study period (LR, DR); (c) ΔT_{max} by regression approaches applied to sub-periods (LR$_{sub}$, DR$_{sub}$); (d) ΔT_{max} by physically-based approaches (OB, RR). Abbreviations of ΔT_{max} approaches according to Table 2.2.
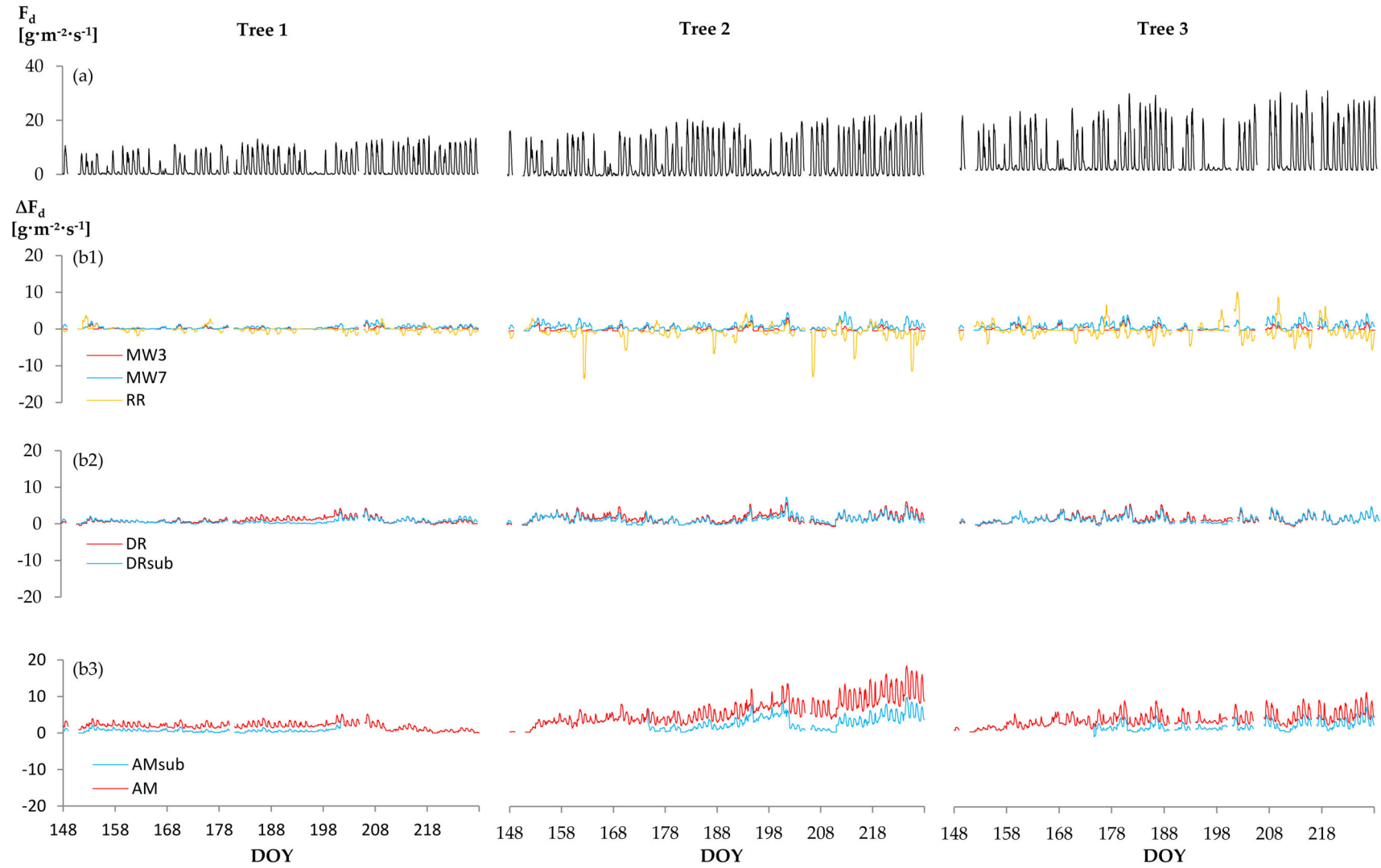
Figure 2.3: (a) Diurnal sap flux density by tree, calculated by the daily ΔT_{max} approach (F_d) and (b) deviations (ΔF_d) from D using those ΔT_{max} approaches that yielded the largest Fd differences among each other (b1): F_d deviations from D by MW3, MW7, RR; (b2): F_d deviations from D by DR applied to complete study period and sub-periods; (b3) F_d deviations from D by AM applied to complete study period and sub-periods). Abbreviations of ΔT_{max} approaches according to Table 2.2.
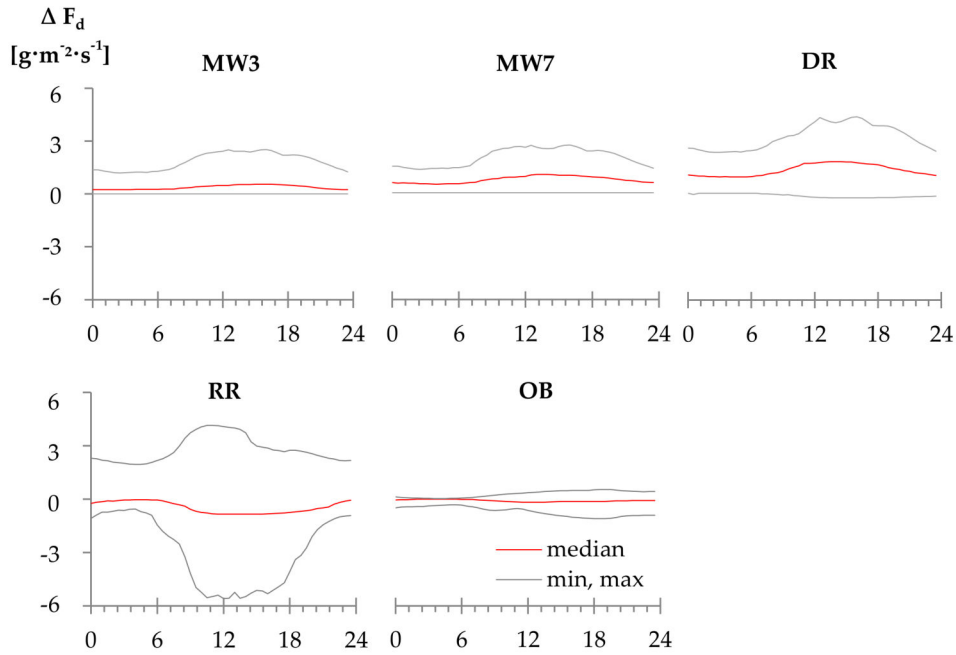
Figure 2.4: Average of the mean, minimum and maximum diurnal sap flux density deviations (ΔF_d) from D using those ΔT_{max} approaches that yielded the largest F_d differences among each other. Abbreviations of ΔT_{max} approaches according to Table 2.2.

2.3.2 Daily scale

Over the entire study period, the physically based approaches and D were evaluated as equal. The empirical ΔT_{max} approaches, in contrast, led to mean daily sap flow densities that significantly differed from those calculated by the D approach ($p = 0.05$, one exception). Among the empirical ΔT_{max} approaches, we found a higher homogeneity on the daily scale than on the sub-daily scale. The most distinct variations were identified between approaches D, MW7, DR and AM. Sap flux density estimates by AM, however, significantly exceeded all alternative F_d estimations ($p = 0.01$) and led to a strongly biased increase of daily sap flow with progressing study period.

Figure 2.5 shows the absolute and relative mean daily F_d and ΔT_{max} increases for different empirical ΔT_{max} approaches. Neglecting the unreliable AM approach, the maximum absolute daily F_d increase was produced by DR, would correspond to a relative F_d increase of 106.0% and was induced by a ΔT_{max} increase of only 0.04 mV (5.52%).

Analyzing the climate response among the ΔT_{max} approaches, we found well-matching relations between daily sap flow estimations, VPD_{air}, VPD_{stand} and radiation (R^2 of 0.51 to 0.84; Figure 2.6). Except for the poor ET_{act} correlations, the D approach showed the strongest climate feedbacks among the tested ΔT_{max} approaches. While the absolute difference of mean daily F_d estimations among the ΔT_{max} approaches was not related to any climate signal, for both MW7 and DR, the mean relative daily sap flux density increase was higher on low radiation days than on days of high radiation ($p = 0.01$).
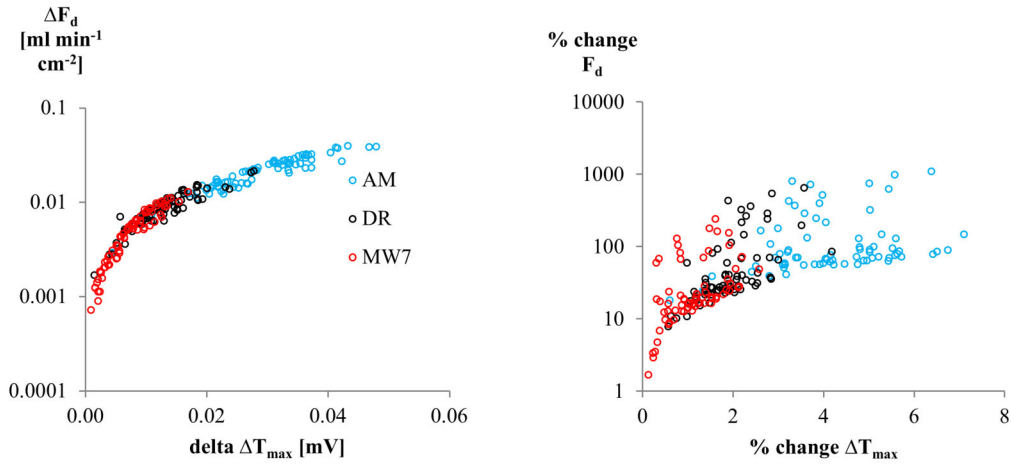
Figure 2.5: Mean (a) absolute variation and (b) percentage change of ΔT_{max} by approach and respective absolute variation and percentage change of mean daily sap flux density estimations. Deviations always with regard to the results obtained using the D approach. Abbreviations of ΔT_{max} approaches according to Table 2.2.
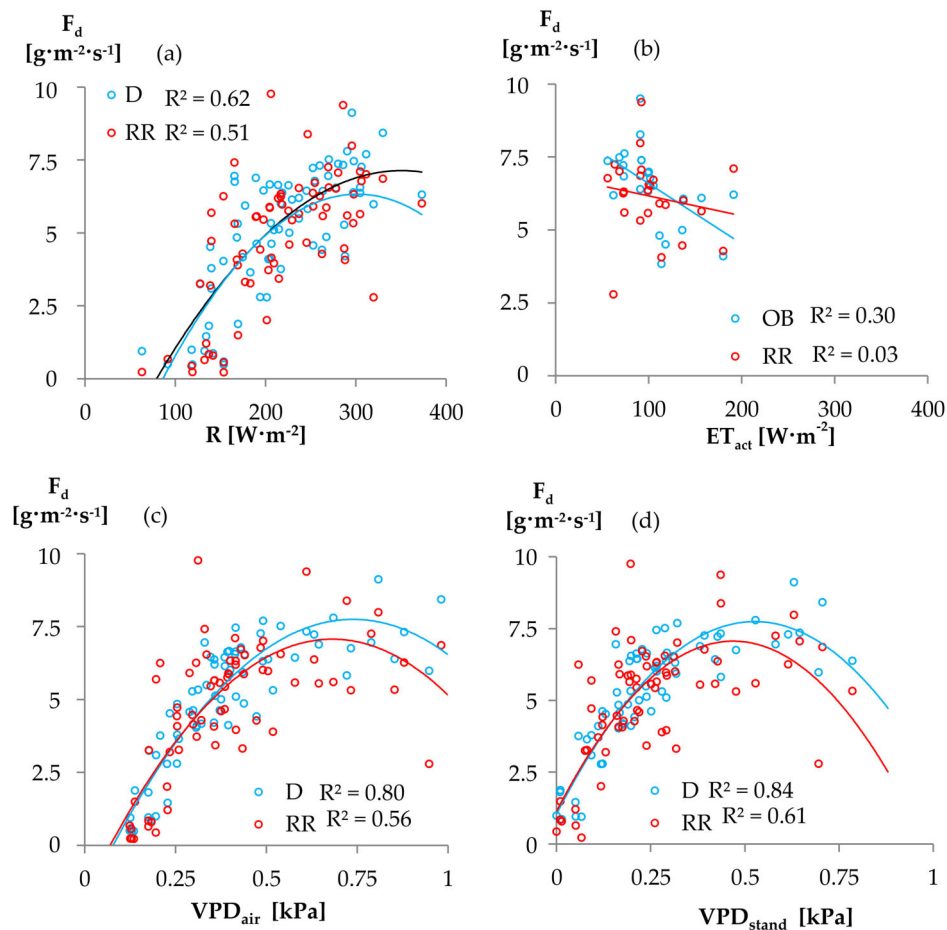
Figure 2.6: Relationship between climate variables and mean daily sap flux density (F_d) for different ΔT_{max} approaches (always best and worse correlation shown). (a) F_d correlation with global radiation R; (b) F_d correlation with actual evapotranspiration ET_{act} (correlation only shown for days of high radiation); (c) F_d correlation with vapor pressure deficit above canopy VPD_{air}; (d) F_d correlation with on site vapor pressure deficit at 2 m above ground VPD_{stand}. Abbreviations of ΔT_{max} approaches according to Table 2.2.

2.3.3 (Intra-)seasonal scale

Dependent on ΔT_{max} approach and data series, mean (intra-)seasonal F_d varied from D by -13.9% (RR) to +137.6% (AM). MW sap flow densities increased with increasing MW width, while F_d response on regression approaches strongly varied by time series and by the reference period they were applied to (Figure 2.7). Mean F_d derived from MW approaches was 12.5% (MW3) to 24.7% (MW9) higher than that derived from D, mean F_d calculated by regression approaches exceeded that of D by 26.0% (LR_{sub}) to 38.5% (DR).
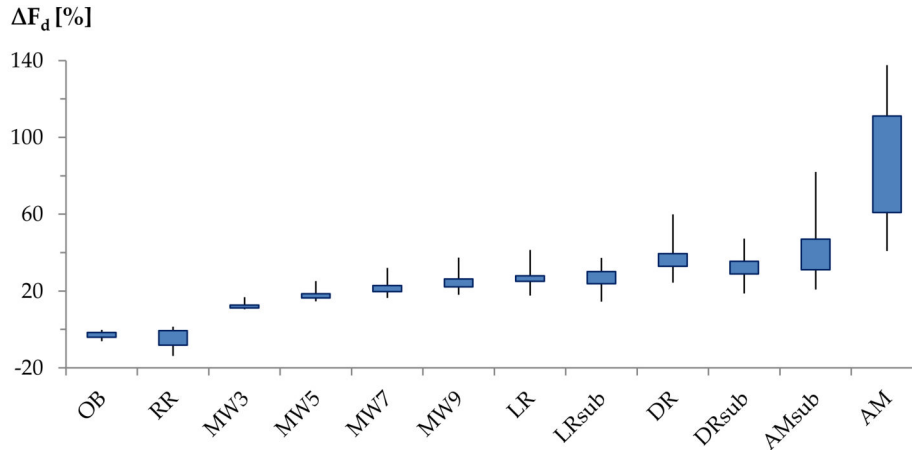
Figure 2.7: Percentage deviation of mean (intra-)seasonal sap flux density estimates using alternative ΔT_{max} approaches from estimates using daily ΔT_{max} (D). Abbreviations of ΔT_{max} approaches according to Table 2.2.

For those approaches that yielded equal results on the daily scale, mean discrepancies between mean (intra-)seasonal F_d did not exceed ±10%. However, discrepancies among the approaches strongly varied by time series, still reaching maximum variations of up to 24%. Except from RR, all alternative ΔT_{max} approaches differed stronger from D on wet days of low radiation than on dry days of high radiation (Table 2.3).

Table 2.3: Percentage deviation of sap flow estimations yielded using alternative ΔT_{max} approaches from estimates using daily ΔT_{max} (D) for different climate conditions. Abbreviations of ΔT_{max} approaches according to Table 2.2.

ΔT_{max} approach	% Deviation from D	
	Dry days, high radiation	Wet days, low radiation
OB	0	6-10
RR	-13	3
MW3	7	25
MW5	12	36
MW7	17	45
MW9	20	53
LR	17	64
DR	24	95
AM	57	202

2.4 Discussion

2.4.1 Sub-daily scale

We observed significant variations between most analyzed ΔT_{max} approaches. Among all ΔT_{max} approaches, the largest difference in sap flux density was computed between RR < D < MW3 < MW7 < DR < AM. Although absolute F_d deviations varied not only by the applied ΔT_{max} approach, but also by tree (Figure 2.3), mean percentage deviations were quite homogenous among the trees (Figure 2.7).

The variations between the MW approaches are particularly critical since MWs of different reference periods are often used in sap flow studies. Considering that we excluded days of likely nocturnal sap flux from our investigations, our results indicate that MW approaches produce a predictable amount of synthetic nighttime flow, and a more than proportional synthetic increase in daytime flux. The same applies for the regression approaches and AM with the limitation, however, that for LR, DR, and AM the outcome is not as predictable as for the MW approaches: As long as the same reference period was being used, we found no difference between sap flow densities calculated by LR and the MW approach LR was based on (MW9). However, LR sap flux density estimates strongly varied with the reference period length and its position within the vegetation period; being based on LR, the same applies for the DR approach. Another drawback of DR is that it does not show a constant relation to other ΔT_{max} approaches.

Not very surprisingly, the most biased sap flow density distributions were produced by AM: ΔT developes dynamically over the growing season and so should ΔT_{max} (Oishi et al., 2008). However, something we can pick from the analysis of AM and other empirical ΔT_{max} approaches is, that the uncertainty of F_d estimates increases with the number of days that lie between the captured ΔT_{max} values. Researchers should be aware of this problem, even when applying physically based ΔT_{max} approaches like OB, because particularly in environments, where zero-flow criteria are not met for a recognizable number of consecutive days, it might become a significant source of uncertainty. One solution to handle this uncertainty could be to define a maximum distance between the captured ΔT_{max} values. To define such a maximum distance, more research would be needed.

In our study, however, the potential problem of non-occurring zero flow criteria for OB sap flow estimations was of minor importance. We only analyzed days of anyway unlikely nocturnal flows and found that, depending on the study period, OB yielded either equal or lower sap flow densities than D. The sometimes slightly lower F_d estimations of OB result from the fact that some of the ΔT values that met the Oishi selection criteria were even lower than the daily maximum ΔT (Figure 2.2 d). Thus, the outcome of OB does not only underline the plausibility of our data exclusion criteria, but also supports our hypothesis that MW and other empirical ΔT_{max} approaches produce kind of artificial day- and nighttime flows.

The finding that RR results in similar F_d estimations as OB indicates that the physically based approaches produce more consistent sap flow estimations than the empirical ΔT_{max} approaches do. Simulating ΔT_{max} from ΔT and micrometeorological variables, the RR approach has the advantage of not being affected by the potential problem of non-occurring zero flow criteria. However, yielding the weakest climate correlations among all tested ΔT_{max} approaches shows

that RR has other drawbacks: The general fit between transformed ET_{pot} (ETp*) and sap flux density has great influence on the number of data points that are selected for ΔT_{max} determination. Thus, on days with differing ETp* and sap flow dynamics, it may happen that ΔT_{max} cannot be calculated due to a lack of fitting data points.

In the study of Regalado and Ritter (2007), this problem seems to having been of minor importance. However, Regalado and Ritter used data with a high temporal resolution of 15 min, so they always found enough data points that met their proportionality criteria. Although we raised the proportionality tolerance to a reasonable level for our 30 min data resolution, we had to exclude several days from our analysis, because the number of selected data points was not sufficient for a solid ΔT_{max} determination. Of course, to some extent, this kind of problem could have been handled by further adapting the proportionality tolerance and also the ETp* limit for night time definition. However, the higher we choose the proportionality tolerance for data selection, the lower turns the coefficient of determination between the selected ETp* and F_d points; and since ΔT_{max} is derived from the correlation between the selected data points, the reliability of the simulated ΔT_{max} values and respective F_d estimations would then decrease as well.

Another drawback of the RR procedure is that the correlation strength between the selected ETp* and F_d values is strongly dependent on actual weather conditions: On wet days with low radiation we yielded mean R^2 between selected ETp* and F_d of 0.72, while on dry days of high radiation mean R^2 was 0.95, which is close to the R^2 values reported by Regalado and Ritter (2007). We therefore conclude that on clear days without precipitation the RR approach may yield reliable ΔT_{max} and respective sap flow estimations, but should be handled with care, when unsteady weather conditions prevail.

Summarizing the above, it seems that for humid conditions without water limitations, D and OB lead to the most reliable sap flux density estimations among the ΔT_{max} approaches. For environments with potentially occurring nocturnal flows, OB might be the better choice, but more research is needed to verify the night-time flow detected by OB against a known standard. One of the main future challenges in this regard is, however, to create such a standard. So far, there is a lack of cost-efficient absolute reference measurements that enable us to detect real night-time flow and calibrate for it.

Lundblad et al. (2001) recalibrated the Granier formula against sap flow measurements of a tissue heat balance system (Cermák et al., 1973). However, the Čermàk system also refers to a reference level of assumed zero flow conditions and is thus not solving the problem of nocturnal flow detection. Other studies use eddy covariance systems as an absolute reference for sap flow as one component of total ecosystem evapotranspiration (Wilson et al., 2001; Ringgaard et al., 2014). However, EC systems have the disadvantage that they only capture total ecosystem fluxes and are known to measure imprecise at nights (Papale et al., 2006). Consequently, it is neither possible to capture single tree transpiration with this method, nor does it make sense to correct nocturnal forest transpiration for EC system measurements.

Ward et al. (2008) conducted whole-tree chamber experiments to detect nocturnal transpiration and calibrate the Granier formula for it. They showed that accounting for real night-time flux is possible and matters. However, chamber experiments are expensive and difficult to im-

plement. Particularly for adult trees and natural forest environments, a convincing solution for nocturnal flow assessment in Granier-type sap flow systems has not yet been found. Consequently, at this state, the most feasible options to deal with the problem of undetected night-time flow are (1) to accept the inability of Granier-type sap flow systems to detect ongoing nocturnal flux as a general constraint of the measuring approach (which holds the risk of underestimating sap flow and absolute sap flow rates matter in forest hydrological research) or (2) to apply physically-based approaches as the Oishi's one including unknown uncertainty caused by the restrictions described above.

2.4.2 Daily scale

Mean daily sap flow densities of the physically based approaches did not significantly differ from those of D. The results of the empirical ΔT_{max} approaches, in contrast, exceeded those of D by 9.8 (MW3) to 31.5% (DR).

This finding is in line with our findings on the sub-daily scale and indicates that the use of empirical ΔT_{max} approaches may become a significant source of uncertainty in daily sap flow estimations. For energy driven environments with unlikely nocturnal sap flow activity, our results suggest the application of D for daily sap flow estimations. D always showed the best correlation with the selected climate parameters, except from ET_{act} which was generally weak (cf. Figure 2.6). However, investigations by Wilson et al. (2001) and Köstner (2001) suggest that better correlations might have been achieved when data for soil evaporation and understory transpiration data had been available and subtracted from ET_{act} measured using an EC tower in advance. While OB yielded results comparable to D and might also be an option for environments with potentially occurring nocturnal flows (cf. 2.4.1), RR should only be applied with care: Although RR yielded absolute mean F_d estimates that did not significantly differ from that of D, it showed the weakest daily climate correlations among all ΔT_{max} approaches (also cf. 2.4.1).

2.4.3 (Intra-)seasonal scale

One important issue of forest hydrological research is the quantification of evapotranspiration and its components. Ringgaard et al. (2012) reviewed that the individually determined evapotranspiration components in forests underestimate EC system measurements by up to 20%. There is broad evidence, that besides scaling issues and miscalculation of other evapotranspiration components, the processing of the raw sap flow signal is one of the main reasons for these discrepancies. However, our results show that the application of alternative ΔT_{max} approaches is not always the appropriate tool to address this problem. Empirical ΔT_{max} determination approaches translate any intermediate ΔT_{max} decrease into nocturnal flow activity, although the seasonal course of ΔT_{max} is also dependent on thermal wood properties and these may vary with tree water status and environmental conditions (Lu et al., 2004; Davis et al., 2012; Tatarinov et al., 2005).

In our study, where conditions of unlikely nocturnal sap flow prevail, this mistranslation of the ΔT_{max} synthetically raised (intra-)seasonal sap flux density estimations of individual trees by between 10.5 (MW3), 57.8 (DR) and 137.6% (AM). In absolute values, (intra-)seasonal sap

flux density estimates of the physically-based approaches were much more consistent and yielded similar results as D. However, applying the RR approach significantly decreased data plausibility on the sub-daily and daily scales. Consequently, OB was the only alternative ΔT_{max} approach that yielded convincing sap flux density estimations and has the potential to detect nocturnal flow, when occurring.

Nevertheless, more research is needed to validate detected night-time flows by absolute reference measurements. For this purpose, applicable measuring techniques are needed, that allow for absolute nocturnal flow detection. Another future challenge will be to deepen the understanding of the natural ΔT_{max} variability and to consider respective findings in the ΔT_{max} determination.

2.5 Conclusions

Based on the analyses of sap flow data of three spruce trees, we showed that the ΔT_{max} determination procedure has a major influence on Granier-based sap flux density estimations. While on days of unlikely nocturnal sap flow, physically-based ΔT_{max} determination approaches yield similar sap flux density estimations as the classic daily ΔT_{max} approach, other, empirical ΔT_{max} approaches produce synthetic flows that (1) significantly raise absolute sap flux density estimations on the sub-daily, daily and (intra-)seasonal scales; (2) affect sub-daily and daily sap flux density dynamics; and (3) reduce data plausibility in terms of climate feedbacks on the daily scale. We therefore conclude that the use of alternative ΔT_{max} approaches may be a significant source of uncertainty in sap flow estimations and complicates the comparability of sap flow studies.

For humid environments with unlikely nocturnal sap flow, our results suggest to apply the original daily ΔT_{max} determination or the physically-based OB approach. RR and other, empirical ΔT_{max} determination approaches were found to yield unsatisfactory results.

To improve Granier-type sap flow estimations, future research should focus more strongly on the development of applicable measuring approaches that allow for absolute nocturnal flow detection and respective recalibration of the Granier formula. Another future research focus should be the deepening of our understanding of the natural ΔT_{max} variability, which is related to wood properties and other eco-physiological parameters. Respective findings should be used to develop new ΔT_{max} approaches that allow for a solid, physically-based ΔT_{max} determination and for reliable absolute sap flux density computations.

3 Using sap flow data to parameterize the Feddes water stress model for Norway spruce

Abbreviations of the original article have been adapted according to the standardized format of this dissertation.

Abstract: Tree water use is a key variable in forest eco-hydrological studies and is often monitored by sap flow measurements. Upscaling these point measurements to the stand or catchment level, however, is still challenging. Due to the spatio-temporal heterogeneity of stand structure and soil water supply, extensive measuring campaigns are needed to determine stand water use from sap flow measurements alone. Therefore, many researchers apply water balance models to estimate stand transpiration. To account for the effects of limited soil water supply on stand transpiration, models commonly refer to plant water stress functions, which have rarely been parameterized for forest trees. The aim of this study was to parameterize the Feddes water stress model for Norway spruce (*Picea abies* [L.] Karst.). After successful calibration and validation of the soil hydrological model HYDRUS-1D, we combined root-zone water potential simulations with a new plant water stress factor derived from sap flow measurements at two plots of contrasting soil moisture regimes. By calibrating HYDRUS-1D against our sap flow data, we determined the critical limits of soil water supply. Drought stress reduced the transpiration activity of mature Norway spruce at root-zone pressure heads < -4100 cm, while aeration stress was not observed. Using the recalibrated Feddes parameters in HYDRUS-1D also improved our water balance simulations. We conclude that the consideration of sap flow information in soil hydrological modeling is a promising way towards more realistic water balance simulations in forest ecosystems.

Keywords: HYDRUS-1D; soil water potential; Norway spruce (*Picea abies*)

3.1 Introduction

Tree water use is a key variable in forest eco-hydrological studies and closely linked to meteorological conditions and soil water availability (Boyer, 1985; Asbjornsen et al., 2011; Blum, 2011; Gartner et al., 2009). To monitor the water use of individual trees, a number of methods are

available (Kool et al., 2014; Wullschleger et al., 1998). Sap flow measurements are most popular, not only because they are cost-efficient and easy to apply. They also yield reasonable information on temporal transpiration patterns and deliver valuable insights into plant-physiological responses to varying hydro-climatic conditions (e.g., soil moisture limitations). Respectively, Steppe et al. (2015) identified sap flow as a "key trait in the understanding of plant hydraulic functioning".

However, to make stem-based sap flow measurements valuable for watershed and land use managers, they need to be scaled to a ground area basis (Asbjornsen et al., 2011). Common scalars in this regard are sapwood area, basal area, diameter or circumference at breast height and leaf area (Asbjornsen et al., 2011; Köstner et al., 1998; Čermák et al., 2004). However, the scaling of sap flow measurements from the tree to the forest stand includes many uncertainties. To begin with, different measuring approaches yield differing estimates of sap flow rates per tree (Čermák et al., 2004; Steppe et al., 2010; Renninger and Schäfer, 2012; Lundblad et al., 2001). This is partly related to uncertainties in signal transformation (Bush et al., 2010; Sun et al., 2012; Rabbel et al., 2016), but also to radial and circumferential variations in sap flow density, which complicates the scaling from the point measurement to water use by tree (Nadezhdina et al., 2002; Ford et al., 2004; Gebauer et al., 2008; Phillips et al., 1996; Fiora and Cescatti, 2006; Čermák et al., 2007). Furthermore, sap flow activity and trans-sectional sapwood distribution vary with tree age, tree dimensions, social position of the tree and also with soil water supply (Gartner et al., 2009; Köstner et al., 2002; Lagergren and Lindroth, 2002; Lundblad and Lindroth, 2002; Střelcová et al., 2013). Thus, extensive measurement campaigns are needed to get a solid estimate of stand water use from sap flow measurements alone.

Alternatively, water balance models can be used to estimate stand transpiration. Such models basically calculate transpiration as a function of atmospheric boundary conditions (potential evapotranspiration), soil water supply and vegetation characteristics from which leaf area index (LAI) and stomatal conductance are the most important (Asbjornsen et al., 2011; Arora, 2002). Under non-limiting conditions, transpiration generally follows the dynamic of atmospheric demand. However, the response of plants to variabilities in soil water supply is highly species-specific. To account for these species-specific feedbacks in the soil-vegetation-atmosphere system, water balance models commonly include plant water stress functions (e.g., van Genuchten (1987) and Feddes et al. (1978)), where critical limits of soil water supply can be adapted according to the vegetation characteristics. For many agricultural crops, such thresholds have already been defined and included into models that help to optimize irrigation scheduling and crop yields (Blum, 2011). However, little is known about the species-specific water-stress-response of forest trees. Since forests play an important role in regional and trans-regional water cycles, there is evidence that an improved knowledge of tree species-specific water stress thresholds would greatly enhance the simulations of water fluxes from the forest stand to the watershed and landscape scale (Asbjornsen et al., 2011; Čermák et al., 2004; Jones, 2007; Verstraeten et al., 2008; Schwärzel et al., 2009).

The aim of this study was: (1) to parameterize the Feddes water stress model for Norway spruce, which is a wide-spread and economically important species in Europe; (2) to investigate if the species-specific calibration of the Feddes parameters can improve water balance simulations

in the soil hydrological model HYDRUS-1D (Šimůnek et al., 2013). In a first step, we used HYDRUS-1D to estimate the root zone water potential for two research plots with contrasting soil water regimes. We derived the Feddes parameters for Norway spruce from correlations of the simulated water potentials and a new sap flow-based plant water stress factor.

3.2 Materials and methods

3.2.1 Study area

The study was conducted in the 27 ha Wüstebach experimental test site (Bogena et al., 2014), which is located in the Rur River catchment close to the German-Belgian border (Figure 3.1). The test site belongs to the TERENO Eifel/Lower Rhine Valley Observatory (Zacharias et al., 2011; Bogena et al., 2016). Altitudes range from 595 m a.s.l. in the north to 628 m a.s.l. in the south. While hillslopes are dominated by shallow Cambisols and Planosols, Gleysols and Histosols have developed in the groundwater-influenced riparian zone along the Wüstebach stream.
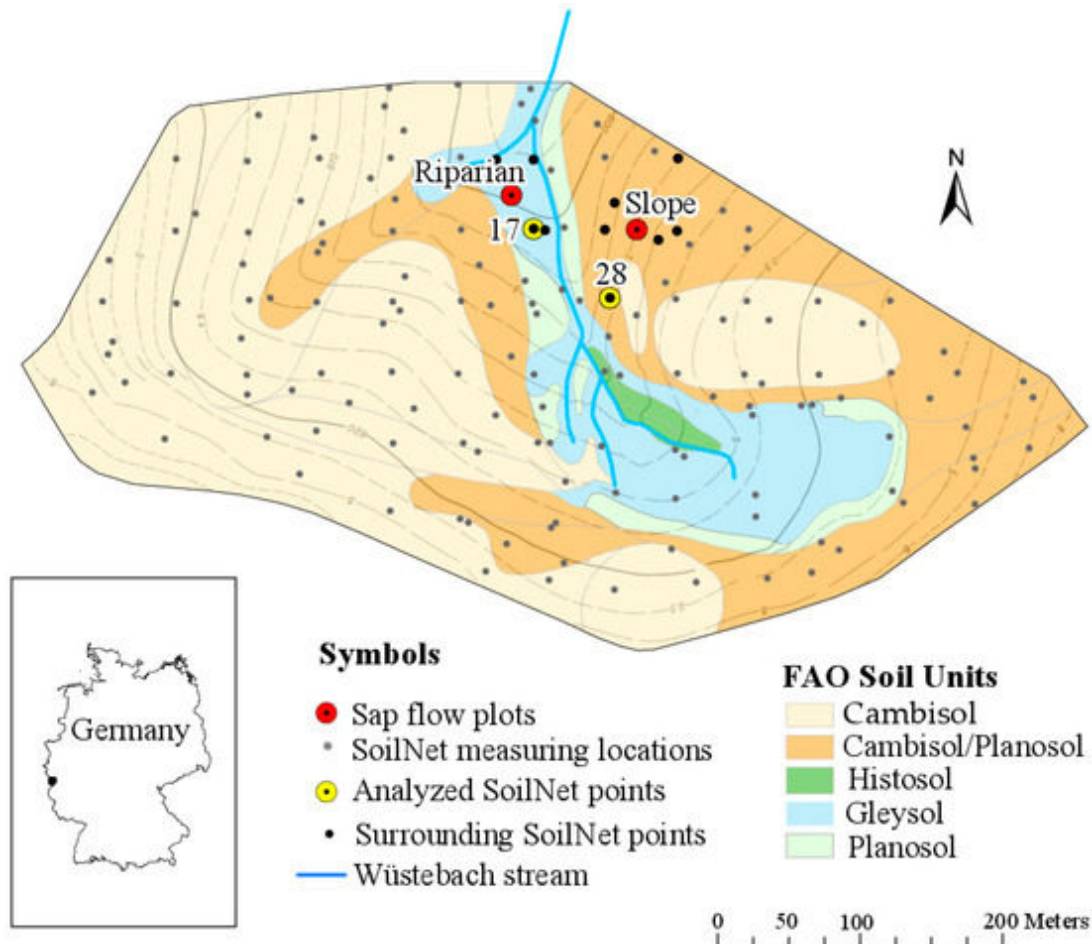
Figure 3.1: Overview of the Wüstebach test site and its location in Germany. The research plots (*Riparian, Slope*) cover differing soil types and topographic situations, which results in contrasting soil moisture regimes (wet and dry). The grey dots indicate the SoilNet sensor network of which two stations have been selected for this study (yellow dots). Black dots show the SoilNet stations we selected to analyze soil moisture variability around the sap flow stations. The difference between the displayed contour lines is 2.5 m.

The soils mainly show a silty clay loam texture with a medium to high coarse material fraction and a litter layer on top (Gottselig et al., 2017). The soils in the valley bottom have slightly higher bulk densities and lower (macro-) porosities and skeleton contents than those on the hillslopes (Gottselig et al., 2017; Rosenbaum et al., 2012; Wiekenkamp et al., 2016).

The climate is characterized by an annual mean temperature of 7 °C (Sciuto and Diekkrüger, 2010) and a mean annual precipitation of 1220 mm (Bogena et al., 2014). The annual potential evapotranspiration of the years 2010–2013 was 630 mm (Graf et al., 2014). The catchment is forested with Norway spruce that were planted in the late 1940s (Etmann, 2009). The trees have now reached a height of about 28 m and the tree density is about 320 trees ha^{-1}.

3.2.2 Data and experimental design

We used sap flow data from two research plots (Figure 3.1) from which one (*Riparian*) is located in the wetter valley bottom (∼600 m a.s.l.), while the other is situated on the drier hillslope (*Slope*, see Figure 3.1) at ∼610 m a.s.l. With a gradient of 2°, the *Riparian* plot is slightly inclined towards N, while the *Slope* plot shows a gradient of 8° in NNW direction. Prevailing soil types are Gleysol (*Riparian*) and Cambisol/Planosol (*Slope*).

At each plot, sap flow of four trees was monitored over 2 years (2009-2010) using improved Granier-type sap flow sensors (SF-L 20/33, Ecomatik, Dachau, Germany). The classic Granier system consists of two sensor probes inserted radially into the sapwood, one above the other. The upper probe is equipped with a heating element and a thermocouple, thus recording the heat dissipation due to sap flow. The lower probe measures the ambient reference temperature of the wood. Our improved sensor version includes another pair of thermocouples that is placed horizontally to the upper heated probe to account for natural inner-wood temperature variations. The mean of the inner-wood temperature variations recorded by these additional reference probes is subtracted from the values recorded by the classic Granier system before applying the Granier formula, where sap flux density is derived from the temperature gradient between the heated and the lower reference probe using the empirical equation (Granier, 1985, 1987):

$$F_{\mathrm{d}} = 119 * \left(\frac{\Delta T_{\max} - \Delta T}{\Delta T} \right)^{1.231} \tag{3.1}$$

in which F_{d} is the sap flux density ($g \cdot m_{-2} \cdot s^{-1}$), ΔT is the actual temperature gradient between the two probes and $\Delta T_{\max}$ the maximum temperature gradient measured between the probes in a given time period. Following Rabbel et al. (2016), who found a daily $\Delta T_{\max}$ determination suitable for the study area, we determined $\Delta T_{\max}$ on the basis of a 24 h moving window (12 h before and 12 h after the actual point of measurement). This dynamic $\Delta T_{\max}$ determination procedure appeared the best opportunity to handle potential drifts in $\Delta T_{\max}$.

The sap flow sensors were installed in the outermost 3.3 cm of the sapwood on the north side of the sample trees at ∼1.5 m above ground. To ensure that the sensor probes were completely surrounded by sapwood (i.e., no heartwood), we determined each tree's sapwood

depth by drill hole analyses before installing the sap flow sensors. We insulated our probes with reflective polystyrene and plastic boxes. The temperature gradients measured and recorded at a datalogger (type CR1000, Campbell Scientific Ltd., Logan, UT, USA) in 30-min time steps. Data gaps were filled using a simple three step procedure: (1) linear regression among all sap flow series within one plot; (2) choice of the data series with the highest coefficient of determination (R^2) with the data series to be gap-filled; (3) interpolation of missing values from the respective regression line. Mean daily sap flow density was calculated from the gap-filled hourly data.

   Soil moisture was monitored by the wireless sensor network SoilNet, which provides catchment-wide information on soil water dynamics in 5, 20 and 50 cm depths at 150 measuring locations (see Figure 3.1). The installed measuring devices are the capacitance soil water content sensors ECH2O EC-5 and ECH2O 5TE (Decagon Devices, Pullman, WA, USA) (Bogena et al., 2010). Sensor calibration was performed according to Rosenbaum et al. (2012). For this study, we used the mean daily soil moisture at 20 and 50 cm depth of two SoilNet stations located close to our sap flow plots (Figure 3.1). Although there are other SoilNet stations closer to the *Slope* plot than the chosen station SN 28, we used this station, because it is located at the same elevation as the sap flow plot. The SoilNet data from 5 cm depth was not considered in this study, because the respective sensors were located in the litter layer and not in the mineral soil we focus on (Figure 3.2).
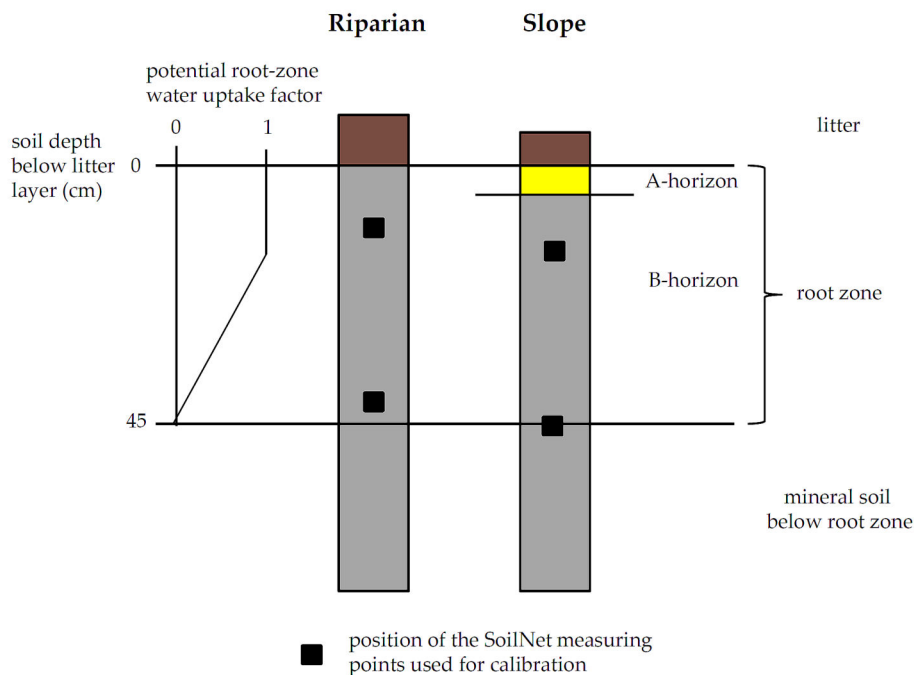
Figure 3.2: Upper part of the soil columns of the research plots as discretized in HYDRUS-1D and position of the SoilNet sensors (black dots) in 20 and 50 cm depth below soil surface. The A horizon at the *Riparian* plot was very thin and therefore neglected in the parameterization.

   Grass reference evapotranspiration ET_0 was calculated using the FAO-Penman-Monteith method (Allen et al., 1998) following Graf et al. (2014), who first calculated hourly ET_0 values and then aggregated these to daily sums. The required input data were obtained from the TERENO weather station Schöneseiffen (3.4 km east of the Wüstebach site). For gap-filling,

linear regression predictors from the same variables of the TERENO station Selhausen (40 km north) were used. To calculate potential evapotranspiration for specific crops (not grass), ET_0 is usually multiplied with the crop coefficient K_c. However, according to Allen et al. (1998) a K_c value of 1 can be used for coniferous forests.

Therefore, we assume ET_0 to represent potential forest transpiration in this study. Daily precipitation was obtained from the Kalterherberg weather station of the German Meteorological Service (DWD), which is located 9.6 km east from of the test site and representative for our study site (Cornelissen et al., 2014). The precipitation data were corrected for systematic measurement errors according to Richter (1995).

The mean leaf area index was determined by averaging respective measurements (SunScan SS1, Delta-T Devices Ltd., Cambridge, UK) at 60 selected SoilNet locations within the Wüstebach site.

3.2.3 Estimating root-zone water potential

The water potential of the root-zone is a measure for the energy needed to extract water from the soil (Jones, 1990). Therefore, we consider the root-zone water potential to be a solid measure to characterize the water availability for plants. However, since water potential is not measured at the SoilNet stations, we used the 1-D Richards equation as implemented in the HYDRUS-1D software (Šimůnek et al., 2013) to inversely determine water potential dynamics from the soil water content (SWC) observations. This is a common approach in soil hydrology, which also allows for the integration of the point scale SWC measurements into vertical soil moisture profiles. In HYDRUS-1D the soil hydraulic properties are parameterized with the Mualem-van Genuchten model (van Genuchten, 1980):

$$\theta(h) = \begin{cases} \theta_r + \dfrac{\theta_s - \theta_r}{[1+|\alpha h|^n]^m} & h < 0 \\\\ \theta_s & h \geq 0 \end{cases} \tag{3.2}$$

$$K(h) = K_s S_e^{0.5} \left[1 - \left(1 - S_e^{0.5/m} \right)^m \right]^2 \tag{3.3}$$

where

$$m = 1 - 1/n \quad n > 1 \tag{3.4}$$

$$S_{\mathrm{e}} = \frac{\theta - \theta_{\mathrm{r}}}{\theta_{\mathrm{s}} - \theta_{\mathrm{r}}} \tag{3.5}$$

where h is the pressure head (cm), θ_{r} is the residual water content ($\mathrm{cm^3\ cm^{-3}}$), θ_{s} the saturated water content ($\mathrm{cm^3\ cm^{-3}}$), α and n are empirical parameters, from which α is related to the air-entry pressure value and n is related to the pore size distribution, m is the retention curve shape parameter, which is dependent on n, K_{s} is the saturated hydraulic conductivity ($\mathrm{cm\ h^{-1}}$), and S_{e} is the relative soil saturation.

Both research plots were modelled separately and in daily time steps. As top boundary conditions, we used the corrected precipitation data and the gap-filled potential evapotranspiration data (see above). The latter was divided into potential evaporation (E_0) and potential transpiration (T_0) on the basis of the leaf area index (LAI) (Allen et al., 1998). In this study, mean LAI on site was 4.8 (with a standard deviation of 0.7) and assumed to be constant in time. Therefore, the differentiation between E_0 and T_0 was of minor importance. However, applying our approach to deciduous trees with seasonal LAI dynamics would require the consideration of the T_0 limitation by LAI. For the hillslope plot (*Slope*) we set the lower boundary condition to free drainage, following Fang et al. (2015), who found this option to provide the best HYDRUS-1D simulation results for the Wüstebach catchment.

To account for the groundwater fluctuations in the riparian zone, the lower boundary condition for the wetter plot (*Riparian*) was set to deep drainage (Leterme et al., 2012). For the deep drainage option, the discharge rate at the bottom of the soil profile is defined as a function of the position of the groundwater table and the empirical parameters A_{qh} and B_{qh} (Hopmans and Stricker, 1989):

$$q(h) = A_{\mathrm{qh}}\ exp(B_{\mathrm{qh}} * |h - GWL_{\mathrm{ref}}|) \tag{3.6}$$

in which q(h) ($\mathrm{cm\ day^{-1}}$) is the discharge rate, h (cm) is the pressure head at the bottom of the soil profile, A_{qh} ($\mathrm{cm\ day^{-1}}$) and B_{qh} ($\mathrm{cm^{-1}}$) are empirical parameters and GWL_{ref} (cm) is the reference groundwater depth. We manually optimized A_{qh} and B_{qh} with regard to the best fit (root-mean-square error) between measured and simulated soil moisture dynamics.

Depending on the local site conditions (Gottselig et al., 2017; Wiekenkamp et al., 2016) we discretized the HYDRUS-1D soil profiles into two *(Riparian)* and three (*Slope*) materials (one/two soil horizons plus an organic litter layer on top; Figure 3.2). The hydraulic properties of the litter layer were parameterized according to Bogena et al. (2013). For the other soil materials, we inversely estimated the Mualem-van-Genuchten parameters from our measured SWC in 20 and 50 cm depth. We therefore used the inverse solution option as implemented in HYDRUS-1D, where the objective function Φ is minimized applying the Levenberg-Marquardt nonlinear least-squares fitting approach (for detailed information on the optimization procedure,

see Šimůnek et al. (2013)). Root water uptake in HYDRUS-1D depends on the root distribution over the soil depth and on soil water availability (Šimůnek et al., 2013). For our Norway spruce plots, we assumed a rooting depth of 45 cm, which is in line with Ammer and Wagner (2005) and Clausnitzer et al. (2011). The root zone was assumed to start below the litter layer, which had a thickness of 6 (*Slope*) and 9 cm (*Riparian*), respectively (Figure 3.2). The root density in spruce forests is typically highest in the upper soil layers (Helmisaari et al., 2007; Puhe, 2003; Schmid, 2002). Therefore, we assumed the potential root water uptake factor to be 1 in the uppermost 15 cm of the mineral soil (one third of the root zone). For the deeper layers, we implemented a linear decrease of the potential root water uptake factor from 1 in 15 cm depth to 0 in 45 cm depth.

To account for reduced water uptake rates in case of water stress (aeration stress and drought stress), we used the Feddes plant water stress function (Feddes et al., 1978) as implemented in HYDRUS-1D. In the Feddes function, a dimensionless water stress factor represents the water stress level of the plant as a function of the root zone water potential (Figure 3.3). This water stress factor corresponds to the ratio of actual (T_{act}) and potential (maximum possible) transpiration (T_0) and thus ranges from 0 (maximum stress/no root water uptake) to 1 (no stress/optimum root water uptake). Optimum root water uptake ($T_0 = T_{act}$) is given between h_2 (field capacity FC) and h_3 (onset of drought stress). The decreasing plant water stress between h_2 and h_1 considers that plants typically experience increasing aeration stress towards saturated conditions; h_4 corresponds to the permanent wilting point (WP), h_1 to the point of maximum aeration stress (anoxic conditions).
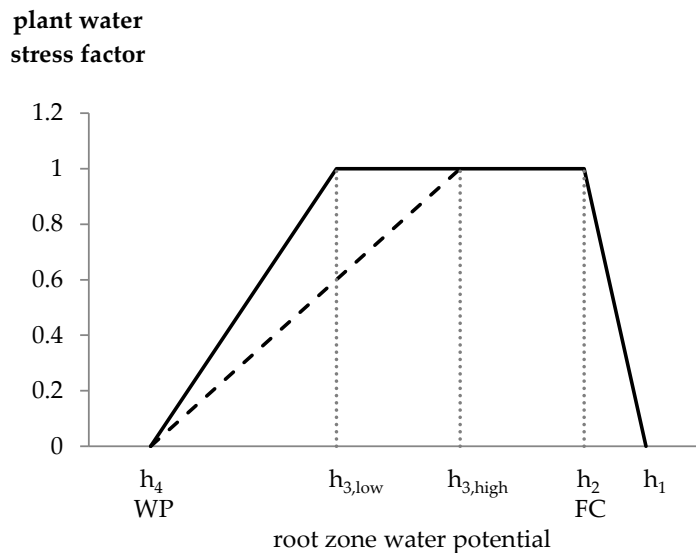
Figure 3.3: Feddes plant water stress function modified after Feddes et al. (1978). Root water uptake commences with the onset of desaturation at h_1 (anoxic moisture conditions), optimum root water uptake is given between h_2 (field capacity, FC) and h_3 (onset of drought stress), where indices high and low refer to the magnitude of potential transpiration rates. From optimum root water uptake towards h_4 (permanent wilting point, WP) the plants experience increasing drought stress.

Presuming that h_3 decreases with decreasing T_0, HYDRUS-1D allows for making h_3 a function of T_0. The range of T_0, within which h_3 becomes a function of T_0 may be defined by the user, but is usually 1-5 mm day^{-1} (default values). The h_3 value for $T_0 < 1$ mm day^{-1} is called $h_{3,low}$,

that for $T_0 > 5$ mm day^{-1} h$_{3,high}$. If T_0 is between 1 and 5 mm day^{-1} and the soil dries out to less than h$_{3,high}$, the critical root-zone water potential, at which potential root water uptake is reduced to the actual root water uptake, is linearly related to T_0 (Šimůnek et al., 2013).

As start values for the model inversion, we used the Feddes parameters (in cm pressure head) as proposed by Vogel et al. (2013) for a 90-years-old spruce site in the Czech Republic, where h$_1$ = h$_2$ = 0 cm, h$_{3,high}$ = -600 cm, h$_{3,low}$ = -1200 cm, and h$_4$ = -15,000 cm. Later, we manually optimized the Feddes parameters on the basis of our sap flow data (see below).

3.2.4 Model validation

We validated our model setup on the basis of the soil moisture measurements in 20 and 50 cm depth using a split-sample approach. To consider the observed drop in soil moisture between the years 2010 and 2011 in the optimization procedure, we chose the years 2009–2011 as the calibration period. For validation, we used another three year period (2012-2014). The goodness-of-fit between observed and simulated data was assessed on the basis of the root mean squared error (RMSE). Our sap flow data was restricted to the years 2009 and 2010 and was therefore not considered for model validation.

3.2.5 Parameterizing the Feddes model using sap flow data

In the classical Feddes approach, plant water stress is derived from the ratio of T_{act} and T_0 (see above). The assumption is that this ratio is mainly dependent on soil water supply. However, Zweifel et al. (2002) showed that Norway spruce reacts to high midday vapor pressure deficits (VPD) by closing stomata. Thus, the trees physiologically reduce their own transpiration activity on many days of the growing season. In order not to mix-up this atmospheric stress reaction with actual soil water stress, we applied a new approach to calculate plant water stress from our sap flow data. This approach was based on the assumption that the micro-climate is identical at both plots; thus, in case of atmospheric stress, all trees (*Riparian* and *Slope* plot) show the same physiological reaction.

For each tree we determined the 6 highest F_d values per day. We averaged these maxima by day and plot and normalized the resulting data series ($F_{d,n,rip}$ for *Riparian* and $F_{d,n,sl}$ for *Slope*).

For the *Riparian* plot, we assumed optimum soil water supply, because due to the constant influence of groundwater the soil at this plot showed relatively high soil water contents throughout the study period and critical levels of soil water supply as reported from other studies (Lagergren and Lindroth, 2002; Lundblad and Lindroth, 2002; Schwärzel et al., 2009; Granier et al., 1999, 2000) were never reached. We calculated a drought stress factor $F_{d,drought}$ (1: optimum water supply; 0: maximum water stress) for the *Slope* plot by dividing $F_{d,n,sl}$ by $F_{d,n,rip}$. To ensure that potential aeration stress at the *Riparian* plot would not affect our drought stress function, we only used data of dry days (3rd day without precipitation). We plotted $F_{d,drought}$ against the simulated *Slope* water potential and analyzed the correlation between $F_{d,drought}$ and root zone h for different levels of soil water shortage. The data which showed the highest significant correlation (R^2 and Student's t-test) between $F_{d,drought}$ and root zone h was used to determine the drought stress trendline. The intersection of this trendline with the x-axis corresponds to

the simulated *Slope* root zone water potential at maximum drought stress ($F_{d,drought} = 0$) and was therefore interpreted as the permanent wilting point h_4.

During model calibration we found that the parameter $h_{3,high}$ was independent from mean daily sap flow dynamics and hence could not be optimized using sap flow measurements. However, it is well-known that at high levels of atmospheric demand, the transpiration rate of spruce forests decreases with increasing vapor pressure deficit (Lagergren and Lindroth, 2002). This was also confirmed by our own sap flow measurements (data not shown). While coupled soil-plant-atmosphere continuum models are able to account for atmospheric stress, this process is not implemented in HYDRUS-1D. Nevertheless, since the Feddes approach is differentiated into $h_{3,high}$ and $h_{3,low}$, atmospheric stress can be considered by adapting the T_0 range at which h_3 is a function of T_0. The study of Zweifel et al. (2002) suggests that spruce trees reduce transpiration when midday vapor pressure deficit exceeds 1250 Pa independent of soil wetness. Accordingly, we analyzed days with maximum VPD of approx. 1250 Pa and found that a T_0 value of 2.7 mm day^{-1} can be used as lower boundary for the h_3-dependent T_0 range. Furthermore, we used T_0 at the day of maximum observed daily F_d (4.8 mm day^{-1}) as the upper boundary for the h_3-dependent T_0 range.

To detect potential aeration stress at the *Riparian* plot, we selected days, for which no drought stress was observed on the *Slope* plot. For these days, $F_{d,n,sl}$ was used as a reference for optimum water supply. We calculated an aeration stress factor $F_{d,aeration}$ (1: optimum water supply; 0: maximum water stress) by dividing $F_{d,n,rip}$ by $F_{d,n,sl}$. To determine the Feddes parameters h_1 and h_2, we plotted $F_{d,aeration}$ against the simulated *Riparian* root-zone water potential and analyzed the observed data trend as described for $F_{d,drought}$.

3.2.6 Relative extractable soil water (REW)

It is well known that absolute soil water contents do not fully reflect the actual soil water status (Jones, 2007; Sadras and Milroy, 1996). Therefore, many researchers refer to the relative extractable soil water (REW) as a measure of soil water status (e.g., Gartner et al. (2009); Lagergren and Lindroth (2002); Sadras and Milroy (1996); Hentschel et al. (2016); Gebauer et al. (2012); Granier et al. (2007)). To compare our Feddes parameters with critical REW values from the literature, we calculated the mean root-zone water contents corresponding to the reported critical REW according to the relations described by Hentschel et al. (2016) and Granier et al. (2007):

$$REW = \frac{\theta - \theta_{WP}}{\theta_{FC} - \theta_{WP}} \tag{3.7}$$

in which θ is the actual water content, θ_{FC} is the water content at field capacity, and θ_{WP} is the water content at permanent wilting point. To be consistent with the literature (Hentschel et al., 2016; Granier et al., 2007), we chose θ at -300 cm pressure head (-0.03 MPa) for θ_{FC} and θ at -16,300 cm pressure head (-1.6 MPa) for θ_{WP}.

3.2.7 Uncertainty assessment

To assess the uncertainty of the simulated root zone water potential related to the assumed rooting depth and the shape of the potential root water uptake function, we performed a sensitivity analysis. First, we ran the model for each plot assuming constant rooting depth (45 cm), but differing root distributions (factor 1 in the uppermost 15/30/45 cm of the mineral soil and linear decrease from 1 to 0 towards the bottom of the root zone). Then, we varied the rooting depth (30/40/50/60 cm) and simulated the respective root zone water potentials assuming a root distribution factor of 1 for the uppermost 15 cm of the mineral soil linearly decreasing from 1 to 0 between 15 cm depth and the final rooting depth.

Test statistics (Mann-Whitney U-test) on the similarity of the simulated root zone water potentials were conducted on the log scale.

To evaluate the small-scale variability of soil water supply around the sap flow stations and to ensure that the selected SoilNet measuring locations are representative for our sap flow plots, we simulated the root zone water potentials of 4 (*Riparian*) and 7 (*Slope*) surrounding SoilNet locations (Figure 3.1). These simulations were again performed on the basis of calibrated and validated Mualem-van Genuchten parameters. From the average root zone water potentials of the surrounding SoilNet locations, we determined the Feddes parameters as described before and compared the results with the water stress thresholds as resulting from the initial research setup.

3.3 Results

3.3.1 Sap flow data

The observed F_d dynamic of both research plots corresponds well to the dynamic of the calculated ET_0 (Figure 3.4). R^2 between mean daily F_d and ET_0 was 0.78 for the *Slope* plot and 0.84 for *Riparian* plot. The differing absolute F_d among trees and plots result from variations in tree diameter and crown size (Table 3.1), which can be explained by small-scale variations in planting density and uneven forest thinning. This becomes particularly apparent for tree 1 of the *Riparian* plot (Figure 3.4b).

At the *Riparian* plot, we observed some data inconsistencies in the winter that were probably caused by frost events and rodent activity. Therefore, the sap flow sensors were checked and readjusted at the beginning of the following vegetation period (May 2010). Since we did not use the noisy data until sensor readjustment, the winter gap at the *Riparian* plot is slightly longer than at the *Slope* plot (Figure 3.4).

a)

b)

c)
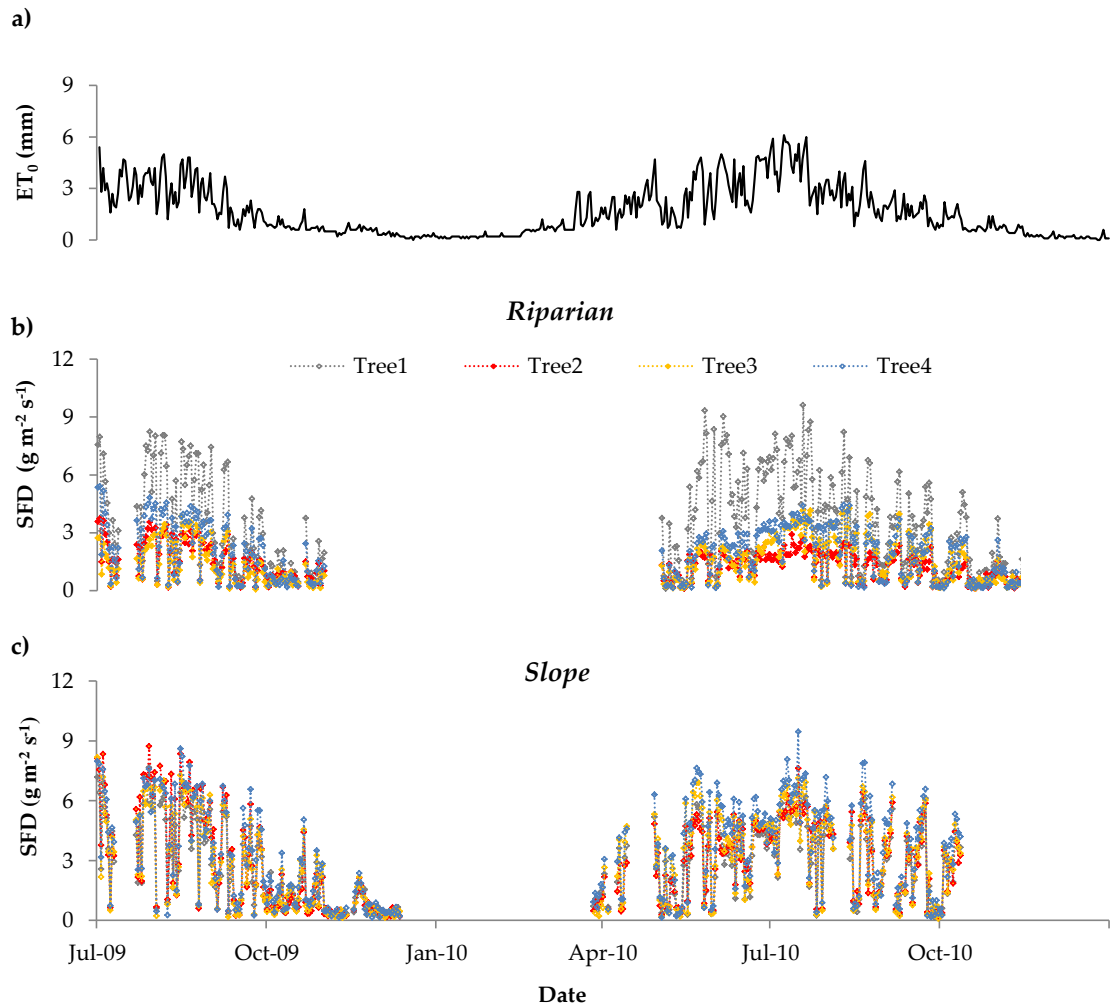
Figure 3.4: Daily potential evapotranspiration (a) and mean daily sap flow density (F_d) by tree and plot ((b) *Riparian*; (c) *Slope*).

Table 3.1: Variation of diameter at breast height (DBH), sapwood depth (SWD), projected crown area (CA) and mean daily sap flow density (F_d) between May and September by plot and sample tree.

Sample tree	*Riparian*				*Slope*			
	DBH	**SWD**	**CA**	**F_d**	**DBH**	**SWD**	**CA**	**F_d**
	cm	**cm**	**m^2**	**g m^{-2} s^{-1}**	**cm**	**cm**	**m^2**	**g m^{-2} s^{-1}**
tree 1	57	6	49.2	4.48	44.7	4.7	56.3	4.52
tree 2	40.3	4.2	23.3	2.25	40.9	4.3	60.4	5.09
tree 3	46.3	4.9	22.2	1.56	44.1	4.6	33.8	4.69
tree 4	40.4	4.2	-*	3.13	48.2	5.1	-*	5.24
mean	46	4.8	31.6	2.9	44.5	4.7	50.2	4.89

*These trees were cut before our survey on CA determination; therefore we estimated CA from the allometric relationships of (Widlowski et al., 2003), where

$$CA = \pi * (0.6122 + 0.0536 * DBH)^2.$$

3.3.2 Simulated soil water dynamics

The Mualem-van Genuchten parameters as resulting from the parameter estimation by HYDRUS-1D show lower residual, but higher saturated water contents for the *Riparian* plot than for the *Slope* plot. At the *Slope* plot, α and K_s decrease with depth (Table 3.2).

Table 3.2: Mualem-van Genuchten parameters as obtained from the HYDRUS-1D inverse modeling procedure by plot and soil layer. θ_r: residual water content, θ_s: saturated water content, α: empirical parameter related to the air-entry pressure value, n: empirical parameter related to the pore size distribution width, K_s saturated hydraulic conductivity (cm day^{-1}).

Soil layer	θ_r	θ_s	α	n	K_s
			Riparian		
B*	0	0.63	0.008	1.58	4
			Slope		
A	0.1	0.52	0.008	1.22	165
B	0.12	0.5	0.001	1.29	78

*The A horizon was very thin and could therefore not be parameterized for this plot.

After inverse modelling, and manual calibration of A_{qh} and B_{qh} for the deep drainage option (-0.85 and -0.012, respectively), the root mean squared errors (RMSE) between observed and simulated data (Figure 3.5) were 3.6 vol % (*Slope*), and 4.6 vol % (*Riparian*). In the validation period, the RMSE of the *Riparian* plot slightly increased (5.3 vol %), while that of the *Slope* remained the same. The manual calibration of the Feddes parameters slightly improved the RMSE at the hillslope plot (3.4 vol % for both calibration and validation period), but had no effect on the RMSE of the *Riparian* plot simulations.

As expected, SWC in the groundwater-influenced plot (*Riparian*) were generally higher than those on the hillslope. The simulated mean annual SWC was 54% for the *Riparian* plot and 36% for the *Slope*). The simulated root zone water potentials (Figure 3.6) highlight the contrasting soil moisture regimes of the two research plots. The mean simulated annual root zone pressure heads were -88 cm (*Riparian*) and -3400 cm (*Slope*). All simulated daily root-zone h values ranged from +27 cm (fully saturated soil column; *Riparian*) to -12,577 cm (very dry conditions near wilting point; *Slope*).
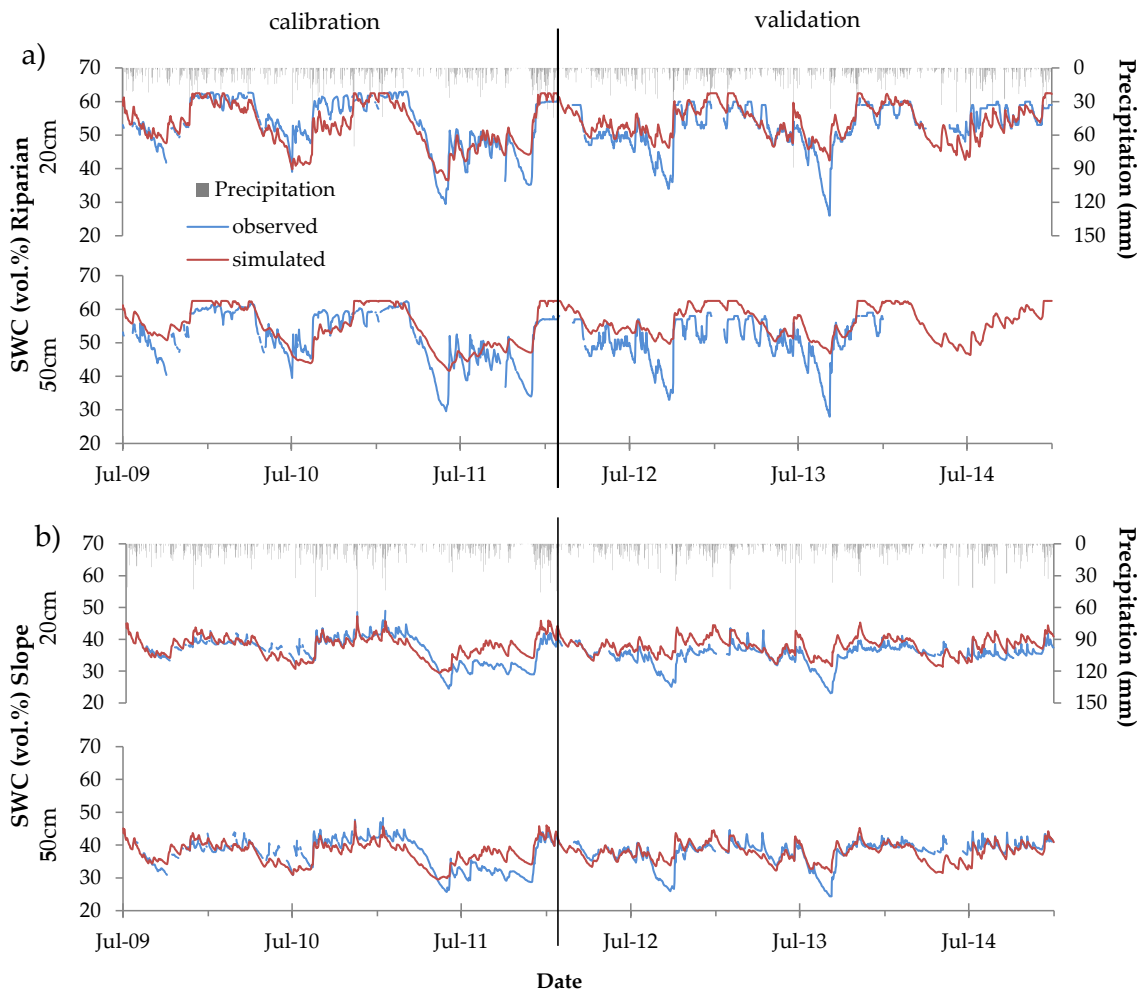
Figure 3.5: Observed (blue) and simulated (red) soil water content (SWC) in 20 and 50 cm depth of the *Riparian* (a) and *Slope* (b) plots. Black vertical lines indicate the border between calibration and validation periods.
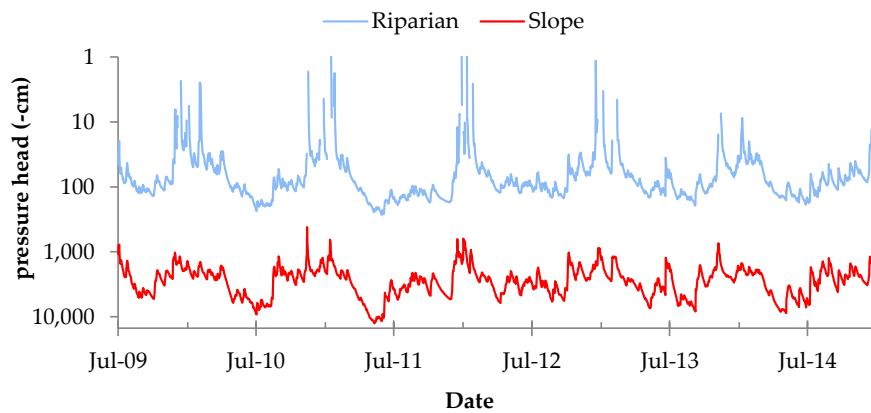
Figure 3.6: Simulated root zone water potential by plot. Note that the pressure head (-cm) is plotted on the log-scale (single positive values cannot be shown).

3.3.3 Feddes parameters for Norway spruce (h_1, h_2, $h_{3,low}$, h_4)

For the *Slope* plot, we found the measured water stress to be dependent on the simulated root-zone water potential (Figure 3.7a). The strongest significant correlation between $F_{d,drought}$ and simulated root-zone h was observed below -4100 cm ($R^2 = 0.77$, $p < 0.001$). Thus, we set $h_{3,low} = $ -4100 cm. Extrapolating the trend-line between $F_{d,drought}$ and simulated root-zone h towards the x-axis, where $F_{d,drought} = 0$ (maximum water stress), resulted in an h_4 value of -15,000 cm which is often used as - a very general - permanent wilting point (Kirkham, 2014). Our data did not indicate the occurrence of aeration stress at our research site (Figure 3.7b). Parameters h_1 and h_2 were therefore set to 0. The Feddes water stress function as resulting from our parameterization shows a higher drought resistance of Norway spruce than previously assumed (Figure 3.7c).
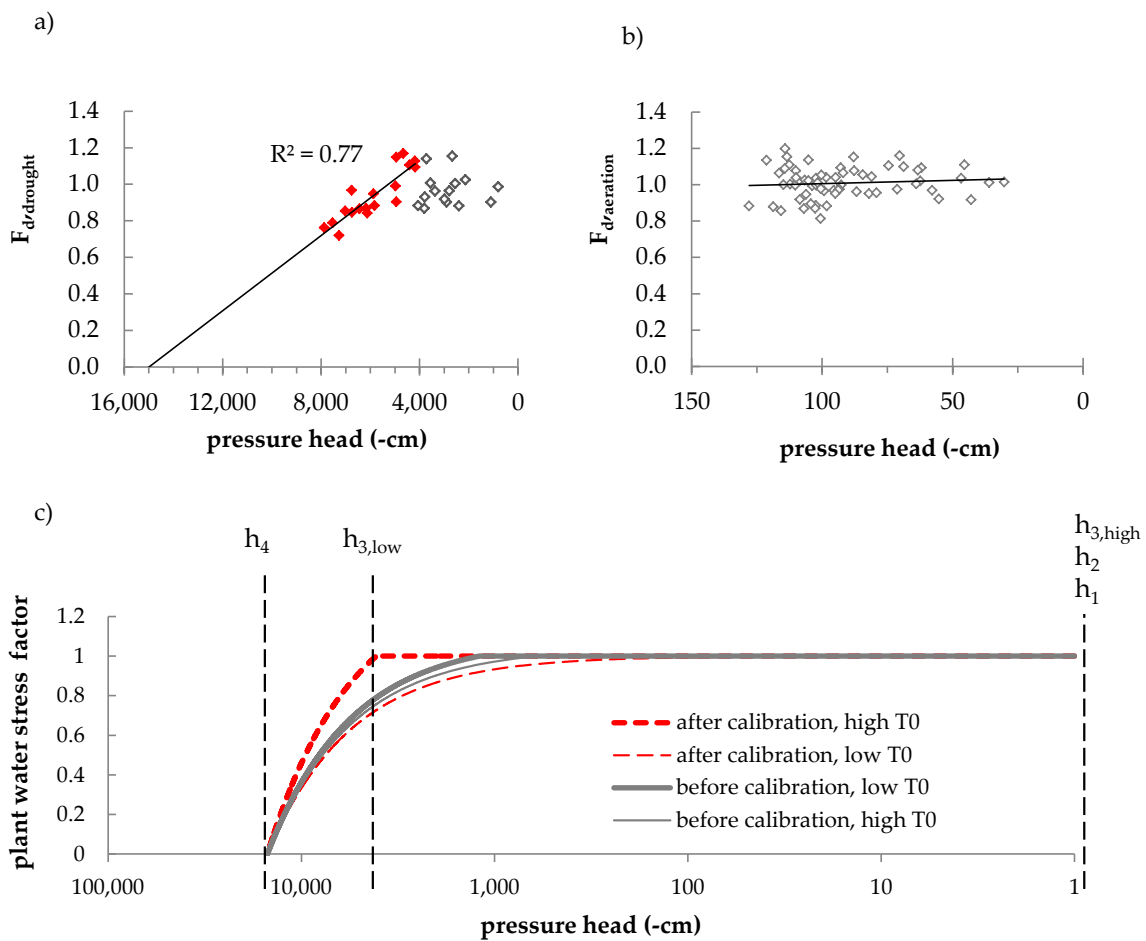
Figure 3.7: (a) Plant water stress as indicated by sap flow data at the *Slope* plot; red dots were used for the extrapolation of the drought stress trend-line (black line); (b) Plant water stress as indicated by sap flow data at the *Riparian* plot (no water stress observed); (c) Calibrated water stress function (red lines) in comparison to the Feddes function used before calibration (grey lines) (cf. Vogel et al. (2013)). Note that the x-axis in figure (c) is displayed on the log-scale.

3.3.4 Simulated water balance before and after calibration

The mean annual simulated water balance of the two research plots indicates generally higher transpiration at the *Riparian* plot compared to the *Slope* plot (Table 3.3). While the water balance of the *Riparian* plot was not affected by the calibration of the Feddes parameters, the calibration raised ET_{act} by 10% for the *Slope* plot. At the same time, drainage decreased by 5%. For all simulation runs, we achieved a very good fit between mean daily sap flow and simulated actual transpiration ($R^2 = 0.82$ at *Slope* and 0.84 at *Riparian* plot). At the *Slope* plot, the correlation between sap flow data and simulated actual transpiration was slightly improved by the calibration of the Feddes parameters ($R^2 = 0.83$). For the *Riparian* plot, R^2 was not affected from the calibration.

Table 3.3: Mean annual simulated water balance (October 2009-September 2014) before and after calibration of the Feddes parameters in HYDRUS-1D. Percentage change of calibrated water balance component in comparison to un-calibrated value is given in brackets. ET_0: potential evapotranspiration, ET_{act}: actual evapotranspiration; all details in mm year^{-1}.

Water Balance Component	*Riparian*		*Slope*	
Precipitation		1321		
ET_0		597		
	un-calibrated	*calibrated*	*un-calibrated*	*calibrated*
ET_{act}	597	597	403	445 (+10%)
Surface runoff	54	54	0	0
Drainage	634	634	841	797 (-5%)

3.3.5 Sensitivity of Feddes parameters to root zone variation and SoilNet measuring location

Variations of the potential root water uptake factor's depth distribution did not lead to significant variations of the simulated root zone h (Mann-Whitney U-test). The same applies for variation of the rooting depths.

The difference between the mean soil water supply of the surrounding SoilNet measuring locations and that of the stations we selected for our study (SN17 and SN28; cf. Figure 3.1) was statistically significant ($p < 0.001$). However, the absolute difference among the simulated SoilNet locations was small and the contrasting soil moisture regimes between the two plots are still clearly visible (Figure 3.8). Respectively, the resulting Feddes parameters were only slightly affected by the selection of the SoilNet measuring location. Parameter $h_{3,low}$ as determined from the mean root zone water potentials of the surrounding SoilNet locations was -3800 cm, which is 300 cm below the $h_{3,low}$ value we determined from SN28. h_4 decreased from -15,000 cm (SN28) to -13,600 cm pressure head (mean of the surrounding SoilNet stations), while h_2 was not affected from the choice of the SoilNet measuring location. This indicates that soil type and elevation were reasonable criteria for the choice of our measuring locations.
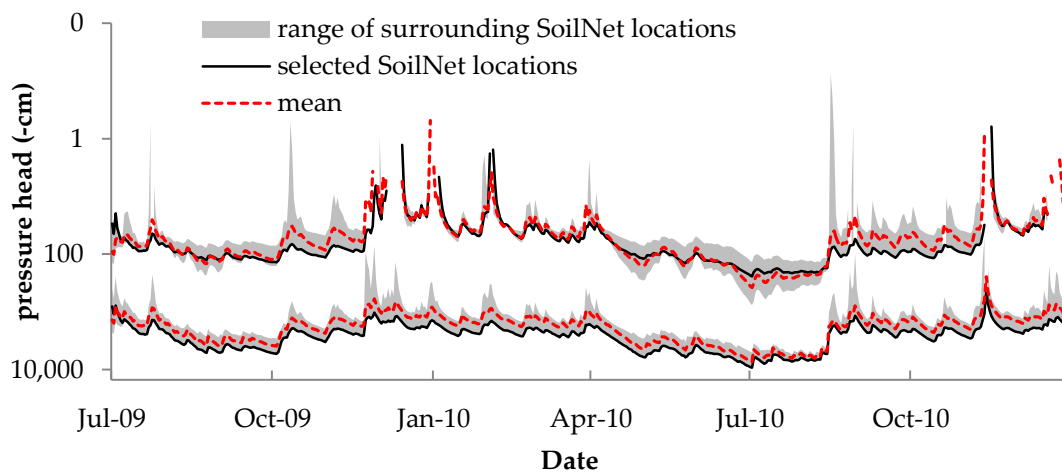
Figure 3.8: Range (grey) and means (red) of simulated root zone water potentials of the SoilNet stations in the surrounding of our sap flow plots (cf. Figure 3.1). Simulated root zone water potentials of SN17 (*Riparian*) and SN28 (*Slope*) are shown in black. Note that the pressure head (-cm) is plotted on the log-scale (single positive values cannot be shown).

3.4 Discussion

3.4.1 Soil moisture simulations

The water balance simulation captured the prevailing soil moisture dynamics reasonably well. Considering the measurement uncertainty of the installed SWC sensors (4-5 vol %; Rosenbaum et al. (2012)) the RMSE of 3.4 to 5.3 vol. % appear very low and are within the range of other HYDRUS-1D studies on the Wüstebach test site (Fang et al., 2015; Bogena et al., 2013). The varying soil hydraulic properties among plots and layers (Table 3.2) fit well to the observations of Gottselig et al. (2017) and Wiekenkamp et al. (2016). The low K_s value in the riparian zone is plausible, because the soils in the valley bottom have a higher bulk density and a lower macro-porosity than the soils on the hillslopes (Rosenbaum et al., 2012; Wiekenkamp et al., 2016).

The simulated mean annual root-zone water potentials (Figure 3.6) highlight the contrasting soil moisture regimes of our research plots (wet and dry). These characteristics become even more pronounced when referring only to the vegetation periods (May-September), where mean root-zone pressure heads are -124 (*Riparian*) and -4308 cm (*Slope*). Covering particularly the stages of critical soil water supply (undersupply/oversupply) our data seems very suitable for investigating the on-set of drought and aeration stress in plants.

3.4.2 Water stress response of Norway spruce

There is evidence that the shallow rooting Norway spruce is more vulnerable to drought than other species with a deeper rooting system (Gartner et al., 2009; Lagergren and Lindroth, 2002; Cienciala et al., 1994). Also, Gartner et al. (2009) and Střelcová et al. (2013) found the sap

flow activity of Norway spruce to decouple from climate variables with increasing soil water shortage. However, critical levels of soil water supply that induce a decline in sap flow rates and transpiration considerably vary among studies.

While Gartner et al. (2009) observed gradually decreasing sap flow rates with increasing soil water shortage for REW < 0.4 (which corresponds to a pressure head of -3240 cm at our *Slope* plot), Lagergren and Lindroth (2002) found Norway spruce to be more drought resistant. Depending on the soil depth considered, they report mean critical REW values of between 0.21 (0-20 cm) and 0.24 (0-50 cm). However, the observed critical REW level strongly varied among trees (REW: 0.18–0.37), which Lagergren and Lindroth (2002) attribute to the heterogeneous soil conditions on site. This is in line with Gartner et al. (2009), who found the stress response of Norway spruce to become increasingly variable between individuals with continuing drought stress. Comparing the water stress response of Norway spruce among more than 60 pure and mixed stands, Lundblad and Lindroth (2002) report difficulties in determining a consistent critical level of REW. For most of the plots, drought limitation of sap flow began around a REW of 0.3. However, the data scatter around this critical limit was large and a clear decrease in transpiration for all stands except peat stands was only observed for REW below 0.25.

In simulation studies, a REW level of 0.3-0.4 is commonly used to indicate the on-set of drought stress in Norway spruce (Schwärzel et al., 2009; Granier et al., 1999, 2000). However, this critical REW range is widely accepted for many species (not only for spruce) and our data show that REW does not represent the actual energy state of the soil. For example, at the *Slope* plot a REW value of 0.3 corresponds to a root-zone pressure head of -4680 cm, which is in the same range (pF 3.7) as the critical h value of -4100 cm (pF 3.6) we observed in our study (Figure 3.7a). However, a REW threshold of 0.3 at the *Riparian* corresponds to a root-zone pressure head of -2140 cm suggesting that drought stress would occur much easier at this site (i.e., at lower soil matric potentials). On the other hand, a critical root-zone water potential of -4100 cm pressure head would here correspond to a REW of 0.17.

One could argue that the poor fit between our critical h and the critical reported REW values for the *Riparian* plot is of minor importance, because critical water contents are never reached (Lundblad and Lindroth, 2002; Calder, 1998). Moreover, the concept of REW seems to apply fairly well to the conditions at the *Slope* plot and to other soils in central European high and low mountain ranges (Gartner et al., 2009; Schwärzel et al., 2009; Granier et al., 1999, 2000). However, Norway spruce is also widely distributed in boreal forest landscapes, where typical critical REW values seem to be lower than 0.3 (Lagergren and Lindroth, 2002; Lundblad and Lindroth, 2002) and soils are often peaty (Bonan and Shugart, 1989), hence showing similar characteristics (low residual water content, high saturated water content; Rezanezhad et al. (2016); Weber et al. (2017); Schwärzel et al. (2006)) as our plot in the riparian zone. Our data indicates that for such soils the concept of REW is likely to fail. This emphasizes the value of soil water potential in comparison to other measures of soil water supply, because, respective water stress thresholds can be applied to any type of soil as long as soil water retention and plant characteristics are known.

However, while critical soil water potentials have been determined for many agricultural crops, little effort has been put into the quantification of Feddes parameters for forest trees. To our

knowledge, the concept of transpiration limiting soil water potentials has hardly been applied in spruce site simulation studies. In the few studies we found, the drought stress threshold was generally assumed to be less negative than the value we determined from our sap flow data ($h_{3,\text{low}}$ = -4100 cm).

Huang et al. (2011) set h_3 to the root-zone h at a SWC of 27.5% of the SWC at field capacity. This corresponds to the mean critical SWC they reviewed from different studies on drought stress in evergreen tree species. Applied to our data and considering field capacity to be represented by SWC at -300 cm pressure head (see above), this threshold corresponds to a pressure head of -3890 cm at the *Riparian* plot, but to h < -10 million cm at the *Slope* site, which is far below the common used value for the permanent wilting point. Dependent on the soil type, Rosenqvist et al. (2010) assumed the onset of drought stress for Norway spruce at water potentials of -500 (coarse sandy soils) to -1000 cm pressure head (clayey soils). However, these texture dependent water stress thresholds contradict the idea that the soil water potential is already a function of SWC and soil properties. From a plant physiological perspective, species-specific water stress thresholds should be used instead. Vogel et al. (2013) set their drought stress thresholds to -1200 ($h_{3,\text{low}}$) and -600 cm pressure head ($h_{3,\text{high}}$). These parameters were derived from other hydrological studies that were conducted on similar soils, but had no plant physiological basis. Nevertheless, applying the parameter set of Vogel et al. (2013) to our simulations, we achieved a very good fit between measured and simulated SWC (RMSE < 5.3 vol %). Also, mean daily sap flow and simulated actual transpiration showed high correlations (R^2 > 0.82). However, although the adaptation of the Feddes function had little impact on the general dynamic of the simulated fluxes, the adjustment of $h_{3,\text{low}}$ significantly changed transpiration (p < 0.001) and drainage fluxes (p < 0.01) at the *Slope* plot (two-sided Mann-Whitney U-test; Table 3.3) and made it more realistic: Based on eddy-covariance measurements, Graf et al. (2014) found the annual ET_{act} in the Wüstebach catchment to cover approximately 90% of ET_0. In our *Slope* plot simulations this ratio was 80% for the uncalibrated Feddes model, but 87% for the calibrated simulation run in the same study period (2010–2013). The runoff ratio (runoff/precipitation) observed by Graf et al. (2014) was 56%, while that in our simulations ranged between 62% (*Slope* plot after calibration of the Feddes model) and 65% *(Slope* plot before calibration of the Feddes model). This result confirms: (1) the finding of Diekkrüger et al. (1995) that a good fit between simulated and measured SWC does not necessarily imply that the simulated water fluxes are correct; and (2) the assumption of Vereecken et al. (2010) that sap flow measurements can help improving root water uptake simulations.

It has to be noted that the impacts of the Feddes model on simulated water fluxes depend on local site conditions. The well-watered *Riparian* plot was not affected by the calibration, because critical pressure heads were never reached. Drought stress simply did not occur and although there is evidence on the vulnerability of Norway spruce to waterlogging (Gartner et al., 2009; Tjoelker et al., 2007), our data did not indicate arising aeration stress in the riparian zone (Figure 3.7b). One reason could be that spruce indeed only suffers from aeration stress at fully saturated soils ($h_1 = h_2 = 0$), which does not apply to the vegetation periods in this study (Figure 3.5). Another possible explanation is that the transpiration limiting effects of aeration stress occur on longer time-scales than the daily scale we were operating at.

Our data show that soil water supply strongly influences the transpiration of Norway spruce. Due to the observed drought stress on the hillslope (Figure 3.7a), the simulated actual transpiration at the *Slope* plot was 13% lower than that of the riparian zone (Table 3.3). This result highlights the importance of considering soil moisture patterns in the modeling of transpiration fluxes from the forest plot to the catchment scale.

3.5 Conclusions

In this study, we confirm the potential of sap flow measurements for the determination of water stress in forest trees. By combining soil hydrological simulations with a water stress factor derived from sap flow data, we were able to parameterize the Feddes water stress function for Norway spruce and improve our water balance simulations on site. Our results show that small-scale variations in soil water supply significantly influence the water balance of spruce sites. Considering soil moisture patterns in the model setup can thus improve the simulation of transpiration fluxes on the catchment scale.

Although additional sap flow stations and a bigger sample size per plot would have provided a more detailed view on the conditions on site, the sampling concept (wet plot against dry plot) delivered valuable insights into the water stress response of Norway spruce. The advantage of our sampling approach is that an upscaling of sap flow density to the tree and plot scale is unnecessary. Hence, uncertainties related to the upscaling procedure (cf. e.g., Steppe et al. (2015); Köstner et al. (1998); Renninger and Schäfer (2012); Lundblad et al. (2001); Bush et al. (2010); Sun et al. (2012); Rabbel et al. (2016); Nadezhdina et al. (2002); Ford et al. (2004)) can be avoided. However, to transfer our finding to other sites and settings, more research on species-specific feedbacks in the soil-vegetation-atmosphere system is needed. There is still a lack of studies determining the critical limits of soil water supply for trees. Since forests play a vital role in regional and trans-regional water cycles and, against the background of climate change, the assessment of respective fluxes becomes increasingly important, future research should focus on: (1) more species-specific investigations on the water stress response of trees; and (2) an improved assessment of small-scale variabilities in soil water supply. With our sampling strategy, we present a simple and cost-efficient approach to achieve these goals, even with a limited number of sample trees.

Author contributions   All authors conceived and designed the experiments; Inken Rabbel performed the experiments, analyzed the data and wrote the paper.

4 Exploring the growth response of Norway spruce (*Picea abies*) along a small-scale gradient of soil water supply

Abbreviations of the original article have been adapted according to the standardized format of this dissertation.

Abstract: The climate-growth response of specific sites and species is one of the main research subjects in classic tree ring studies. Traditional sampling approaches therefore aim at maximizing the climate signal of the analyzed tree ring series, which is typically achieved by focusing on dominant trees or on sites located in particularly temperature or moisture limited environments. However, there is increasing evidence that these selective sampling strategies cannot yield chronologies that are representative for entire populations. One promising approach to gain a deeper understanding of forest dynamics and climate-growth responsiveness is the analysis of climate signal ranges among trees. This individualistic approach requires random sampling and the integration of information on small-scale heterogeneities in site and tree characteristics. Here, we analyze the climate-growth response of 144 Norway spruce trees (*Picea abies* Karst.) on difference levels of data aggregation. The aim of our study is to investigate the relevance of small-scale heterogeneities in site conditions, particularly in soil water supply, for the detected climate-growth signal. We identify soil water supply and site characteristics, which indirectly modify the water availability for trees, as dominating growth factors across scales. The driest sites show the strongest climate-growth reaction, while the growth response of wetter sites is weak or even insignificant. Therefore, we conclude that integrating small-scale information on site characteristics, particularly on soil water supply, can help to gain a deeper understanding of species-specific growth limitations.

4.1 Introduction

Investigating the climate-growth response of specific sites and species is one of the main research subjects in classic tree ring studies. Hence, site and tree selection typically aim at maximizing the climate signal in the inspected growth chronology (Nehrbass-Ahles et al., 2014; Primicia et al., 2015; Sullivan and Csank, 2016). Respectively, many researchers follow a selective sampling focusing either on "dominant, large and healthy trees" (Nehrbass-Ahles et al., 2014) or on sites located in particularly temperature or moisture limited environments (Esper et al., 2007; Sullivan and Csank, 2016).

However, even though selective sampling is acknowledged as appropriate approach for climate growth analysis and climate reconstructions (Nehrbass-Ahles et al., 2014), there is increasing evidence that the resulting tree ring chronologies are likely to miss representativeness for the tree population (Carrer, 2011; Nehrbass-Ahles et al., 2014; Sullivan and Csank, 2016), because the climate sensitivity of individual trees largely depends on site and tree characteristics (Carrer, 2011; Galván et al., 2014; Primicia et al., 2015). Recent studies show that the growth responsiveness of trees to climate is related to forest management and composition (Pretzsch and Dieler, 2011; Primicia et al., 2015), physical and chemical soil properties (Braun et al., 2010; Pretzsch and Dieler, 2011; Tromp-van Meerveld and McDonnell, 2006; Ibáñez et al., 2018), soil water state (Ashiq and Anand, 2016; Helama et al., 2016; Jiang et al., 2016; Lévesque et al., 2014; Linares et al., 2010; Primicia et al., 2015; Zhang et al., 2018), canopy structure (Adams and Kolb, 2004; Linares et al., 2010; Martín-Benito et al., 2008; Primicia et al., 2015), tree to tree competition (Linares et al., 2010; Primicia et al., 2015; Gleason et al., 2017; Piutti and Cescatti, 1997), tree size (Carrer and Urbinati, 2004; Linares et al., 2010), and tree age as a proxy for other, size related effects (Carrer and Urbinati, 2004; Primicia et al., 2015).

Consequently, researchers increasingly seek for randomized sampling strategies that allow for both (1) the extraction of a mean climate-growth response and (2) the investigation of the range of climate signals among trees (Carrer, 2011; Nehrbass-Ahles et al., 2014; Sullivan and Csank, 2016). However, to draw ecological conclusions from heterogeneities in the individual climate-growth response of trees, a comprehensive sampling design including quantitative data on tree and site characteristics is indispensable (Babst et al., 2013; Nehrbass-Ahles et al., 2014).

In this study, we analyze tree ring chronologies of 144 Norway spruce trees (*Picea abies* Karst) on different levels of data aggregation with the aim to identify the relevance of small-scale heterogeneities in site conditions for the detected climate-growth signal. Since Norway spruce is known to be particularly vulnerable to drought (Boden et al., 2014; Bouriaud et al., 2005; Neuwirth, 2010; Zang et al., 2012, 2014), we focus on small-scale variabilities in simulated soil water supply and on site characteristics, which indirectly modify the water availability for trees. Further potentially growth relevant factors we consider in our analysis are soil nutrient states and pH level. The study area is an even-aged Norway spruce plantation in the Eifel National Park (western Germany). Hence, age-related modifications of the climate-growth signal do not play a role in our study.

4.2 Materials and methods

4.2.1 Study area and data base

This study was conducted in the 27 ha Wüstebach experimental test site, which belongs to the TERENO Eifel/Lower Rhine Valley Observatory and is located in the Eifel National Park close to the German Belgian border (Bogena et al., 2018). The area is forested with Norway spruce that were planted in the late 1940ies (Etmann, 2009). In 2013, one quarter of the trees (8.6 ha) was removed to investigate the effects of deforestation on hydrological and biogeochemical cycling (Bogena et al., 2014). Altitudes range from 595 m a.s.l. in the north to 628 m a.s.l. in the south. While the hillslopes are dominated by shallow Cambisols and Planosols, Gleysols and Histosols have developed in the Riparian zone (a map of the study area is given in the 4.3 section). The soil texture is mainly silty clay loam with a medium to high coarse material fraction (Gottselig et al., 2017). The mean annual temperature and precipitation sum for the period 1970-2000 are 7.9 °C (DWD weather station Kall-Sistig in 13.1 km distance to the test-site) and 1280 mm (DWD weather station Kalterherberg in 9.6 km distance to the test-site), respectively.

We analyzed tree ring data of 48 microsites with slightly varying soil water supply to explore small-scale variations in the climate-growth relations. Soil moisture was monitored with the TERENO sensor network SoilNet (Bogena et al., 2010). SoilNet provides catchment-wide information on soil water dynamics in 5, 20 and 50 cm depths with 15 min resolution since 2009 using ECH2O EC-5 and ECH2O 5TE sensors (Decagon Devices, Pullman, WA, USA). We used the soil hydrological model HYDRUS-1D (Šimůnek et al., 2013) to generate long-term information on soil water supply from the SoilNet data. First, we inversely estimated the soil hydraulic properties for each of our micro-sites as described in Rabbel et al. (2018a) using SoilNet data from 2010 to 2012 for the model calibration and data from 2013 to 2015 for the model validation. Based on the validated model setup we conducted long-term simulations of soil water supply in terms of root-zone pressure heads for the period 1951 to 2000. Daily climate and precipitation data for the long-term simulations were taken from the DWD weather stations Kall-Sistig and Kalterherberg, respectively. We considered the effect of forest growth on the water balance by using a dynamic leaf area index (LAI) as obtained from long-term simulations with the process-based forest hydrological model LWF-Brook90 (Hammel and Kennel, 2001). For more detailed information on the climate data processing and simulated LAI, we refer to Cornelissen (2016). Through logarithmic transformation and aggregation of the daily modelled pressure heads we obtained mean monthly root-zone pF values for each of our microsites. As additional growth relevant factors, we considered planting density and soil properties as microsite characteristics in our study. In this context, we made use of the comprehensive spatially distributed biogeochemistry dataset of the Wüstebach (Gottselig et al., 2017). For this study we selected information on soil horizon depths and horizon-wise bulk density, pH and C-, N- and P-contents.

4.2.2 Tree ring data and chronology building

We selected our microsites with regard to the existing SoilNet measuring locations to draw the closest possible link between tree ring data and local site conditions. However, since our

sampling campaign took place after the deforestation event in 2013, Gleysol sites could not be considered in this study. Each microsite consists of three trees in direct proximity (< 10 m) to one of the SoilNet stations. We used a HAGLÖF increment corer with 5 mm diameter to extract two opposite cores at breast height per tree. The sample preparation followed standard procedures (Stokes and Smiley, 1968). Ring widths were measured at the dendrochronological lab DeLaWi Tree Ring Analyses (Windeck, Germany) using the moveable object table Lintab 5 (Rinntech, Heidelberg, Germany) and a stereo microscope (Carl Zeiss, Jena, Germany) in a measuring accuracy of 10 μm. Synchronization and cross-dating were carried out with the software tools TSAP-WIN (Rinn, 2003) and COFECHA (Holmes, 1983). Tree mean curves (TMC) were calculated with TSAP-WIN. We detrended each TMC using a high-pass filter based on binomially weighted 5-year running means (Schweingruber, 1988) to remove age-related trends and emphasize inter-annual growth variations. Indices (RWI) were calculated as ratio between actual tree ring widths and the filtered value. In total, we considered 144 trees to create 48 SoilNet related microsite chronologies (SN) and one regional chronology across all microsites in the Wüstebach catchment (WÜ). To avoid data inconsistencies, we excluded the juvenile phase from our investigations and thus only used the period 1970 to 2000 for further analyses. More recent years were not considered, because of a multi-year data gap in the Kall-Sistig weather station data. Applying the hierarchical cluster analysis after Ward, which has already been proven to provide a clear distinction of growth clusters in previous studies (e.g., Friedrichs et al. (2009)), we used the squared Euclidian distance as a measure of similarity to detect SN chronologies (RWI series) with similar growth dynamics. These were aggregated to respective cluster chronologies (CL) using arithmetic means.

4.2.3 Statistical analysis

We analyzed the climate-growth relationships in the Wüstebach catchment at different levels of data aggregation using Pearson's product-moment correlations. WÜ, CL and SN chronologies were correlated with monthly temperature and precipitation data and mean monthly root-zone pF over a 18-month window from May of the previous year (denoted with the index p) until October of the current year of ring formation. Additionally, we considered temperature means, precipitation sums and mean simulated root-zone pF for the periods March-May (MAM), June-August (JJA), September-November (SON), April-October (VEG), and annual values (CAL) for the previous and current year of ring formation.

We correlated the climate signal strength (Pearson's r) observed on the SN level with the respective microsite characteristics (exposition, inclination, planting density, mean root-zone pF, and soil biogeochemistry) to identify the relevance of site characteristics for the detected climate signal. We conducted this analysis (1) for all 48 SN microsites across the Wüstebach catchment and (2) for each growth cluster separately.

Since the cluster characteristics considered in this study typically exhibit non-normal distributions, we used U-tests instead of T-tests to identify statistically significant differences in the mean cluster characteristics and therewith to explain the cluster formation itself. In this context, we applied the software package R (R Core Team, 2018). Significance for both Pearson's correlations and U-tests was tested on the 95% significance level ($p < 0.05$).

4.3 Results and discussion

4.3.1 Regional climate-growth relations

For the WÜ chronology (Fig. 4.1a), we found significant negative correlations between mean monthly and seasonal temperatures and RWI for JULp, JJAp and VEGp (Fig. 4.1b), whereas the strong correlation of RWI and JULp (r=-0.55) seems to dominate the observed seasonal temperature-growth relations. Significant positive correlations with RWI were observed for OCTp, JJAp, SONp, and VEGp precipitation sums (Fig. 4.1b). In this case, the strong correlation of RWI and OCTp (r=0.61) dominates the observed significant correlation of RWI and SONp. The sensitivity to high summer temperatures and low precipitation of the previous year is typical for Norway spruce in lower altitudes (Fischer and Neuwirth, 2012; Hartl-Meier et al., 2014; Mäkinen et al., 2002; van der Maaten-Theunissen et al., 2013).

The interplay between positive correlations of RWI with precipitation and negative correlations with temperature for the same periods (JJAp and VEGp) suggests that radial growth rates in the Wüstebach catchment are mainly controlled by water availability. This finding is supported by the significant negative correlations of RWI with the mean monthly (JULp, AUGp, OCTp, NOVp), seasonal (JJAp, SONp, VEGp), and annual (CALp) root-zone pF (4.1b) and in line with other studies reporting the particularly high vulnerability of Norway spruce to drought (Boden et al., 2014; Bouriaud et al., 2005; Neuwirth, 2010; Zang et al., 2012, 2014).

a)

b)
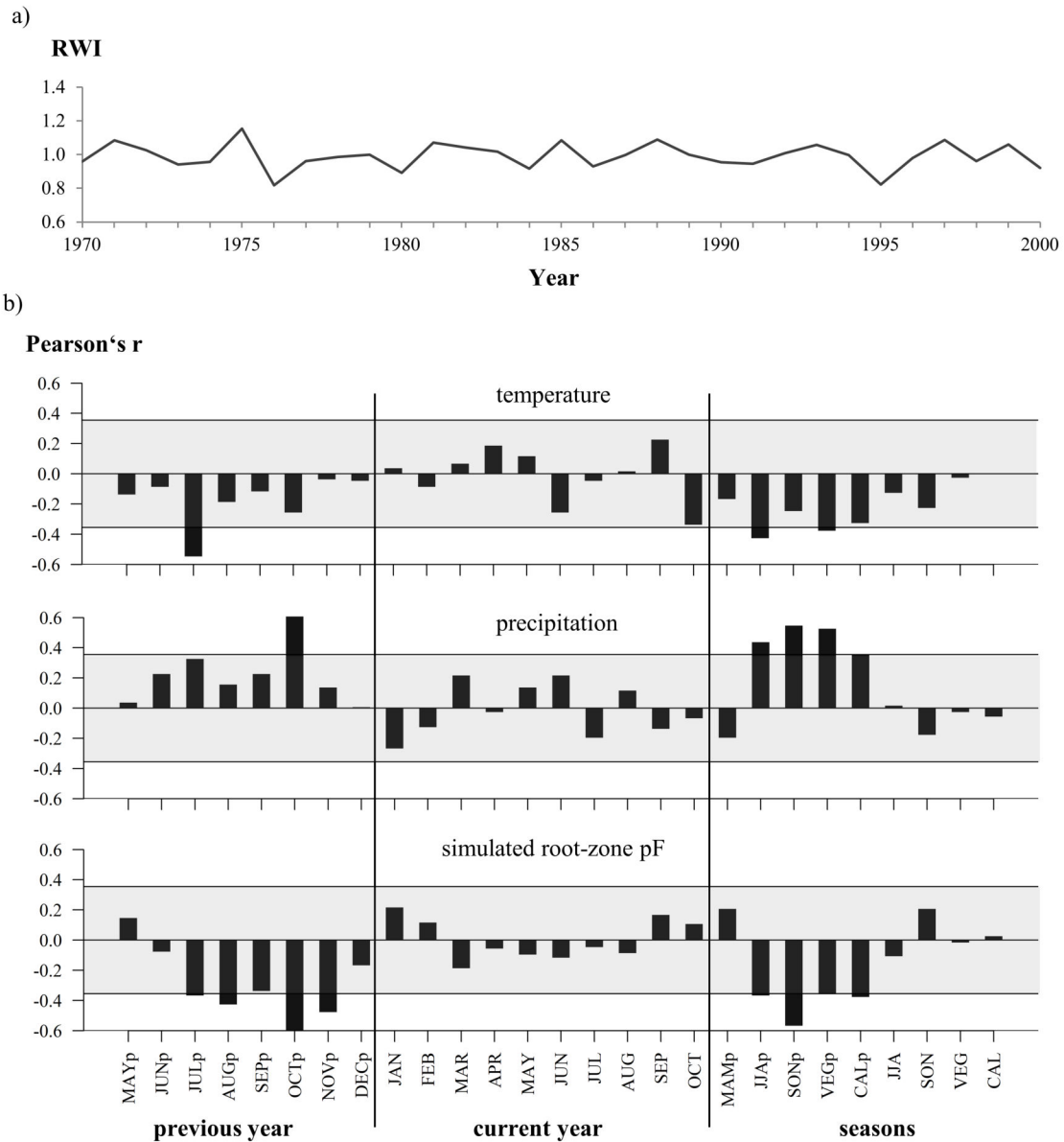
Figure 4.1: WÜ chronology (a) and correlation between respective RWI values and monthly/seasonal temperatures, precipitation sums, and simulated root-zone pF values (b). Horizontal black lines in figure b represent the 95% significance level.

4.3.2 Climate growth relations across microsites

The SN chronologies show a considerable scatter in RWI values (Fig. 4.2a). Nevertheless, the general growth dynamic is similar among SN chronologies. For most of the SN series, we observed negative RWI peaks in the years 1976 and 1995, which have already been identified as negative pointer years for the Wüstebach area in a previous study (Thomas et al., 2018). Particularly high ranges of RWI values among SN chronologies were found for the years 1970 (0.31), 1977 (0.36), and 1996 (0.33) and hence for years that follow negative pointer years (Thomas et al., 2018). This indicates that the recovery of growth rates after drought years depends on small-scale environmental conditions.
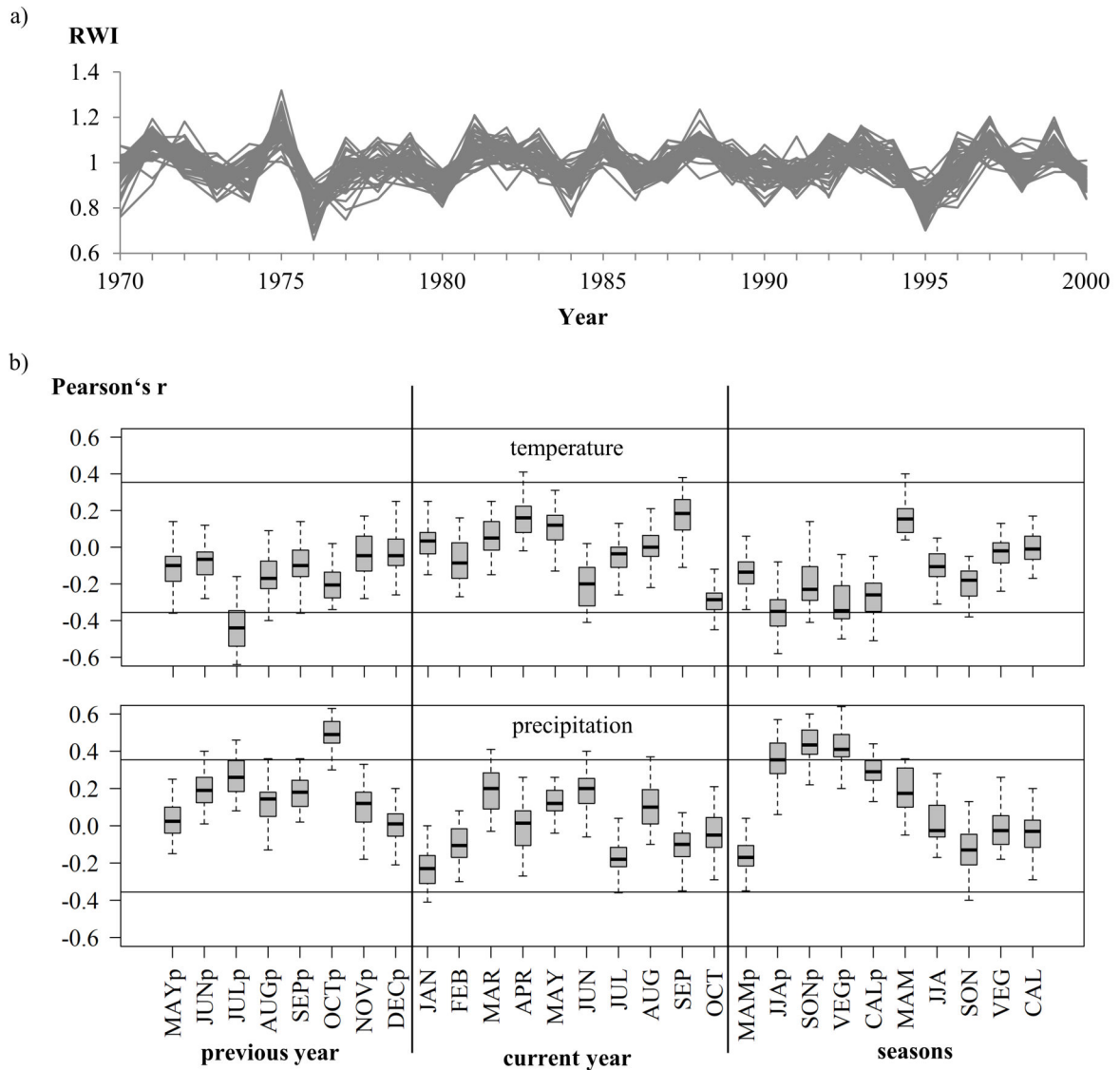
Figure 4.2: SN chronologies (a) and correlation between respective RWI values and monthly/seasonal temperatures and precipitation sums (b). Black horizontal lines represent the 95% significance level.

The monthly/seasonal climate signals among SN chronologies are strongly scattered (Fig. 4.2b), which we attribute to small-scale variabilities in the microsite conditions (e.g., soil properties).

We found significant negative correlations between the SN chronologies' temperature signals and the simulated summer root-zone pF of the previous year (JJAp; Fig. 4.3a). Hence, drier microsites react stronger to high summer temperatures than wetter microsites, which was also found by other studies on the regional scale (Ashiq and Anand, 2016; Helama et al., 2016; Jiang et al., 2016; Lévesque et al., 2014; Zhang et al., 2016). Significant negative correlations with seasonal temperature signals (JJAp, VEGp) were also found for the local planting density (Fig. 4.3b).This effect indicates an increasing competition for soil water with increasing number of trees per ground area, which was already observed by Linares et al. (2010) and Primicia et al. (2015).
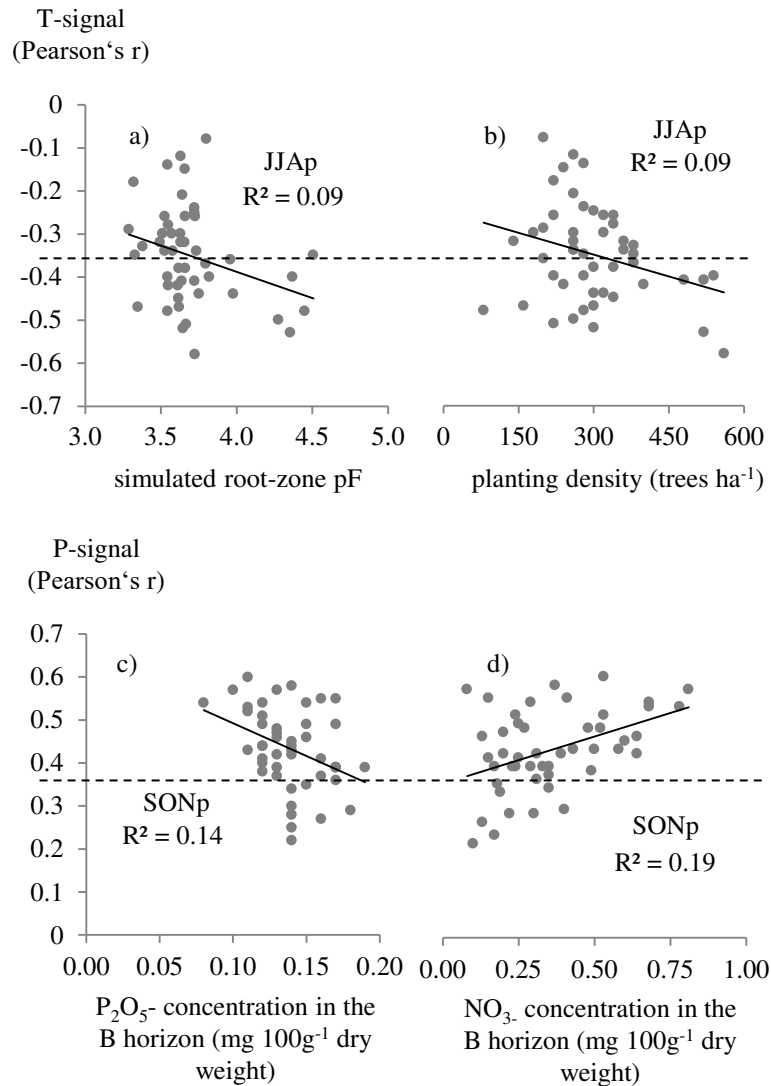
Figure 4.3: Correlation between SN climate signal strength (Pearson's r) and simulated root-zone pF (a), planting density (b), P_2O_5 concentration (c), and NO_{3-} concentration (d). The dashed black lines indicate the 95% significance level for the observed climate-growth relations. T-signal: temperature signal as resulting from the correlation of the SN chronologies and mean monthly/seasonal temperatures; P-signal: precipitation signal as resulting from the correlation of the SN chronologies and monthly/seasonal precipitation sums; reference periods for the illustrated climate signals: JJAp: Juli to August of the previous year; SONp: September to November of the previous year.

Interestingly, we did not find any correlations between the precipitation signal of the SN chronologies and water related microsite characteristics. Instead, seasonal precipitation signals (SONp, VEGp) were significantly related to the microsite's soil N and P states. We observed decreasing precipitation signals with increasing plant available P (P_2O_5) indicating that insufficient P supply increases the drought vulnerability of Norway spruce (Fig. 4.3c).

Nitrate N (NO_{3-}), in contrast, shows a significantly positive correlation with the precipitation signal strength (Fig. 4.3d). One possible explanation is that the enhanced N levels in the Wüstebach catchment as indicated by C/N ratios well below 25 (Gundersen et al., 1998) reduce fine-root growth and limit the uptake of other nutrients. The resulting negative effects of excess N on tree growth and vitality have been described before and may result in a decreased tolerance

against soil-related stress factors (Braun et al., 2010; Kazda, 1990; Mohren et al., 1986; Puhe, 2003; Seith et al., 1996; Thelin et al., 1998). Hence, it seems reliable that microsites of excess N supply are more vulnerable to water stress than microsites with a more balanced nutrient supply.

4.3.3 Cluster formation and characteristics

Our cluster analysis resulted in three primary growth clusters with 18 (CL1), 21 (CL2), and 9 SN members (CL3) (Fig. 4.4a). The spatial proximity of the SN sites was not important for cluster formation (Fig. 4.4b). Instead, the site characteristics of the clusters mainly differed in the mean simulated soil water supply (Fig 4.5). However, while the mean simulated root-zone pF of cluster 1 was significantly higher than that of cluster 2 and 3, no significant difference was found between the moisture regimes of cluster 2 and 3.
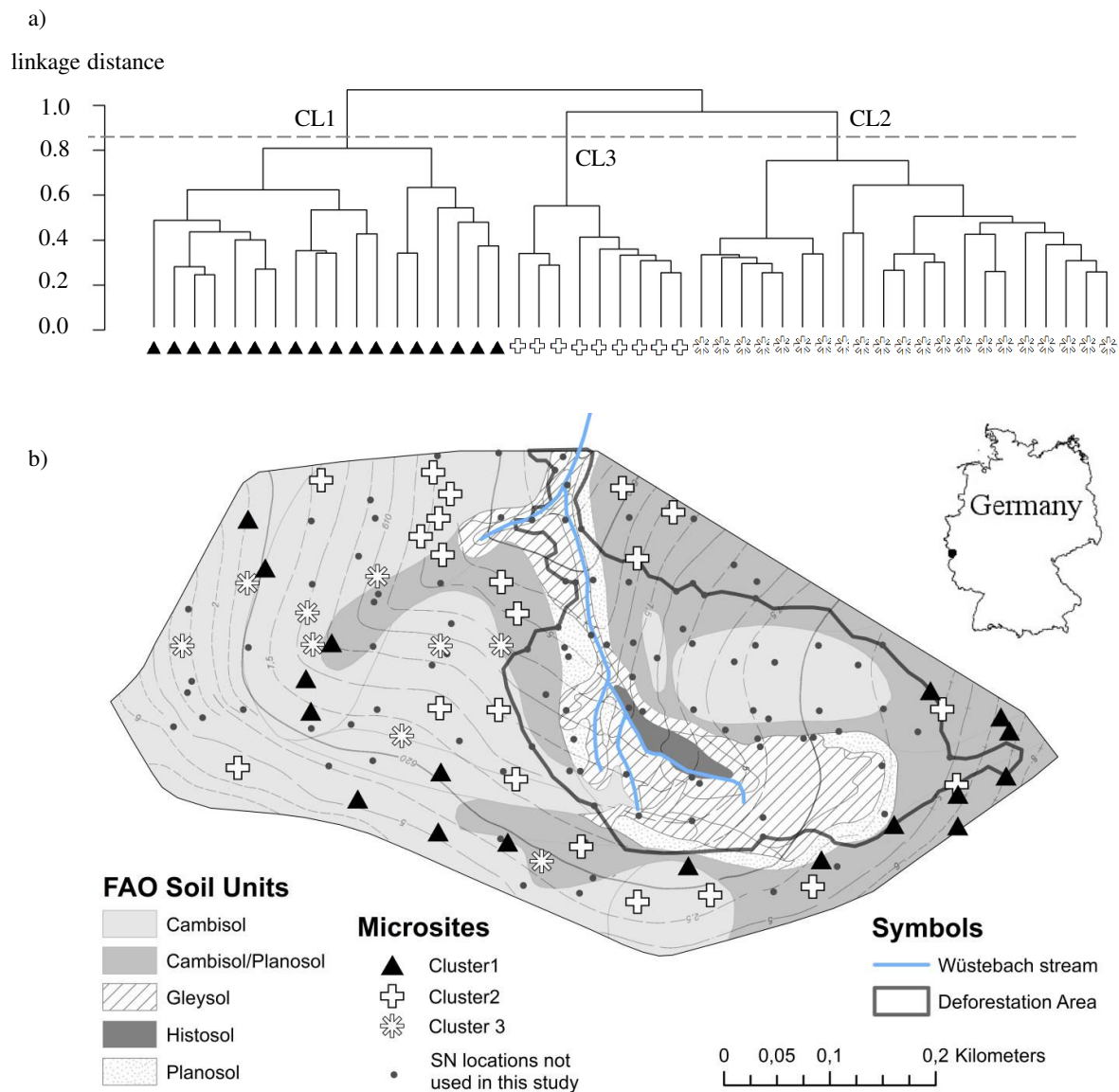

Figure 4.4: Dendrogram as resulting from the hierarchical cluster analysis after Ward (a) and spatial distribution of the clusters within the Wüstebach catchment (b).
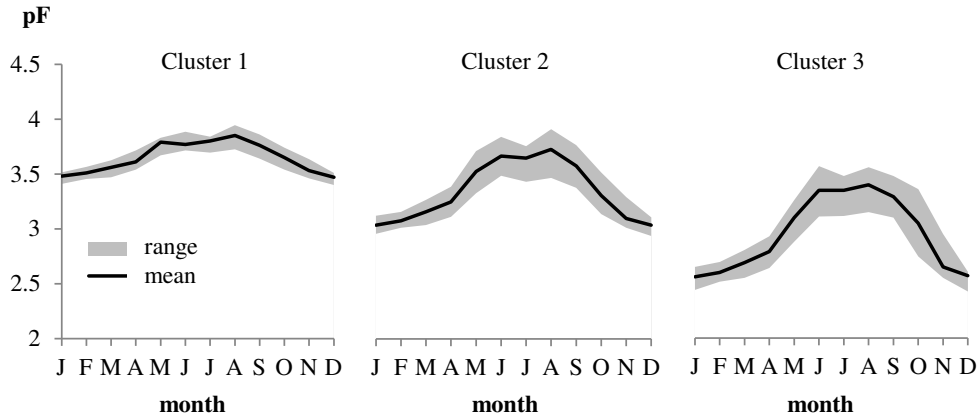
Figure 4.5: Simulated mean monthly soil water supply (black line) and inter-annual variation of the simulated mean monthly soil water supply (grey) for the period 1970-2000 by growth cluster. Field capacity and permanent wilting point are generally assumed for pF 2-2.5 and 4.2, respectively.

Nevertheless, the cluster's climate signal strength was clearly connected to the observed gradient in the mean cluster's soil water supply: The cluster chronology of the driest cluster (CL1, Fig. 4.6a) showed the strongest correlation with monthly/seasonal mean temperatures (JULp, JJAp, CALp, VEGp), while the wettest cluster (CL3) did not show significant temperature-growth relations at all (Fig. 4.6b). Also, the temperature signal of CL1 was even 0.06 (JULp) to 0.08 (VEGp) points stronger than that of the mean WÜ chronology. This indicates that our small-scale clustering approach can help to improve the extraction of a regional climate signal.

The precipitation signal of the cluster chronologies was also modified by mean soil water supply. However, the effect was not as strong as for the temperature signal. Even though the precipitation signal strength decreased with increasing root-zone pF, all cluster chronologies still showed significant correlations with mean seasonal precipitation sums (JJAp, SONp, VEGp). The OCTp precipitation signal was highly significant ($p < 0.001$) for all cluster chronologies and the only signal appearing to be independent from the soil moisture regime.

Internal relations between SN climate signal and microsite characteristics varied among clusters. The analyzed microsite characteristics within the clusters were found to be independent from each other and also from absolute soil water states. In contrast to our findings on the regional scale, cluster internal SN temperature signals were not correlated with the simulated soil water supply. Instead, temperature signals significantly correlated with the planting density (Fig. 4.7a), which reflects the above described increased competition for water resources under drought, and with the bulk density of the B horizon (Fig. 4.7b). The increasing climate sensitivity with increasing bulk density can be explained, because Norway spruce is known to preferably root humus-rich soil horizons. High skeleton contents and clay-rich B horizons as present in the Wüstebach catchment hamper the development of the deeper rooting system, which is particularly important to compensate water shortage under drought (Puhe, 2003).

The cluster internal SN precipitation signals were significantly correlated to soil NO_{3-} (positive correlation, Fig. 4.7c) and P_2O_5 (negative correlation, Fig. 4.7d). Furthermore, increasing sensitivities to monthly/seasonal precipitation sums can be observed with increasing bulk densities (Fig. 4.6e), decreasing soil depth (Fig. 4.7f) and ongoing soil acidification (Fig. 4.7g).
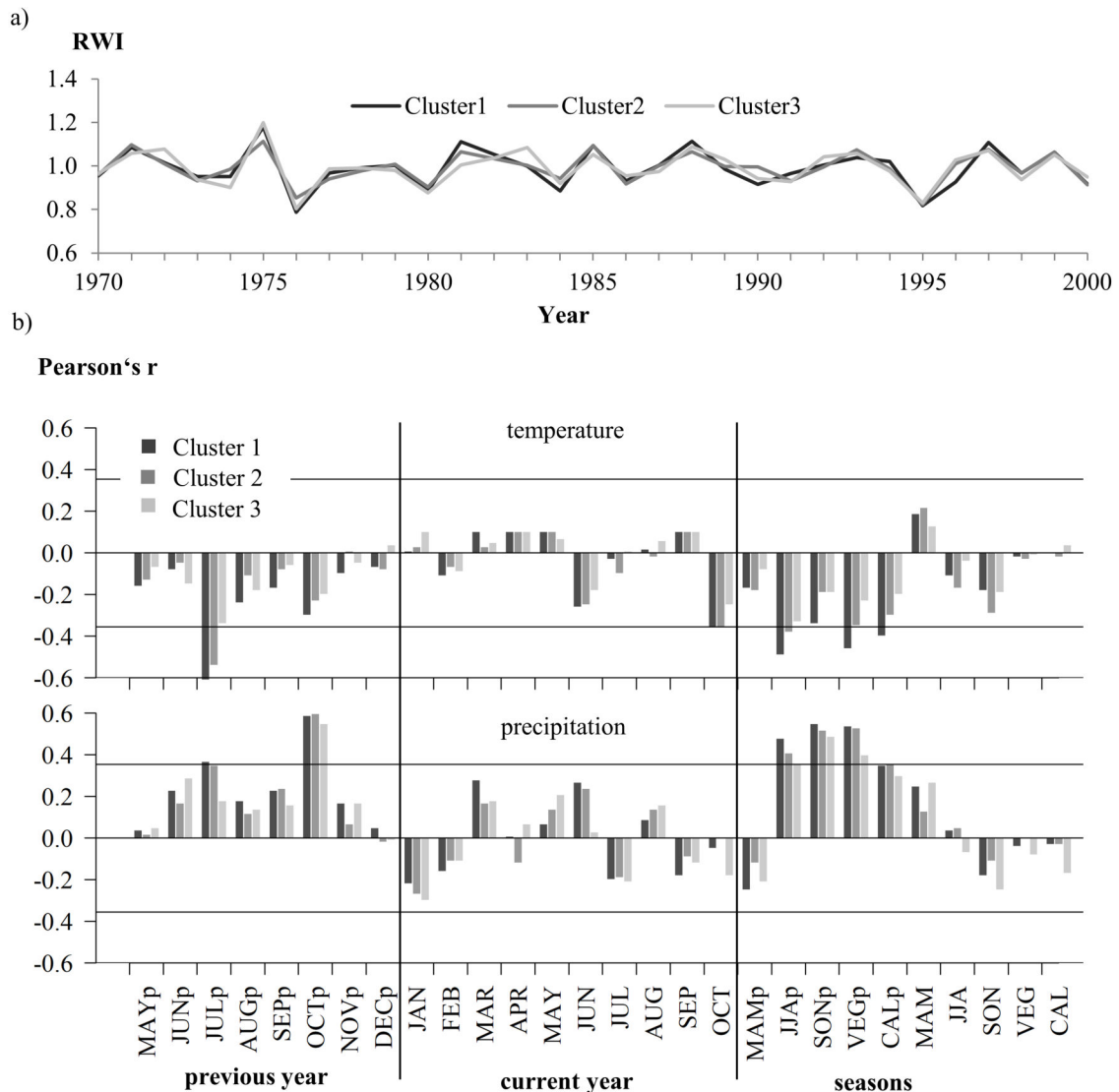
Figure 4.6: Cluster chronologies (a) and respective correlation between RWI values and monthly/seasonal temperatures and precipitation sums (b). Black horizontal lines represent the 95% significance level.

We found a noteworthy negative correlation between soil depth and drought sensitivity, which is reasonable as total soil water storage increases with increasing soil depth. This finding is also in correspondence to other studies (e.g., Tromp-van Meerveld and McDonnell (2006)), who explained patterns in forest basal area with spatial variations in soil depth.

The negative effect of soil acidification on root growth and thus on the potential water uptake of Norway spruce has been reviewed by Puhe (2003) and explains the negative correlation between soil pF and SN precipitation signal.

Apart from the mean soil water supply, we did not find significant differences in the microsite characteristics among clusters. Therefore, we attribute the observed cluster-internal dependencies of climate-growth relations from microsite characteristics to the underlying cluster moisture regimes.
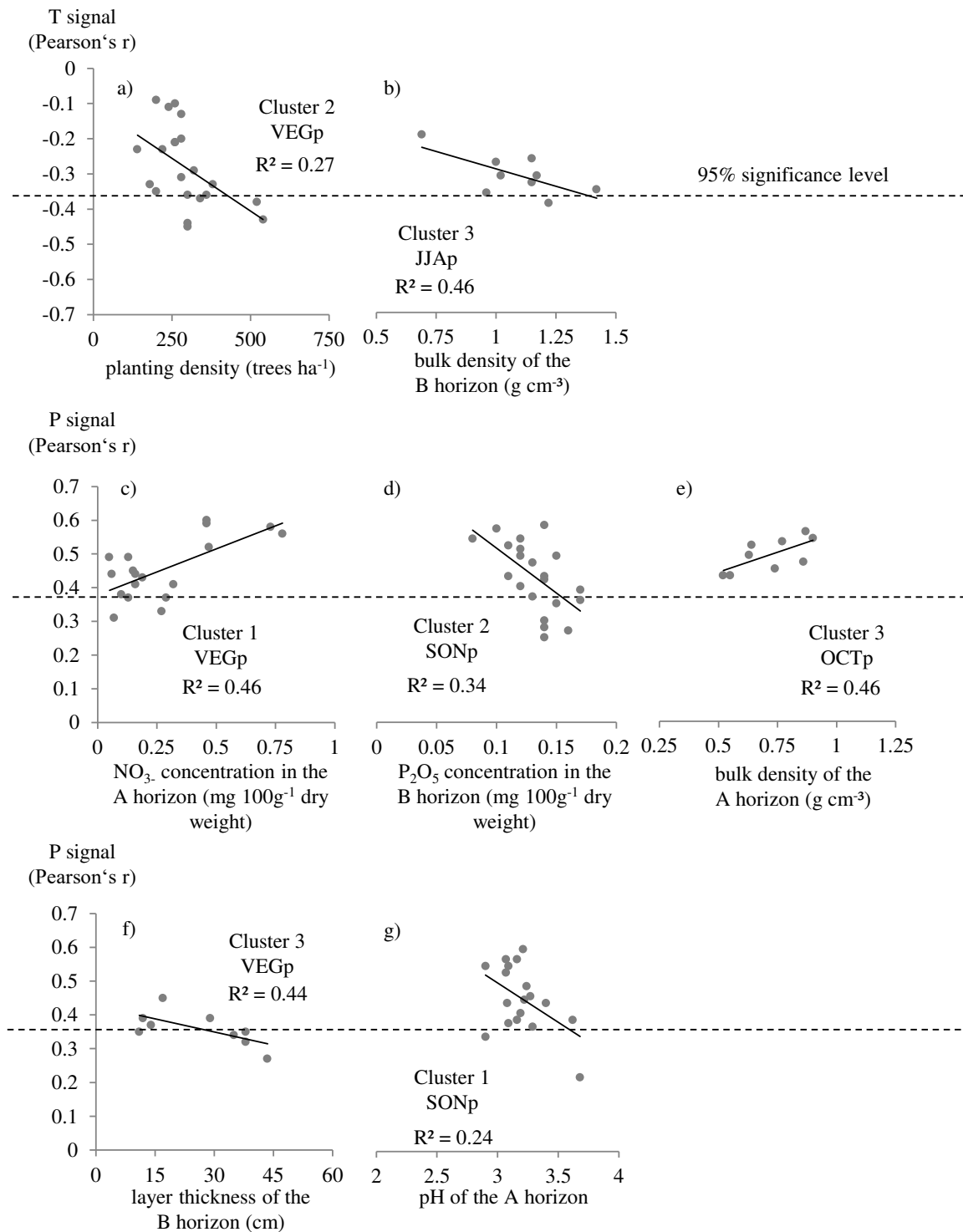
Figure 4.7: Correlation between cluster internal SN climate signal strength (Pearson's r) and microsite characteristics for cluster and season as given in the plots. The dashed black lines indicate the 95% significance level for the observed climate-growth relations. T-signal: temperature signal as resulting from the correlation of the SN chronologies and mean monthly/seasonal temperatures; P-signal: precipitation signal as resulting from the correlation of the SN chronologies and monthly/seasonal precipitation sums; reference periods for the illustrated climate signals: OCTp: October of the previous year; JJAp: Juli to August of the previous year; SONp: September to November of the previous year; VEGp: April to October of the previous year.

4.4 Conclusion: soil water supply as a dominating growth factor across scales

In this study, we explored the growth response of Norway spruce along a small-scale gradient of soil water supply. We used different levels of data aggregation to identify the relevance of the soil water regime and other microsite characteristics on the climate-growth relations in the Wüstebach catchment. We found significant impacts of soil water supply across all levels of data aggregation.

On the regional scale (WÜ chronology), the mean seasonal simulated root-zone pF showed similar (SONp, CALp) or slightly weaker (JJAp, VEGp) correlations with tree growth than the mean seasonal precipitation sums. However, on the monthly scale, growth variability was better explained by soil water supply than by monthly precipitation sums (Fig. 4.1b). This emphasizes the function of the soil as a buffer of precipitation and is in line with other studies comparing the growth response of trees to soil related wetness indices and to precipitation sums alone (Scharnweber et al., 2011; van der Maaten-Theunissen et al., 2013).

Across all 48 microsites (SN chronologies), the temperature-growth response was directly (simulated root-zone pF) and indirectly (planting density) related to local soil water supply. Cluster-internally, correlations between simulated root-zone pF and climate growth response were not observed. However, we identified the local soil water supply to be the most dominating factor in the formation of the growth clusters. Hence, cluster-internal feedbacks between SN climate signal strength and microsite characteristics already represent a second level of signal modification. Significant correlations of cluster-internal SN climate-signals were found for planting density, soil depth, and bulk density and hence for site characteristics that indirectly modify the availability of soil water for trees (Fig. 4.7).

Author contributions Inken Rabbel, Burkhard Neuwirth and Bernd Diekkrüger conceived and designed the study; Inken Rabbel performed the experiments and analyzed the data; Heye Bogena contributed to the discussion of methods and results; Inken Rabbel wrote the paper.

5 Synthesis

This dissertation was set up to analyze feedbacks in the soil-vegetation-atmosphere system of the Wüstebach catchment in the Eifel National Park in western Germany. Being exposed to rising temperatures and a precipitation shift from summer to winter (Zacharias et al., 2011), the region is highly susceptible to climate change (Simmer et al., 2015).

Respective changes in the water cycle are likely to drive present plant species towards their physiological limits (Bréda et al., 2006; Thompson et al., 2009). This particularly applies for the Wüstebach catchment, where the dominating species is Norway spruce (*Picea abies* [L.] H. Karst.), a tree species, which is known to be particularly vulnerable to drought (Boden et al., 2014; Bouriaud et al., 2005; Neuwirth, 2010; Zang et al., 2012, 2014).

To improve the understanding of climate change impacts on ecosystem processes and fluxes, ***this work aimed at***...

...a better understanding and quantification of species specific transpiration limitations under consideration of the soil conditions: An alternative water stress factor was derived from sap flow data and used to parameterize the Feddes water stress model (Feddes et al., 1978) for Norway spruce. The newly parameterized Feddes function was implemented in site specific water balance simulations (chapter 3; Rabbel et al. (2018a));

. . . a better understanding of the role of soil conditions for the climate growth response of trees: The Feddes parameters developed in chapter 3 were implemented in long-term water balance simulations. The resulting information on long-term spatiotemporal variations of soil water supply were set into context with tree ring data from 48 microsites (chapter 4; Rabbel et al. (2018b)).

The selection of the sap flow data processing procedure for chapter 3 was based on a comparative study of different data processing approaches (cf. chapter 2; Rabbel et al. (2016)). With that, the research presented in chapter 2 was a prerequisite for the subsequent investigations and aimed at ***a more reliable quantification of tree water use***.

Results and conclusions of chapter 2-4 are summarized below. Also, limitations of the studies and consequential future perspectives are discussed.

Chapter 2: Sap flow data processing

How does the parameterization of the Granier formula affect absolute sap flow density estimates on sub-daily, daily and (intra-) seasonal scales and which parameterization approach yields the most reliable results?

The parameterization of the Granier formula strongly affects absolute sap flow density estimates. The most critical parameter to determine is ΔT_{max}, which is the maximum temperature gradient between the heated probe and the reference probe below and represents a state of zero sap flux. Such zero flow conditions were originally assumed to occur every night (Granier, 1985, 1987). However, it has been proven that sap flow may continue throughout the night as well (Zeppel et al., 2013; Phillips et al., 2010; Daley and Phillips, 2006).

To improve nocturnal sap flow detection, researchers have developed empirical and physical approaches to determining ΔT_{max}. All approaches are based on the assumption that zero flow is related to erratically occurring ambient conditions. Empirical approaches presume the recurrence of zero flow within a given time period, during which ΔT_{max} is determined, while physically based approaches define ΔT_{max} when accompanying environmental measures suggest that presumed zero flow conditions have been met.

On the sub-daily scale, significant variations in sap flow density were observed between most analyzed ΔT_{max} determination approaches. During the day, variations among the approaches were generally higher than during the night. On the daily scale, empirical ΔT_{max} approaches yielded 9.8 to 31.5% higher sap flow densities than physically-based. Also, the data plausibility in terms of climate feedbacks was lower for empirically based approaches than for the physically-based. On the (intra-) seasonal scale, sap flow densities derived from empirical ΔT_{max} approaches exceeded those from physically-based by 10.5 to 57.8%.

In conclusion, the choice of the data processing may become a significant source of uncertainty in Granier-based sap flow estimates. Most reliable sap flow densities were derived from a physically-based parameterization of the Granier formular. The so-called Oishi baseliner (Oishi et al., 2008, 2016) defines a baseline upon ΔT_{max} values that were observed on days with particularly low vapor pressure deficit. In humid environments, as prevailing in the Wüstebach catchment, the classic daily ΔT_{max} determination also yielded reasonable results.

However, it has been shown that the uncertainty of Granier-based sap flow density estimates varies not only with the data processing approach, but also with the species the technique is applied to (Sun et al., 2012; Steppe et al., 2010). To improve the understanding of the natural and species-specific ΔT_{max} variability and consequences for Granier-based sap flow estimates, comparative studies including different sites and species, longer study periods, and a bigger sample size should be targeted in future studies.

Shortly after publication of the manuscript (Rabbel et al., 2016), this concern was indeed adressed by other researchers of the community. Peters et al. (2018) quantified uncertainties in Granier-based sap flux densities of two conifer species (*Larix decidua* Mill. and *Picea abies* (L.) Karst) caused by different ΔT_{max} determination approaches, dampening and sensor calibration. The study included data of 131 individual trees from 18 sites with climatic conditions ranging

from 1.4 to 19.8°C mean annual temperature and 428–1452 mm mean annual precipitation and confirmed the potential of a physically-based ΔT_{max} determination towards more reliable sap flow density estimates in conifers.

Respective investigations on deciduous trees could further improve our understanding of uncertainties in Granier-based sap flow measurements. However, the recent progress on the development of free software tools for physically-based Granier-type sap flow data processing (Oishi et al., 2016; Ward et al., 2017) is already an important step towards "more harmonized, transparent and reproducible sap flow data" (Peters et al., 2018).

Chapter 3: Water balance simulations

Does the implementation of sap flow data help to improve forest water balance simulations?

The implementation of sap flow data indeed improved the water balance simulations presented in chapter 3. However, first of all, the study confirmed the potential of sap flow measurements for the determination of water stress in trees. By combining soil hydrological simulations with a water stress factor derived from sap flow data of two DHC-stations with contrasting soil moisture regimes, the Feddes water stress model was parameterized for Norway spruce. The onset of drought stress was observed at a root-zone pressure head of -4100 cm water column (-402 kPa). With that, the trees showed a higher drought resistance than previously assumed. Maximum drought stress was determined for a root zone pressure head of -15,000 cm water column (-1471 kPa). This values is commonly accepted as a very general permanent wilting point (Kirkham, 2014); aeration stress was not observed.

Implementing the newly parametrized Feddes function in the soil hydrological model HYDRUS-1D improved the water balance simulations for a plot with temporarily limited soil water supply. Considering soil moisture patterns and species specific critical limits of soil water supply in the model setup can thus improve the simulation of transpiration fluxes on the catchment scale.

Probably, additional sap flow stations and a bigger sample size per plot would have provided a more detailed view on the stress conditions on site. Nevertheless, an extension of the measuring network is also a question of funds and logistics, and the simple sampling design provided a cost-efficient opportunity to gain valuable insights into the water stress of Norway spruce. Since no common alternative is available to quantify the water stress response of forest trees, the parameterization of the Feddes function on the basis of sap flow data and the resulting improvement of the forest water balance simulations is a good success.

In comparison to classic water stress factors, where actual evpotranspiration is simply divided by potential evapotranspiration (Blum, 2011), the sap flow based water stress concept even holds one considerable advantage: The reduction of transpiration due to stomata closing under atmospheric stress is not considered as soil water stress. This is particularly valuable for the determination of critical soil water limits for heat sensitive species, as for example Norway spruce. These close stomata on many days of the growing season to avoid disproportionate water loss due elevated vapour pressure deficits (Zweifel et al., 2002). Attributing this kind of

transpiration reduction to soil water shortage would be misleading and yield unrealistically high stress levels already at low levels of soil water depletion.

Summarizing the above, sap flow data can be used to quantify the water stress of trees. Implementing this in models is a promising way towards more realistic forest water balance simulations. These are needed to assess the role of forests in regional and transregional water cycles and to reduce the uncertainty in the prediction of forest traits under climate change (Ammer et al., 2018; Keenan, 2015; Thompson et al., 2009; Bréda et al., 2006). However, there is still a lack of studies determining soil water stress of forest trees. Therefore, more research on the species-specific water stress response of trees seems an important future perspective.

Chapter 4: Climate-growth response

How important are small-scale heterogeneities in soil water supply for the growth responsiveness of trees?

Small-scale heterogeneities in soil water supply significantly affect the growth responsiveness of trees. As shown in chapter 4, the local soil water regime and other microsite characteristics, which indirectly modify the water availability for trees, are dominating growth factors across different levels of data aggregation.

On the regional scale, inter-annual growth variations of Norway spruce were better explained by soil water supply than by monthly precipitation sums. Also the formation of growth clusters in the Wüstebach catchment mainly followed spatial patterns of soil water supply. While the driest cluster showed the strongest climate-growth reaction, the climate-growth response of the wettest cluster was almost completely insignificant. Across all investigated microsites within the test-site, the climate-growth response was directly (simulated soil suction of the root-zone) and indirectly (planting density) related to local soil water supply.

Hence, small-scale information on site conditions, particularly on soil water supply, should be considered in investigations of species specific growth limitations.

With the SoilNet at hand, the setting in the Wüstebach test-site provided ideal conditions to analyse the role of small-scale variations in soil water supply for the growth responsiveness of trees. Nevertheless, the synthetic character of the test-site, which is an even-aged plantation without considerable herb and shrub layer, has some drawbacks. It is well known that species diversity and stand structure have huge effects on the stress resilience and stress responsiveness of trees and forests (Thompson et al., 2009). These effects remained completely unconsidered in this study. To evaluate the transferability of the results, it would be interesting to conduct similar investigations in a mixed or near-natural forest system.

Also, it would be interesting to link the observed long-term feedbacks between tree growth and soil conditions with intra-annual growth dynamics. To this end, existing dendrometer data and wood anatomical features could be combined and set into context with intra-seasonal dynamics of soil water supply. Unfortunately, it was well beyond the scope of this dissertation to put the idea into practice. Nevertheless, it could be worth implementing it in future research projects.

This dissertation aimed at an improved uncertainty assessment for tree based transpiration estimates and at a better understanding of the species specific stress response of Norway spruce. Special emphasis was put on the response of transpiration and growth to climate forcings and soil water supply.

Summarizing the above, I think that these objectives were achieved. My comparative study on sap flow data processing approaches already found its way to the community and provided a hook for a comprehensive large-scale investigation of uncertainties in sap flow measurements. To me this is a great success. Also, I gained detailed insights into the stress response of Norway spruce. I was able to quantify species-specific transpiration limitations and found strong feedbacks between the climate-growth response of Norway spruce and small-scale variations in the soil water supply. Of course, all results are closely linked to the special setting of the Wüstebach test-site. The transferability to other sites and settings still needs to be proved. However, besides the Norway spruce related details, I contributed new methodological approaches, from which I hope that one or another will be recognized in future investigations.

Bibliography

Adams, H. D. and Kolb, T. E. (2004). Drought responses of conifers in ecotone forests of northern Arizona: Tree ring growth and leaf δ13C. *Oecologia*, 140(2):217–225.

Allen, R. G., Pereira, L. S., Raes, D., and Smith, M. (1998). Crop evapotranspiration: Guidelines for computing crop water requirements. *Irrigation and Drainage Papers*, 56. Food and Agriculture Organization of the United Nations, Rome, Italy.

Ammer, C., Fichtner, A., Fischer, A., Gossner, M., Meyer, P., Seidl, R., Thomas, F., Annighöfer, P., Kreyling, J., Ohse, B., Berger, U., Feldmann, E., Häberle, K.-H., Heer, K., Heinrichs, S., Huth, F., Krämer-Klement, K., Mölder, A., Mueller, J., Mund, M., Opgenoorth, L., Schall, P., Scherer-Lorenzen, M., Seidel, D., Vogt, J., and Wagner, S. (2018). Key ecological research questions for promoting the state of Central European forests. *Basic and Applied Ecology*, 3:3–25.

Ammer, C. and Wagner, S. (2005). An approach for modelling the mean fine-root biomass of Norway spruce stands. *Trees*, 19(2):145–153.

Arora, V. (2002). Modeling vegetation as a dynamic component in soil-vegetation-atmosphere transfer schemes and hydrological models. *Reviews of Geophysics*, 40(2):1006–1031.

Asbjornsen, H., Goldsmith, G. R., Alvarado-Barrientos, M. S., Rebel, K., Van Osch, F. P., Rietkerk, M., Chen, J., Gotsch, S., Tobón, C., Geissert, D. R., Gómez-Tagle, A., Vache, K., Dawson, T. E., Tobon, C., Geissert, D. R., Gomez-Tagle, A., Vache, K., and Dawson, T. E. (2011). Ecohydrological advances and applications in plant-water relations research: A review. *Journal of Plant Ecology*, 4(1-2):3–22.

Ashiq, M. and Anand, M. (2016). Spatial and temporal variability in dendroclimatic growth response of red pine (Pinus resinosa Ait.) to climate in northern Ontario, Canada. *Forest Ecology and Management*, 372:109–119.

Babst, F., Poulter, B., Trouet, V., Tan, K., Neuwirth, B., Wilson, R., Carrer, M., Grabner, M., Tegel, W., Levanic, T., Panayotov, M., Urbinati, C., Bouriaud, O., Ciais, P., and Frank, D. (2013). Site- and species-specific responses of forest growth to climate across the European continent. *Global Ecology and Biogeography*, 22(6):706–717.

Blum, A. (2011). *Plant breeding for water limited environments.* Springer, New York, USA.

Boden, S., Kahle, H.-P., von Wilpert, K., and Spiecker, H. (2014). Resilience of Norway spruce (Picea abies (L.) Karst) growth to changing climatic conditions in Southwest Germany. *Forest Ecology and Management*, 315:12–21.

Bogena, H., Borg, E., Brauer, A., Dietrich, P., Hajnsek, I., Heinrich, I., Kiese, R., Kunkel, R., Kunstmann, H., Merz, B., Priesack, E., Pütz, T., Schmid, H. P., Wollschläger, U., Vereecken, H., and Zacharias, S. (2016). TERENO: German network of terrestrial environmental observatories. *Journal of large-scale research facilities*, 52:1–8.

Bogena, H., Herbst, M., Huisman, J., Rosenbaum, U., Weuthen, A., and Vereecken, H. (2010). Potential of wireless sensor networks for measuring soil water content variability. *Vadose Zone Journal*, 9(4):1002–1013.

Bogena, H., Montzka, C., Huisman, J., Graf, A., Schmidt, M., Stockinger, M., von Hebel, C., Hendricks-Franssen, H., van der Kruk, J., Tappe, W., Lücke, A., Baatz, R., Bol, R., Groh, J., Pütz, T., Jakobi, J., Kunkel, R., Sorg, J., and Vereecken, H. (2018). The TERENO-Rur hydrological observatory: A multiscale multi-compartment research platform for the advancement of hydrological science. *Vadose Zone Journal*, 17(1):1–22.

Bogena, H. R., Bol, R., Borchard, N., Brüggemann, N., Diekkrüger, B., Drüe, C., Groh, J., Gottselig, N., Huisman, J. a., Lücke, A., Missong, A., Neuwirth, B., Pütz, T., Schmidt, M., Stockinger, M., Tappe, W., Weihermüller, L., Wiekenkamp, I., and Vereecken, H. (2014). A terrestrial observatory approach to the integrated investigation of the effects of deforestation on water, energy, and matter fluxes. *Science China Earth Sciences*, 57(1):61–75.

Bogena, H. R., Huisman, J. A., Baatz, R., Hendricks Franssen, H. J., and Vereecken, H. (2013). Accuracy of the cosmic-ray soil water content probe in humid forest ecosystems: The worst case scenario. *Water Resources Research*, 49(9):5778–5791.

Bonan, G. B. (2008). Forests and climate change: Forcings, feedbacks, and the climate benefits of forests. *Science*, 320(5882):1444–1449.

Bonan, G. B. and Shugart, H. H. (1989). Ecological processes in boreal forests. *Annual Review of Ecology, Evolution, and Systematics*, 20:1–28.

Bouriaud, O., Leban, J.-M., Bert, D., and Deleuze, C. (2005). Intra-annual variations in climate influence growth and wood density of Norway spruce. *Tree Physiology*, 25(6):651–660.

Boyer, J. S. (1985). Water Transport. *Annual Review of Plant Physiology*, 36(1):473–516.

Braun, S., Thomas, V. F., Quiring, R., and Flückiger, W. (2010). Does nitrogen deposition increase forest production? The role of phosphorus. *Environmental Pollution*, 158(6):2043–2052.

Bräuning, A. and Steppe, K. (2016). Editorial note for the special issue on 'Sap flow and hydraulic functioning' of TREES: structure and function. *Trees*, 30(1):1–3.

Bréda, N., Huc, R., Granier, A., and Dreyer, E. (2006). Temperate forest trees and stands under severe drought: a review of ecophysiological responses, adaptation processes and long-term consequences. *Annals of Forest Science*, 63(6):625–644.

Bush, S. E., Hultine, K. R., Sperry, J. S., and Ehleringer, J. R. (2010). Calibration of thermal dissipation sap flow probes for ring- and diffuse-porous trees. *Tree Physiology*, 30(12):1545–54.

Calder, I. R. (1998). Water use by forests, limits and controls. *Tree Physiology*, 18(8–9):625–631.

Carrer, M. (2011). Individualistic and time-varying tree-ring growth to climate sensitivity. *PLoS One*, 6(7):e22813.

Carrer, M. and Urbinati, C. (2004). Age-dependent tree-ring growth responses to climate in Larix decidua and Pinus cembra. *Ecology*, 85(3):730–740.

Cermák, J., Deml, M., and Penka, M. (1973). A new method of sap flow rate determination in trees. *Biologia Plantarum*, 15(3):171–178.

Čermák, J., Kucera, J., Bauerle, W. L., Phillips, N., and Hinckley, T. M. (2007). Tree water storage and its diurnal dynamics related to sap flow and changes in stem volume in old-growth Douglas-fir trees. *Tree Physiology*, 27(2):181–198.

Čermák, J., Kučera, J., and Nadezhdina, N. (2004). Sap flow measurements with some thermodynamic methods, flow integration within trees and scaling up from sample trees to entire forest stands. *Trees*, 18(5):529–546.

Cienciala, E., Lindroth, A., Cermák, J., Hällgren, J.-E., and Kucera, J. (1994). The effects of water availability on transpiration, water potential and growth of Picea abies during a growing season. *Journal of Hydrology*, 155:57–71.

Clausnitzer, F., Köstner, B., Schwärzel, K., and Bernhofer, C. (2011). Relationships between canopy transpiration, atmospheric conditions and soil water availability - Analyses of long-term sap-flow measurements in an old Norway spruce forest at the Ore Mountains/Germany. *Agricultural and Forest Meteorology*, 151(8):1023–1034.

Cocozza, C., Palombo, C., Tognetti, R., La Porta, N., Anichini, M., Giovannelli, A., and Emiliani, G. (2016). Monitoring intra-annual dynamics of wood formation with microcores and dendrometers in Picea abies at two different altitudes. *Tree Physiology*, 36(7):832–846.

Cornelissen, T. (2016). 3D-Modeling of unsaturated flow dynamics and patterns. Potentials and limitations at different spatial and temporal scales. *Dissertation*, Rheinische Friedrich-Wilhelms Universität Bonn, Germany.

Cornelissen, T., Diekkrüger, B., and Bogena, H. R. (2014). Significance of scale and lower boundary condition in the 3D simulation of hydrological processes and soil moisture variability in a forested headwater catchment. *Journal of Hydrology*, 516:140–153.

Cruiziat, P., Cochard, H., and Ameglio, T. (2002). Hydraulic architecture of trees: main concepts and results. *Annals of Forest Science*, 59(7):723–752.

Daley, M. J. and Phillips, N. G. (2006). Interspecific variation in nighttime transpiration and stomatal conductance in a mixed New England deciduous forest. *Tree Physiology*, 26(4):411–419.

Davis, T. W., Kuo, C.-M., Liang, X., and Yu, P.-S. (2012). Sap flow sensors: Construction, quality control and comparison. *Sensors*, 12(1):954–971.

De Schepper, V. and Steppe, K. (2010). Development and verification of a water and sugar transport model using measured stem diameter variations. *Journal of Experimental Botany*, 61(8):2083–2099.

Deckers, J. (2010). Feinkartierung eines Fichtenforstes als Basis für ein Langzeitmonitoring. *Natur in NRW*, 35(4):26–29.

Deslauriers, A., Fonti, P., Rossi, S., Rathgeber, C. B. K., and Gričar, J. (2017). *Ecophysiology and plasticity of wood and phloem formation.* In: Amoroso, M., Daniels, L., Baker, P., and Camarero, J. (Eds.): Dendroecology: Tree-ring analyses applied to ecological studies. Ecological Studies 231, Springer, Dordrecht, The Netherlands:13–33.

Deslauriers, A., Rossi, S., and Anfodillo, T. (2007). Dendrometer and intra-annual tree growth: What kind of information can be inferred? *Dendrochronologia*, 25(2):113–124.

Diekkrüger, B., Söndgerath, D., Kersebaum, K., and McVoy, C. (1995). Validity of agroecosystem models a comparison of results of different models applied to the same data set. *Ecological Modelling*, 81:3–29.

Drew, D. M. and Downes, G. M. (2009). The use of precision dendrometers in research on daily stem size and wood property variation: A review. *Dendrochronologia*, 27(2):159–172.

Drüe, C., Graf, A., Heinemann, G., and Pütz, T. (2012). *Observation of atmosphere-forest exchange processes at the new TERENO site Wüstebach.* Presentation at the 20th Symposium on boundary layers and turbulence, 09-13 July 2012, Boston, USA.

Ecomatik (2000). *SF-L Sap flow sensor. User manual version 1.3.* Ecomatik Umweltmess- und Datentechnik, Munich, Germany.

Esper, J., Frank, D. C., and Luterbacher, J. (2007). *On selected issues and challenges in dendroclimatology.* In: Kienast, F., Wildi, O., and Gosh, S. (Eds.): A changing world. Landscape Series 8, Springer, Dordrecht, The Netherlands:113–132.

Etmann, M. (2009). Dendrologische Aufnahmen im Wassereinzugsgebiet Oberer Wüstebach anhand verschiedener Mess- und Schätzverfahren. *Diploma thesis*, Westfälische Wilhelms-Universität Münster, Germany.

Fang, Z., Bogena, H., Kollet, S., Koch, J., and Vereecken, H. (2015). Spatio-temporal validation of long-term 3D hydrological simulations of a forested catchment using empirical orthogonal functions and wavelet coherence analysis. *Journal of Hydrology*, 529:1754–1767.

Feddes, R. A., Kowalik, P. J., and Zaradny, H. (1978). *Simulation of field water use and crop yield.* Centre for Agricultural Publishing and Documentaion, Wageningen, The Netherlands.

Fiora, A. and Cescatti, A. (2006). Diurnal and seasonal variability in radial distribution of sap flux density: implications for estimating stand transpiration. *Tree Physiology*, 26(9):1217–1225.

Fischer, S. and Neuwirth, B. (2012). Climate sensitivity of Douglas-fir in Eifel and Kellerwald. *Allgemeine Forst- und Jagdzeitung*, 183(1-2):23–33.

Ford, C. R., Hubbard, R. M., Kloeppel, B. D., and Vose, J. M. (2007). A comparison of sap flux-based evapotranspiration estimates with catchment-scale water balance. *Agricultural and Forest Meteorology*, 145(3-4):176–185.

Ford, C. R., McGuire, M. A., Mitchell, R. J., and Teskey, R. O. (2004). Assessing variation in the radial profile of sap flux density in Pinus species and its effect on daily water use. *Tree Physiology*, 24(3):241–249.

Friedrichs, D. A., Neuwirth, B., Winiger, M., and Löffler, J. (2009). Methodologically induced differences in oak site classifications in a homogeneous tree-ring network. *Dendrochronologia*, 27(1):21–30.

Galván, J. D., Camarero, J. J., and Gutiérrez, E. (2014). Seeing the trees for the forest: Drivers of individual growth responses to climate in Pinus uncinata mountain forests. *Journal of Ecology*, 102(5):1244–1257.

Gartner, K., Nadezhdina, N., Englisch, M., Čermak, J., and Leitgeb, E. (2009). Sap flow of birch and Norway spruce during the European heat and drought in summer 2003. *Forest Ecology and Management*, 258(5):590–599.

Gebauer, T., Horna, V., and Leuschner, C. (2008). Variability in radial sap flux density patterns and sapwood area among seven co-occurring temperate broad-leaved tree species. *Tree Physiology*, 28(12):1821–1830.

Gebauer, T., Horna, V., and Leuschner, C. (2012). Canopy transpiration of pure and mixed forest stands with variable abundance of European beech. *Journal of Hydrology*, 442-443:2–14.

Gleason, K. E., Bradford, J. B., Bottero, A., D'Amato, A. W., Fraver, S., Palik, B. J., Battaglia, M. A., Iverson, L., Kenefic, L., and Kern, C. C. (2017). Competition amplifies drought stress in forests across broad climatic and compositional gradients. *Ecosphere*, 8(7):e01849.

Gottselig, N., Wiekenkamp, I., Weihermüller, L., Brüggemann, N., Berns, A. E., Bogena, H. R., Borchard, N., Klumpp, E., Lücke, A., Missong, A., Pütz, T., Vereecken, H., Huisman, J. A., and Bol, R. (2017). A three-dimensional view on soil biogeochemistry: A dataset for a forested headwater catchment. *Journal of Environmental Quality*, 46(1):210–218.

Graf, A., Bogena, H. R., Drüe, C., Hardelauf, H., Pütz, T., Heinemann, G., and Vereecken, H. (2014). Spatiotemporal relations between water budget components and soil water content in a forested tributary catchment. *Water Resources Research*, 50:4840–4847.

Granier, A. (1985). Une nouvelle méthode pour la mesure du flux de séve brute dans le tronc des arbres. *Annales des Sciences Forestieres*, 42(2):193–200.

Granier, A. (1987). Evaluation of transpiration in a Douglas-fir stand by means of sap flow measurements. *Tree Physiology*, 3(4):309–320.

Granier, A., Biron, P., Breda, N., Pontailler, J.-Y., and Saugier, B. (1996). Transpiration of trees and forest stands: short and long-term monitoring using sapflow methods. *Global Change Biology*, 2(3):265–274.

Granier, A., Bréda, N., Biron, P., and Villette, S. (1999). A lumped water balance model to evaluate duration and intesity of drought constraints in forest stands. *Ecological Modeling*, 116:269–283.

Granier, A., Loustau, D., and Breda, N. (2000). A generic model of forest canopy conductance dependent on climate, soil water availability and leaf area index. *Annals of Forest Science*, 57(8):755–765.

Granier, A., Reichstein, M., Breda, N., Janssens, I. A., Falge, E., Ciais, P., Grünwald, T., Aubinet, M., Berbigier, P., Bernhofer, C., Buchmann, N., Facini, O., Grassi, G., Heinesch, B., Ilvesniemi, H., Keronen, P., Knohl, A., Köstner, B., Lagergren, F., Lindroth, A., Longdoz, B., Loustau, D., Mateus, J., Montagnani, L., Nys, C., Moors, E., Papale, D., Peiffer, M., Pilegaard, K., Pita, G., Pumpanen, J., Rambal, S., Rebmann, C., Rodrigues, A., Seufert, G., Tenhunen, J., Vesala, T., and Wang, Q. (2007). Evidence for soil water control on carbon and water dynamics in European forests during the extremely dry year: 2003. *Agricultural and Forest Meteorology*, 143(1-2):123–145.

Gundersen, P., Callesen, I., and De Vries, W. (1998). Nitrate leaching in forest ecosystems is related to forest floor C/N ratios. *Environmental Pollution*, 102:403–407.

Hacke, U. G. and Sperry, J. S. (2015). Functional and ecological xylem anatomy. *Perspectives in Plant Ecology, Evolution and Systematics*, 4(2):97–115.

Hammel, K. and Kennel, M. (2001). *Charakterisisierung und Analyse der Wasserverfügbarkeit und des Wasserhaushalts von Waldstandorten in Bayern mit dem Simulationsmodell BROOK90.* Forstliche Forschungsberichte München 185, Munich, Germany.

Hanewinkel, M., Cullmann, D. A., Schelhaas, M. J., Nabuurs, G. J., and Zimmermann, N. E. (2013). Climate change may cause severe loss in the economic value of European forest land. *Nature Climate Change*, 3(3):203–207.

Hartl-Meier, C., Zang, C., Dittmar, C., Esper, J., Göttlein, A., and Rothe, A. (2014). Vulnerability of Norway spruce to climate change in mountain forests of the European Alps. *Climate Research*, 60(2):119–132.

Helama, S. (2015). Expressing tree-ring chronology as age-standardized growth measurements. *Forest Science*, 61(5):817–828.

Helama, S., Läänelaid, A., Bijak, S., and Jaagus, J. (2016). Contrasting tree-ring growth response of Picea abies to climate variability in western and eastern Estonia. *Geografiska Annaler, Series A: Physical Geography*, 98(2):155–167.

Helmisaari, H.-s., Derome, J., Nöjd, P., and Kukkola, M. (2007). Fine root biomass in relation to site and stand characteristics in Norway spruce and Scots pine stands. *Trees*, 27:1493–1504.

Hentschel, R., Hommel, R., Poschenrieder, W., Grote, R., Holst, J., Biernath, C., Gessler, A., and Priesack, E. (2016). Stomatal conductance and intrinsic water use efficiency in the drought year 2003 - A case study of a well-established forest stand of European beech. *Trees*, 30:153–174.

Holmes, R. L. (1983). Computer-assisted quality control in tree-ring dating and measurement. *Tree-Ring Bulletin*, 43:69–78.

Hopmans, J. W. and Stricker, J. N. M. (1989). Stochastic analysis of soil water regime in a watershed. *Journal of Hydrology*, 105:57–84.

Huang, M., Lee Barbour, S., Elshorbagy, A., Zettl, J., and Cheng Si, B. (2011). Water availability and forest growth in coarse-textured soils. *Canadian Journal of Soil Science*, 91(2):199–210.

Ibáñez, I., Zak, D. R., Burton, A. J., and Pregitzer, K. S. (2018). Anthropogenic nitrogen deposition ameliorates the decline in tree growth caused by a drier climate. *Ecology*, 99(2):411–420.

Jackson, L. W. R. (1952). Radial Growth of Forest Trees in the Georgia Piedmont. *Ecology*, 33(3):336–341.

Jiang, X., Huang, J.-G., Stadt, K., Comeau, P., and Chen, H. (2016). Spatial climate-dependent growth response of boreal mixedwood forest in western Canada. *Global and Planetary Change*, 139:141–150.

Johnson, S. and Schweingruber, F. (2012). *Trees and wood in dendrochronology: Morphological, anatomical, and tree-ring analytical characteristics of trees frequently used in dendrochronology.* Springer, Berlin, Heidelberg, Germany.

Jones, H. (1990). Physiological aspects of the control of water status in horticultural crops. *Horticultural Science*, 25(1):19–26.

Jones, H. G. (2007). Monitoring plant and soil water status: Established and novel methods revisited and their relevance to studies of drought tolerance. *Journal of Experimental Botany*, 58(2):119–130.

Kaennel, M. and Schweingruber, F. (1995). *Multilingual glossary of dendrochronology.* Verlag Paul Haupt, Berne, Switzerland.

Kazda, M. (1990). Indications of unbalanced nitrogen nutrition of Norway spruce stands. *Plant and Soil*, 128(1):97–101.

Keenan, R. J. (2015). Climate change impacts and adaptation in forest management: a review. *Annals of Forest Science*, 72(2):145–167.

Kirkham, M. (2014). *Principles of soil and plant water relations.* Elsevier, Amsterdam, Waltham, San Diego.

Kool, D., Agam, N., Lazarovitch, N., Heitman, J. L., Sauer, T. J., and Ben-Gal, A. (2014). A review of approaches for evapotranspiration partitioning. *Agricultural and Forest Meteorology*, 184:56–70.

Köstner, B. (2001). Evaporation and transpiration from forests in Central Europe – relevance of patch-level studies for spatial scaling. *Meteorology and Atmospheric Physics*, 76(1):69–82.

Köstner, B., Biron, P., Siegwolf, R., and Granier, A. (1996). Estimates of water vapor flux and canopy conductance of Scots pine at the tree level utilizing different xylem sap flow methods. *Theoretical and Applied Climatology*, 53:105–113.

Köstner, B. and Clausnitzer, F. (2011). Die Transpiration eines Fichten – und Buchenbestandes unter Bodentrockenheit im Tharandter Wald. *Waldökologie, Landschaftsforschung und Naturschutz*, 12:29–35.

Köstner, B., Falge, E., and Tenhunen, J. D. (2002). Age-related effects on leaf area/sapwood area relationships, canopy transpiration and carbon gain of Norway spruce stands (Picea abies) in the Fichtelgebirge, Germany. *Tree Physiology*, 22(8):567–574.

Köstner, B., Granier, A., and Cermák, J. (1998). Sapflow measurements in forest stands: methods and uncertainties. *Annals of Forest Science*, 55(1-2):13–27.

Kottek, M., Grieser, J., Beck, C., Rudolf, B., and Rubel, F. (2006). World map of the Köppen-Geiger climate classification updated. *Meteorologische Zeitschrift*, 15:259–263.

Krokene, P., Nagy, N. E., and Krekling, T. (2008). *Traumatic resin ducts and polyphenolic parenchyma cells in conifers.* In: Schaller, S. (Ed.): Induced plant resistance to herbivory. Springer, Dordrecht, The Netherlands :147–169.

Lagergren, F. and Lindroth, A. (2002). Transpiration response to soil moisture in pine and spruce trees in Sweden. *Agricultural and Forest Meteorology*, 112(2):67–85.

Lehmkuhl, F., Loibl, D., and Borchardt, H. (2010). Geomorphological map of the Wüstebach (Nationalpark Eifel, Germany) - an example of human impact on mid-European mountain areas. *Journal of Maps*, 6(1):520–530.

Leo, M., Oberhuber, W., Schuster, R., Grams, T. E. E., Matyssek, R., and Wieser, G. (2014). Evaluating the effect of plant water availability on inner alpine coniferous trees based on sap flow measurements. *European Journal of Forest Research*, 133(4):691–698.

Leterme, B., Mallants, D., and Jacques, D. (2012). Sensitivity of groundwater recharge using climatic analogues and HYDRUS-1D. *Hydrology and Earth System Sciences*, 16(8):2485–2497.

Lévesque, M., Rigling, A., Bugmann, H., Weber, P., and Brang, P. (2014). Growth response of five co-occurring conifers to drought across a wide climatic gradient in Central Europe. *Agricultural and Forest Meteorology*, 197:1–12.

Linares, J. C., Camarero, J. J., and Carreira, J. A. (2010). Competition modulates the adaptation capacity of forests to climatic stress: Insights from recent growth decline and death in relict stands of the Mediterranean fir Abies pinsapo. *Journal of Ecology*, 98(3):592–603.

Lu, P., Urban, L., and Zhao, P. (2004). Granier's thermal dissipation probe (TDP) method for measuring sap flow in trees: Theory and practice. *Acta Botanica Sinica*, 46(6):631–646.

Lundblad, M., Lagergen, F., and Lindroth, A. (2001). Evaluation of heat balance and heat dissipation methods for sapflow measurements in pine and spruce. *Annals of Forest Science*, 58:625–638.

Lundblad, M. and Lindroth, A. (2002). Stand transpiration and sapflow density in relation to weather, soil moisture and stand characteristics. *Basic and Applied Ecology*, 3(3):229–243.

Mäkinen, H., Nöjd, P., Kahle, H.-P., Neumann, U., Tveite, B., Mielikäinen, K., Röhle, H., and Spiecker, H. (2002). Radial growth variation of Norway spruce (Picea abies (L.) Karst.) across latitudinal and altitudinal gradients in central and northern Europe. *Forest Ecology and Management*, 171(3):243–259.

Martín-Benito, D., Cherubini, P., Del Río, M., and Cañellas, I. (2008). Growth response to climate and drought in Pinus nigra Arn. trees of different crown classes. *Trees*, 22(3):363–373.

Michelot, A., Simard, S., Rathgeber, C., Dufrêne, E., and Damesin, C. (2012). Comparing the intra-annual wood formation of three European species (Fagus sylvatica, Quercus petraea and Pinus sylvestris) as related to leaf phenology and non-structural carbohydrate dynamics. *Tree Physiology*, 32(8):1033–1045.

Mohren, G. M. J., van den Burg, J., Burger, F. W., and Oterdoom, J. H. (1986). Phosphorus deficiency induced by nitrogen input in Douglas fir stands. *Nederlands Bosbouwtijdschrift*, 58(9):238–245.

Moore, G. W., Cleverly, J. R., and Owens, M. K. (2008). Nocturnal transpiration in riparian Tamarix thickets authenticated by sap flux, eddy covariance and leaf gas exchange measurements. *Tree Physiology*, 28(4):521–528.

Moore, G. W. and Owens, M. K. (2011). Transpirational water loss in invaded and restored semiarid riparian forests. *Restoration Ecology*, 20(3):1–6.

Nadezhdina, N., Cermák, J., and Ceulemans, R. (2002). Radial patterns of sap flow in woody stems of dominant and understory species: scaling errors associated with positioning of sensors. *Tree Physiology*, 22(13):907–918.

Nehrbass-Ahles, C., Babst, F., Klesse, S., Nötzli, M., Bouriaud, O., Neukom, R., Dobbertin, M., and Frank, D. (2014). The influence of sampling design on tree-ring-based quantification of forest growth. *Global Change Biology*, 20(9):2867–2885.

Neuwirth, B. (2010). *Interannuelle Klima-Wachstums-Beziehungen zentraleuropäischer Bäume von AD 1901 bis 1971*. Edwin Ferger Verlag, Bergisch Gladbach, Germany.

Oishi, A. C., Hawthorne, D. A., and Oren, R. (2016). Baseliner: An open-source, interactive tool for processing sap flux data from thermal dissipation probes. *SoftwareX*, 5:139–143.

Oishi, A. C., Oren, R., and Stoy, P. C. (2008). Estimating components of forest evapotranspiration: A footprint approach for scaling sap flux measurements. *Agricultural and Forest Meteorology*, 148(11):1719–1732.

Oliveras, I. and Llorens, P. (2001). Medium-term sap flux monitoring in a Scots pine stand: analysis of the operability of the heat dissipation method for hydrological purposes. *Tree Physiology*, 21(7):473–480.

Papale, D., Reichstein, M., Aubinet, M., Canfora, E., Bernhofer, C., Kutsch, W., Longdoz, B., Rambal, S., Valentini, R., Vesala, T., Papale, D., Reichstein, M., Aubinet, M., Canfora, E., and Bernhofer, C. (2006). Towards a standardized processing of net ecosystem exchange measured with eddy covariance technique: algorithms and uncertainty estimation. *Biogeosciences*, 3(4):571–583.

Perämäki, M. (2005). A physical analysis of sap flow dynamics in trees. *Dissertation*, University of Helsinki, Finland.

Peters, R. L., Fonti, P., Frank, D. C., Poyatos, R., Pappas, C., Kahmen, A., Carraro, V., Prendin, A. L., Schneider, L., Baltzer, J. L., Baron-Gafford, G. A., Dietrich, L., Heinrich, I., Minor, R. L., Sonnentag, O., Matheny, A. M., Wightman, M. G., and Steppe, K. (2018). Quantification of uncertainties in conifer sap flow measured with the thermal dissipation method. *New Phytologist*, 219(4):1283–1299.

Phillips, N., Oren, R., and Zimmermann, R. (1996). Radial patterns of xylem sap flow in non-, diffuse- and ring-porous tree species. *Plant, Cell and Environment*, 19(8):983–990.

Phillips, N. G., Lewis, J. D., Logan, B. A., and Tissue, D. T. (2010). Inter- and intra-specific variation in nocturnal water transport in Eucalyptus. *Tree Physiology*, 30(5):586–596.

Pilcher, J. (2013). *Sample preparation, cross-dating, and measurement.* In: Cook, E., and Kairiukstis, L. (Eds.): Methods of dendrochronology: Applications in the environmental sciences. Springer, Dordrecht, The Netherlands:40–50.

Piutti, E. and Cescatti, A. (1997). A quantitative analysis of the interactions between climatic response and intraspecific competition in european beech. *Canadian Journal of Forest Research*, 27(3):277–284.

Pretzsch, H. and Dieler, J. (2011). The dependency of the size-growth relationship of Norway spruce (Picea abies [L.] Karst.) and European beech (Fagus sylvatica [L.]) in forest stands on long-term site conditions, drought events, and ozone stress. *Trees*, 25(3):355–369.

Primicia, I., Camarero, J. J., Janda, P., Čada, V., Morrissey, R. C., Trotsiuk, V., Bače, R., Teodosiu, M., and Svoboda, M. (2015). Age, competition, disturbance and elevation effects on tree and stand growth response of primary Picea abies forest to climate. *Forest Ecology and Management*, 354:77–86.

Puhe, J. (2003). Growth and development of the root system of Norway spruce (Picea abies) in forest stands: A review. *Forest Ecology and Management*, 175:253–273.

R Core Team (2018). *R: A Language and Environment for Statistical Computing.* R Foundation for Statistical Computing, Vienna, Austria.

Rabbel, I., Bogena, H., Neuwirth, B., and Diekkrüger, B. (2018a). Using sap flow data to parameterize the feddes water stress model for Norway spruce. *Water*, 10(3).

Rabbel, I., Diekkrüger, B., Voigt, H., and Neuwirth, B. (2016). Comparing ΔT_{max} determination approaches for Granier-based sapflow estimations. *Sensors*, 16(1):1–16.

Rabbel, I., Neuwirth, B., Bogena, H., and Diekkrüger, B. (2018b). Exploring the growth response of norway spruce (picea abies) along a small-scale gradient of soil water supply. *Dendrochronologia*, 52:123–130.

Regalado, C. M. and Ritter, A. (2007). An alternative method to estimate zero flow temperature differences for Granier's thermal dissipation technique. *Tree Physiology*, 27(8):1093–1102.

Renninger, H. J. and Schäfer, K. V. R. (2012). Comparison of tissue heat balance- and thermal dissipation-derived sap flow measurements in ring-porous oaks and a pine. *Frontiers in Plant Science*, 3:1–9.

Reyes-García, C., Andrade, J. L., Simá, J. L., Us-Santamaría, R., and Jackson, P. C. (2012). Sapwood to heartwood ratio affects whole-tree water use in dry forest legume and non-legume trees. *Trees*, 26(4):1317–1330.

Rezanezhad, F., Price, J. S., Quinton, W. L., Lennartz, B., Milojevic, T., and Van Cappellen, P. (2016). Structure of peat soils and implications for water storage, flow and solute transport: A review update for geochemists. *Chemical Geology*, 429:75–84.

Richter, D. (1995). *Ergebnisse methodischer Untersuchungen zur Korrektur des systematischen Meßfehlers des Hellmann Niederschlagsmessers.* Berichte des Deutschen Wetterdienstes 194, Offenbach, Germany.

Ringgaard, R., Herbst, M., and Friborg, T. (2012). Partitioning of forest evapotranspiration: The impact of edge effects and canopy structure. *Agricultural and Forest Meteorology*, 166-167:86–97.

Ringgaard, R., Herbst, M., and Friborg, T. (2014). Partitioning forest evapotranspiration: Interception evaporation and the impact of canopy structure, local and regional advection. *Journal of Hydrology*, 517:677–690.

Rinn, F. (2003). *TSAP-Win. Time series analysis and presentation for dendrochronology and related applications. Version 4.64 for Microsoft Windows.* Rinntech, Heidelberg, Germany.

Rosenbaum, U., Bogena, H. R., Herbst, M., Huisman, J. a., Peterson, T. J., Weuthen, A., Western, a. W., and Vereecken, H. (2012). Seasonal and event dynamics of spatial soil moisture patterns at the small catchment scale. *Water Resources Research*, 48(10):1–22.

Rosenqvist, L., Hansen, K., Vesterdal, L., and van der Salm, C. (2010). Water balance in afforestation chronosequences of common oak and Norway spruce on former arable land in Denmark and southern Sweden. *Agricultural and Forest Meteorology*, 150(2):196–207.

Sadras, V. O. and Milroy, S. P. (1996). Soil-water treshold for the responses of leaf expansion and gas exchange: a review. *Field Crop Research*, 47:253–266.

Sakuratani, T. (1981). A heat balance method for measuring water flux in the stem of intact plants. *Journal of Agricultural Meteorology*, 37:9–17.

Scharnweber, T., Manthey, M., Criegee, C., Bauwe, A., Schröder, C., and Wilmking, M. (2011). Drought matters - Declining precipitation influences growth of Fagus sylvatica L. and Quercus robur L. in north-eastern Germany. *Forest Ecology and Management*, 262(6):947–961.

Schmid, I. (2002). The influence of soil type and interspecific competition on the fine root system of Norway spruce and European beech. *Basic and Applied Ecology*, 3(4):339–346.

Schwärzel, K., Feger, K.-H., Häntzschel, J., Menzer, A., Spank, U., Clausnitzer, F., Köstner, B., and Bernhofer, C. (2009). A novel approach in model-based mapping of soil water conditions at forest sites. *Forest Ecology and Management*, 258(10):2163–2174.

Schwärzel, K., Šimůnek, J., Van Genuchten, M. T., and Wessolek, G. (2006). Measurement and modeling of soil-water dynamics and evapotranspiration of drained peatland soils. *Journal of Plant Nutrition and Soil Science*, 169(6):762–774.

Schweingruber, F. (1990). *Anatomie europäischer Hölzer: ein Atlas zur Bestimmung europäischer Baum-, Strauch-, und Zwergstrauchhölzer*. Verlag Paul Haupt, Berne, Switzerland.

Schweingruber, F., Kairiukstis, L., and Shiyatov, S. (2013). *Sample selection*. In: Cook, E., and Kairiukstis, L. (Eds.): Methods of dendrochronology: Applications in the environmental sciences. Springer, Dordrecht, The Netherlands:23–34.

Schweingruber, F. H. (1988). *Tree rings: basics and applications of dendrochronology*. Kluwer Academic Publishers, Dordrecht.

Schweingruber, F. H. (1996). *Tree rings and environment: dendroecology*. Verlag Paul Haupt, Berne, Switzerland.

Schweingruber, F. H. (2007). *Wood Structure and Environment*. Springer, Berlin, Heidelberg, Germany.

Sciuto, G. and Diekkrüger, B. (2010). Influence of soil heterogeneity and spatial discretization on catchment water balance modeling. *Vadose Zone Journal*, 9(4):955–969.

Seith, B., George, E., Marschner, H., Wallenda, T., Schaeffer, C., Einig, W., Wingler, A., and Hampp, R. (1996). Effects of varied soil nitrogen supply on Norway spruce (Picea abies [L.] Karst.): I. Shoot and root growth and nutrient uptake. *Plant and Soil*, 184(2):291–298.

Simmer, C., Thiele-Eich, I., Masbou, M., Amelung, W., Bogena, H., Crewell, S., Diekkrüger, B., Ewert, F., Hendricks Franssen, H. J., Huisman, J. A., Kemna, A., Klitzsch, N., Kollet, S., Langensiepen, M., Löhnert, U., Rahman, A. S., Rascher, U., Schneider, K., Schween, J., Shao, Y., Shrestha, P., Stiebler, M., Sulis, M., Vanderborght, J., Vereecken, H., Van Der Kruk, J., Waldhoff, G., and Zerenner, T. (2015). Monitoring and modeling the terrestrial system from pores to catchments: The transregional collaborative research center on patterns in the soil-vegetation-atmosphere system. *Bulletin of the American Meteorological Society*, 96(10):1765–1787.

Šimůnek, J., M. Šejna, A., Saito, H., Sakai, M., and Genuchten, M. T. V. (2013). The HYDRUS-1D software package for simulating the movement of water, heat, and multiple solutes in variably saturated media, Version 4.17, HYDRUS Software Series 3, Department of Environmental Sciences, University of California Riverside, Riverside, USA.

Smith, D. M. and Allen, S. J. (1996). Measurement of sap flow in plant stems. *Journal of Experimental Botany*, 47(305):1833–1844.

Střelcová, K., Kurjak, D., Leštianska, A., Kovalčíková, D., Ditmarová, u., Škvarenina, J., and Ahmed, Y. A. R. (2013). Differences in transpiration of Norway spruce drought stressed trees and trees well supplied with water. *Biologia*, 68(6):1118–1122.

Steppe, K., De Pauw, D. J. W., Doody, T. M., and Teskey, R. O. (2010). A comparison of sap flux density using thermal dissipation, heat pulse velocity and heat field deformation methods. *Agricultural and Forest Meteorology*, 150(7-8):1046–1056.

Steppe, K., De Pauw, D. J. W., Lemeur, R., and Vanrolleghem, A. (2005). A mathematical model linking tree sap flow dynamics to daily stem diameter fluctuations and radial stem growth. *Tree Physiology*, 26:257–273.

Steppe, K., Vandegehuchte, M. W., Tognetti, R., and Mencuccini, M. (2015). Sap flow as a key trait in the understanding of plant hydraulic functioning. *Tree Physiology*, 35(4):341–345.

Stokes, M. A. and Smiley, T. L. (1968). *An introduction to tree-ring dating*. University of Arizona Press, Tucson, USA.

Sullivan, P. F. and Csank, A. Z. (2016). Contrasting sampling designs among archived datasets: Implications for synthesis efforts. *Tree Physiology*, 36(9):1057–1059.

Sun, H., Aubrey, D. P., and Teskey, R. O. (2012). A simple calibration improved the accuracy of the thermal dissipation technique for sap flow measurements in juvenile trees of six species. *Trees*, 26(2):631–640.

Tatarinov, F. A., Kučera, J., and Cienciala, E. (2005). The analysis of physical background of tree sap flow measurement based on thermal methods. *Measurement Science and Technology*, 16(5):1157–1169.

Thelin, G., Rosengren-Brinck, U., Nihlgård, B., and Barkman, A. (1998). Trends in needle and soil chemistry of Norway spruce and Scots pine stands in South Sweden 1985-1994. *Environmental Pollution*, 99(2):149–158.

Thomas, F., Rzepecki, A., Lücke, A., Wiekenkamp, I., Rabbel, I., and Pütz, T. (2018). Growth and wood isotopic signature of Norway spruce (Picea abies) along a small-scale gradient of soil moisture. *Tree Physiology*, tpy100.

Thompson, I., Mackey, B., McNulty, S., and Mosseler, A. (2009). *Forest resilience, biodiversity, and climate change: a synthesis of the biodiversity/resilience/stability relationship in forest ecosystems.* Secretariat of the Convention on Biological Diversity, Montreal, Canada, Technical Series 43:1-67.

Tjoelker, M. G., Boratyński, A., and Bugala, W. (2007). *Biology and Ecology of Norway Spruce*. Springer, Dordrecht, The Netherlands.

Tromp-van Meerveld, H. J. and McDonnell, J. J. (2006). On the interrelations between topography, soil depth, soil moisture, transpiration rates and species distribution at the hillslope scale. *Advances in Water Resources*, 29(2):293–310.

Tyree, M. T. (1997). The Cohesion-Tension theory of sap ascent: current controversies. *Journal of Experimental Botany*, 48(10):1753–1765.

van der Maaten-Theunissen, M., Kahle, H. P., and Van Der Maaten, E. (2013). Drought sensitivity of Norway spruce is higher than that of silver fir along an altitudinal gradient in southwestern Germany. *Annals of Forest Science*, 70(2):185–193.

van Genuchten, M. T. (1980). A closed-form equation for predicting the hydraulic conductivity of unsaturated soils. *Soil Science Society of America Journal*, 44(5):892.

van Genuchten, M. T. (1987). Numerical model for water and solute movement in and below the root zone. U.S. Salinity laboratory, USDA, ARS, Riverside, USA.

Vereecken, H., Huisman, J. A., Bogena, H., Vanderborght, J., Vrugt, J. A., and Hopmans, J. W. (2010). On the value of soil moisture measurements in vadose zone hydrology: A review. *Water Resources Research*, 46(4):1–21.

Verstraeten, W. W., Veroustraete, F., and Feyen, J. (2008). Assessment of Evapotranspiration and Soil Moisture Content Across Different Scales of Observation. *Sensors*, 8(1):70–117.

Vogel, T., Dohnal, M., Dusek, J., Votrubova, J., and Tesar, M. (2013). Macroscopic modeling of plant water uptake in a forest stand involving root-mediated soil water redistribution. *Vadose Zone Journal*, 12(1):1:12.

Wald und Holz NRW (2017). Leistungsbericht 2017. Wald, Wasser, Wildnis. Leistungsbericht der Nationalparkverwaltung Eifel, Schleiden-Gemünd, Germany.

Ward, E. J., Domec, J.-C., King, J., Sun, G., McNulty, S., and Noormets, A. (2017). Tracc: an open source software for processing sap flux data from thermal dissipation probes. *Trees*, 31(5):1737–1742.

Ward, E. J., Oren, R., Sigurdsson, B. D., Jarvis, P. G., and Linder, S. (2008). Fertilization effects on mean stomatal conductance are mediated through changes in the hydraulic attributes of mature Norway spruce trees. *Tree Physiology*, 28(4):579–96.

Weber, T. K. D., Iden, S. C., and Durner, W. (2017). A pore-size classification for peat bogs derived from unsaturated hydraulic properties. *Hydrology and Earth System Sciences*, 21(12):6185–6200.

Widlowski, J.-L., Verstraete, M., Pinty, B., and Gobron, N. (2003). Allometric relationships of selected European tree species. EC joint Research Centre, TP440, Ispra, Italy.

Wiekenkamp, I., Huisman, J. A., Bogena, H. R., Lin, H. S., and Vereecken, H. (2016). Spatial and temporal occurrence of preferential flow in a forested headwater catchment. *Journal of Hydrology*, 534:139–149.

Williams, D. G., Cable, W., Hultine, K., Hoedjes, J. C. B., Yepez, E. A., Simonneaux, V., Er-Raki, S., Boulet, G., de Bruin, H. A. R., Chehbouni, A., Hartogensis, O. K., and Timouk, F. (2004). Evapotranspiration components determined by stable isotope, sap flow and eddy covariance techniques. *Agricultural and Forest Meteorology*, 125(3-4):241–258.

Wilson, K. B., Hanson, P. J., Mulholland, P. J., Baldocchi, D. D., and Wullschleger, S. D. (2001). A comparison of methods for determining forest evapotranspiration and its components : sap-flow , soil water budget , eddy covariance and catchment water balance. *Agricultural and Forest Meteorology*, 106(2):153–168.

Wullschleger, S. D., Meinzer, F. C., and Vertessy, R. A. (1998). A review of whole-plant water use studies in trees. *Tree Physiology*, 18:499 – 512.

Zacharias, S., Bogena, H., Samaniego, L., Mauder, M., Fuß, R., Pütz, T., Frenzel, M., Schwank, M., Baessler, C., Butterbach-Bahl, K., Bens, O., Borg, E., Brauer, A., Dietrich, P., Hajnsek, I., Helle, G., Kiese, R., Kunstmann, H., Klotz, S., Munch, J. C., Papen, H., Priesack, E., Schmid, H. P., Steinbrecher, R., Rosenbaum, U., Teutsch, G., and Vereecken, H. (2011). A network of terrestrial environmental observatories in Germany. *Vadose Zone Journal*, 10(3):955.

Zang, C., Hartl-Meier, C., Dittmar, C., Rothe, A., and Menzel, A. (2014). Patterns of drought tolerance in major European temperate forest trees: Climatic drivers and levels of variability. *Global Change Biology*, 20(12):3767–3779.

Zang, C., Pretzsch, H., and Rothe, A. (2012). Size-dependent responses to summer drought in Scots pine, Norway spruce and common oak. *Trees*, 26(2):557–569.

Zeppel, M., Logan, B., Lewis, J. D., Phillips, N., and Tissue, D. (2013). Why lose water at night? Disentangling the mystery of nocturnal sap flow, transpiration and stomatal conductance - When, where, who? *Acta Horticulturae*, 991:307–312.

Zhang, J., Gou, X., Zhang, Y., Lu, M., Xu, X., Zhang, F., Liu, W., and Gao, L. (2016). Forward modeling analyses of Qilian Juniper (Sabina przewalskii) growth in response to climate factors in different regions of the Qilian Mountains, northwestern China. *Trees*, 30(1):175–188.

Zhang, L., Jiang, Y., Zhao, S., Jiao, L., and Wen, Y. (2018). Relationships between tree age and climate sensitivity of radial growth in different drought conditions of Qilian Mountains, northwestern China. *Forests*, 9(3).

Zweifel, R., Böhm, J. P., and Häsler, R. (2002). Midday stomatal closure in Norway spruce–reactions in the upper and lower crown. *Tree Physiology*, 22:1125–1136.